TECHNICAL REPORT S-73-5

SEEPAGE IN MISSISSIPPI RIVER BANKS

Report 1

ANALYSIS OF TRANSIENT SEEPAGE USING A VISCOUS-FLOW MODEL AND THE FINITE DIFFERENCE AND FINITE ELEMENT METHODS

by

C. S. Desai

May 1973

Sponsored by U. S. Army Engineer Division, Lower Mississippi Valley

Conducted by U. S. Army Engineer Waterways Experiment Station
Soils and Pavements Laboratory
Vicksburg, Mississippi

TECHNICAL REPORT S-73-5

SEEPAGE IN MISSISSIPPI RIVER BANKS

Report 1

ANALYSIS OF TRANSIENT SEEPAGE USING A VISCOUS-FLOW MODEL AND THE FINITE DIFFERENCE AND FINITE ELEMENT METHODS

by

C. S. Desai

May 1973

Sponsored by U. S. Army Engineer Division, Lower Mississippi Valley

Conducted by U. S. Army Engineer Waterways Experiment Station
Soils and Pavements Laboratory
Vicksburg, Mississippi

ARMY-MRC VICKSBURG, MISS.

THE CONTENTS OF THIS REPORT ARE NOT TO BE USED FOR ADVERTISING, PUBLICATION, OR PROMOTIONAL PURPOSES. CITATION OF TRADE NAMES DOES NOT CONSTITUTE AN OFFICIAL ENDORSEMENT OR APPROVAL OF THE USE OF SUCH COMMERCIAL PRODUCTS.

FOREWORD

The study of transient seepage phenomena in Mississippi River banks was initiated by the Soils and Pavements Laboratory, U. S. Army Engineer Waterways Experiment Station (WES), Vicksburg, Mississippi, at the request of the U. S. Army Engineer Division, Lower Mississippi Valley (LMVD).

The investigations described in this report were performed by Dr. C. S. Desai. The tests were conducted by Dr. Desai, assisted by Messrs. A. L. Sullivan and W. L. Hanks. This report was prepared by Dr. Desai and was reviewed and approved by LMVD prior to publication. The work was accomplished under the direction of Messrs. J. P. Sale, W. C. Sherman, and C. L. McAnear of the Soils and Pavements Laboratory. Useful comments and suggestions by Mr. S. J. Johnson of WES, Messrs. R. I. Kaufman, F. J. Weaver, and L. H. Cave of LMVD, and Dr. R. S. Sandhu of Ohio State University are gratefully acknowledged.

Directors of WES during the investigation were COL Levi A. Brown, CE, and COL Ernest D. Peixotto, CE. Technical Directors were Messrs. J. B. Tiffany and F. R. Brown.

CONTENTS

NOTATION

A	Matrix
A_x, A_y	Constants
b	Half width of gap
B	Boundary, matrix
c	Constant, rate of rise of flood
C_x	Constant
D	Matrix, operator, constant
erfc	Error function
exp	Exponential
f	Function
g	Gravitational constant
h	Head, vector, potential
h_o	Maximum upstream head
h_1, h_2	Upstream and downstream heads
$\bar{h}$	Mean head
H	Head, total head
i	Index
I	Modified Bessel function
j	Index
J	Jacobian matrix
J_s	Bessel function
k	Index, coefficient of permeability (L/T)
k_o	Permeability (L^2)
K	Matrix
L	Length of model
L_r	Length scale ratio

m	Coefficient of permeability of gap, index
n	Porosity
N_j	Interpolating functions for the finite elements
p	Pressure, exponent
P	Matrix
q	Rate of flow
Q	Matrix
r	Coordinate, number of degrees of freedom
R,RR	Matrix
s	Coordinate, factor
t	Time
T	Period, temperature
T_r	Time scale ratio
u	Head, velocity component, function
$\bar{u}$	Mean velocity component
U	Parameter
v	Velocity component
$\bar{v}$	Mean velocity component
v_p	Particle velocity
V	Volume
V_r	Velocity ratio
w	Velocity component
W	Model width
x	Coordinate
X	Body force component, vector
y	Coordinate
Y	Body force component
z	Coordinate
Z	Body force component
α	Constant, angle
α_1,α_2	Constants
β_x,β_y	Factors
γ	Density
Δt	Time interval

Δx	Interval in x direction
Δy	Interval in y direction
$\Delta \tau$	Small time interval
η	Normal to surface
θ	Angular coordinate
λ	Constant
μ	Viscosity
ν	Kinematic viscosity
ρ	Mass density
τ	Factor
Ψ	Function, total fluid head
ω	Frequency
Ω	Potential function
∇	Operator
∂	Partial differential operator

CONVERSION FACTORS, BRITISH TO METRIC UNITS OF MEASUREMENT

British units of measurement used in this report can be converted to metric units as follows:

Multiply	By	To Obtain
inches	2.54	centimeters
feet	0.3048	meters
pounds per square inch	0.6894757	newtons per square centimeter
Fahrenheit degrees	5/9	Celsius or Kelvin degrees*

* To obtain Celsius (C) temperature readings from Fahrenheit (F) readings, use the following formula: $C = (5/9)(F - 32)$. To obtain Kelvin (K) readings, use: $K = (5/9)(F - 32) + 273.15$.

SUMMARY

The stability of the banks of the Mississippi River is dependent in part upon seepage conditions induced by variations in the river level. Specifically, the drawdown conditions become significant for the design of stable riverbank slopes and protective structures. Conventionally, the slopes are designed on the basis of sudden drawdown conditions, which have often been found to be conservative. For realistic design analysis, it is necessary to evolve methods that permit computations of the timewise fluctuations of the phreatic surface as a consequence of the variations in the river level.

Closed-form solutions for the transient, unconfined seepage posed by the foregoing situation are suitable only for simplified geometries and physical conditions. Such numerical techniques as the finite difference and finite element methods can provide general solutions for complex geometries and material properties. These methods were employed in this research.

A parallel-plate, viscous-flow model was designed and constructed at the WES for the purpose of conducting tests that simulate seepage conditions and variations of external water levels in the field. This report presents a description of the viscous-flow model and the theory governing fluid flow through the model. Various experiments were performed using the model, and a special finite difference scheme was developed for solving approximate equations governing one- and two-dimensional fluid flow. Comparisons were made between the numerical and experimental solutions. A study was performed to examine the numerical characteristics of the finite difference solution scheme.

The finite element method for analysis of one- and two-dimensional fluid flow situations was developed. The one-dimensional flow situation was based on an approximate equation, and the two-dimensional situation was based on the division of the transient problem into a number of steady-state problems governed by the Laplace equation. The numerical solutions were compared with typical experimental results and with field observations along typical sections of the Mississippi River. Analyses were also performed to arrive at the conclusions regarding discretization of infinite soil media as occurring in riverbanks.

Applications of the proposed techniques for obtaining head distribution and flow nets in the domain of fluid seepage are presented in the report. Work to be performed and to be included in the final report (Report 2) is briefly described.

SEEPAGE IN MISSISSIPPI RIVER BANKS

ANALYSIS OF TRANSIENT SEEPAGE USING A VISCOUS-FLOW MODEL AND THE FINITE DIFFERENCE AND FINITE ELEMENT METHODS

PART I: INTRODUCTION

Background

1. Prior to revetment construction along the Mississippi River, the riverbank slopes are graded to help ensure their stability under various river stages, including drawdown. During a fall in the river level, the free water or the phreatic surface in the earth bank lags behind the falling level of water in the river, and it is generally difficult to compute the location of such a free-water surface. Conventionally, the designs are based on the free-water surface that results after full drawdown. This procedure is, however, conservative for many cases and requires slopes that are flatter than necessary.

2. The stability of an earth slope subjected to the effects of changing river stages is dependent on, among other factors, the pore pressures induced within the earth mass due to seepage. The pore pressures are generally estimated from flow net analysis obtained under steady-state conditions. However, a more precise determination of pore pressures is warranted in the case of a continuously moving free surface. In recent years, extensive piezometer installations at selected locations along the banks of the Mississippi River have provided valuable data on the development of free-water surfaces and pore pressures as functions of changing river levels.

3. The U. S. Army Engineer Division, Lower Mississippi Valley (LMVD), engaged the U. S. Army Engineer Waterways Experiment Station (WES) to investigate the transient flow in earth banks under conditions of variable rates of rise or fall in river level and to evolve some

rational methods for predicting the location of free-water surface and the distribution of pore pressures for use in design and stability analyses. The study described herein forms a part of these investigations.

4. Closed-form solutions to the governing equation of the transient flow are available for simple material and boundary conditions.[1-6] However, increased use of high-speed computers has now made possible the use of certain numerical techniques that allow the introduction of complex material and boundary conditions. Numerical methods for the equivalent problems in unsteady gas and heat flow equations have been developed.[7-10]

5. The problem of unconfined seepage through porous soils is, however, complicated by the occurrence of the so-called "phreatic surface" and "surface of seepage" and thus requires special schemes for handling them. In a previous study, Schnitter and Zeller[11] considered flow in earth dams and, on the basis of a simplified falling surface, employed a numerical procedure for the closed-form solution of the Boussinesq equation. A parallel-plate, viscous-flow model was used for comparisons with the analytical solutions. On the basis of an approximate approach,[12] Newlin and Rossier[13] obtained comparisons between their analytical results and experiments with a polyethylene-bead model. In most of the previous work, the applications were restricted to homogeneous, isotropic materials, relatively short model lengths, and a well defined impervious surface (core).

Approaches

6. With the increasing use of numerical techniques in conjunction with digital computers, it is now possible to solve many complex situations in seepage analysis that were impossible or difficult to handle with conventional methods. The two numerical techniques adopted in this study were: (a) the finite difference method and (b) the finite element method. Reviews of published work using these methods are presented in Parts III and IV of this report.

7. In order to develop confidence in using such numerical methods

for design analysis, it is necessary to obtain comparisons between the numerical solutions and laboratory and/or field observations. A number of laboratory experiments were performed by the WES with the parallel-plate, viscous-flow model.[14,15] The model simulated the rise and drawdown conditions caused by variations in the river stages and permitted observations of the movements of the free surface with such variations. In addition, the field observations of river levels and the corresponding heads in piezometers over a period of years along certain sections of the Mississippi River provided field data for useful comparisons.

8. Comparisons between laboratory and field observations and the numerical solutions have been obtained. The laboratory tests included gradual rise and drawdown tests and sudden drawdown tests with the viscous-flow model. Field data included two typical sections along the Mississippi.

9. Design curves for certain common situations along the Mississippi, use of a higher order isoparametric element, numerical stability of the procedures, and some other topics that are under investigation and will be included in Report 2 of this series are described briefly in Part V.

PART II: THE VISCOUS-FLOW MODEL

10. A parallel-plate, viscous-flow model[14,16-19] was constructed to simulate the flow conditions in the riverbanks under changing flood levels. Results from the experiments with the model permitted comparisons with the solutions from the numerical techniques. This part of the report describes salient features of the model and presents the theory of fluid flow through the closely spaced parallel plates in the model.

Description of the Model

11. The viscous-flow model (fig. 1) consists of two 0.5-in.-thick (1.27 cm), parallel glass plates with a plastic base plate, resting on an adjustable I-beam that is supported on two columns. The glass

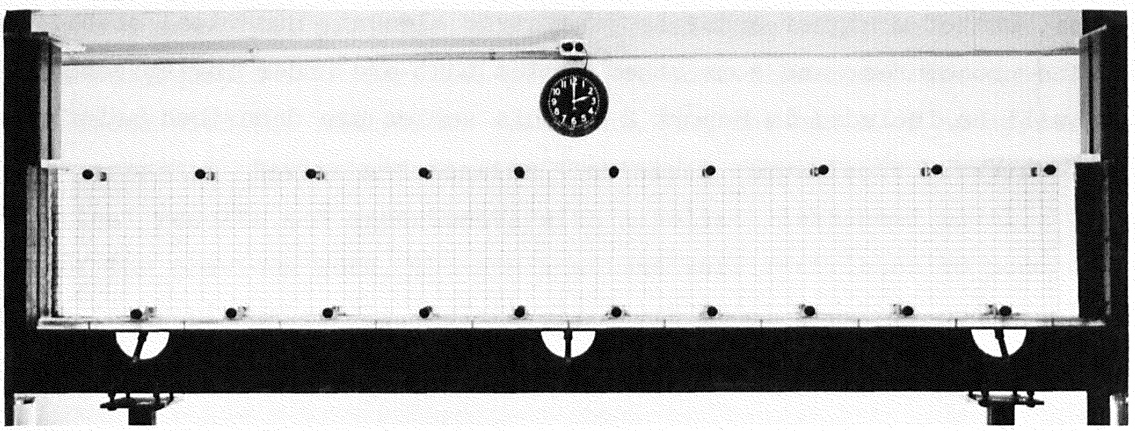

Fig. 1. View of parallel-plate, viscous-flow model

plates are 11 ft (about 335 cm) long and 20 in. (about 50 cm) in height. Two plastic plates, each 0.25 in. (0.635 cm) thick, are inserted between the glass plates so that a desired width of gap between them is obtained. The plastic plates can be shaped to simulate any desired prototype configuration. A reservoir, approximately 8 in. square (20.3 cm square), is provided at each end of the glass plates. Each reservoir is provided with a means for controlling the level of liquid in the reservoir.

Fluid used in the model

12. The fluid used for the experiments was Silicone SF-96-1000,* manufactured by General Electric Company. The following description of the fluid was given by the manufacturer:

> Silicone fluid is chemically inert to most common materials of construction, and its density and viscosity do not change appreciably with temperature. The fluid has excellent stability under very high temperatures for long periods of time. It is self-extinguishing with flash point above 550 F** and autoignition temperature in the range of 820 to 860 F. It has low surface tension, which is largely independent of viscosity (about 21 dynes per cm at 25 C, over a viscosity range of 20 to 100,000 centistokes). The thermal conductivity of the Silicone fluid is relatively constant over a wide range of temperature.

13. The actual viscosity-temperature relation of the fluid was determined at the WES (fig. 2). The density-temperature relationship is shown in fig. 3. At a temperature of 24 C, the viscosity of the Silicone fluid is about 9.7 poises, and this value is used for numerical computations described subsequently. At this temperature level, the density of the fluid is approximately 0.97 g/cm^3. The bulk modulus of the SF-96-1000 fluid is about 150,000 psi (10,500 kg/cm^2); that of water is about 300,000 psi (21,100 kg/cm^2). Although the liquid is nearly twice as compressible as water, the pressures in the prototype and in the model are not large enough to cause concern.

14. The Silicone fluid is colorless; therefore, it was necessary to add a coloring agent to it in order to obtain a distinct and clear free surface. The coloring material, Sudan Red 4BA, was supplied by the General Dyestaff Company of New York.

15. A Randolph pump, Model 500, manufactured by the Randolph Company of Houston, Texas, was installed to pump the liquid into the reservoir.

---

* The number "1000" in the designation of the fluid stands for the nominal viscosity of 1000 centistokes.

** A table of factors for converting British units of measurement to metric units is presented on page xiii.

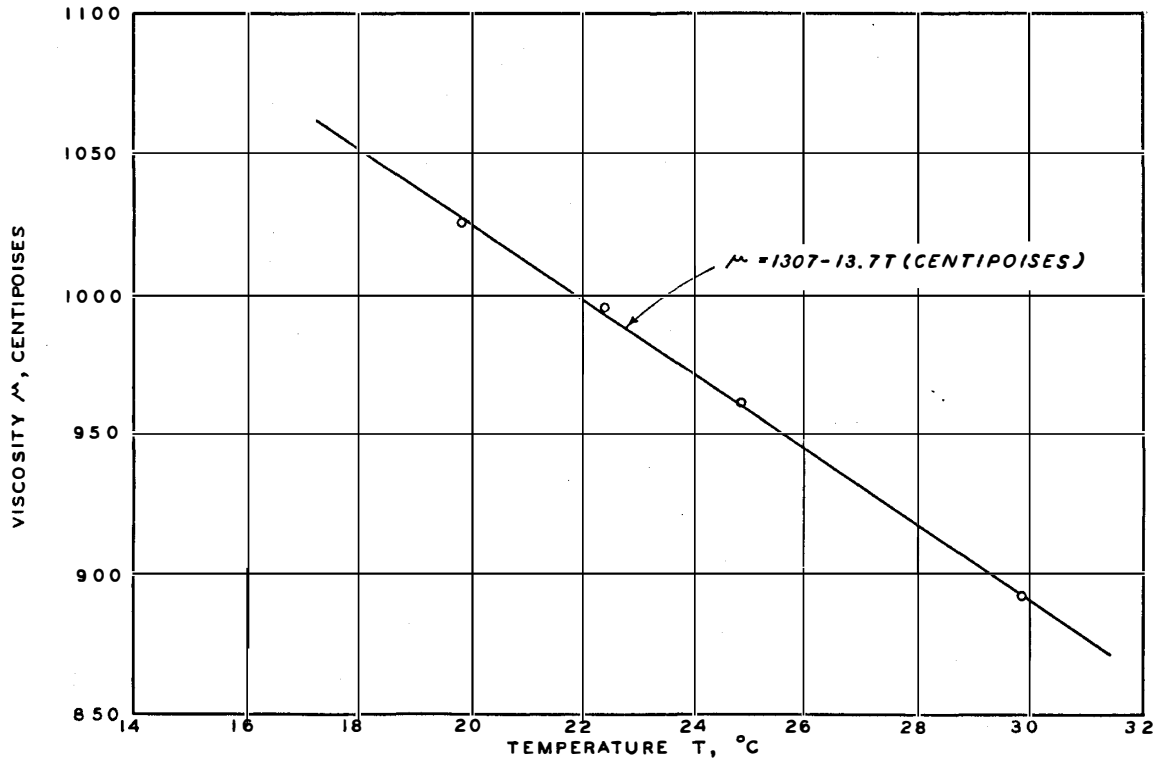

Fig. 2. Viscosity-temperature relationship for Silicone SF-96-1000 fluid

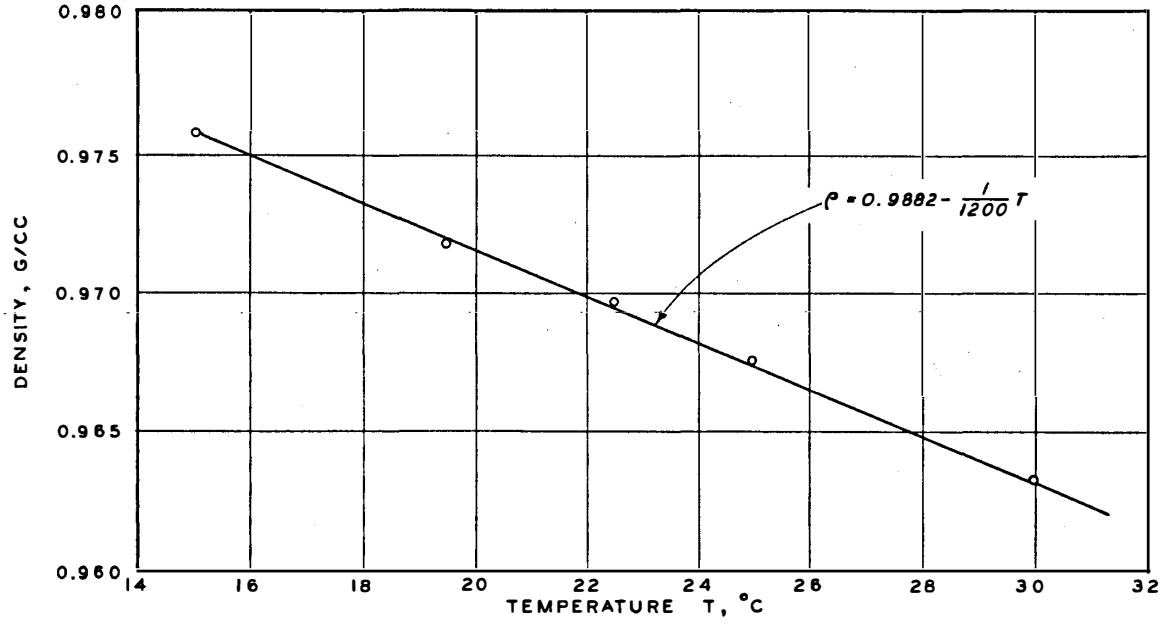

Fig. 3. Density-temperature relationship for Silicone SF-96-1000 fluid

Device for varying
external fluid levels

16. For the rising conditions in the external fluid level, the liquid was pumped into the reservoir at one end of the model. A movable pipe passing through the bottom of the graduated reservoir was adjusted to achieve desired heights of fluid levels. Thus, the free surface changed with the change in level in the reservoir. A desired rate of rise of level in the reservoir could be set by means of the electronic control panel (fig. 4). The free surface was permitted to stabilize

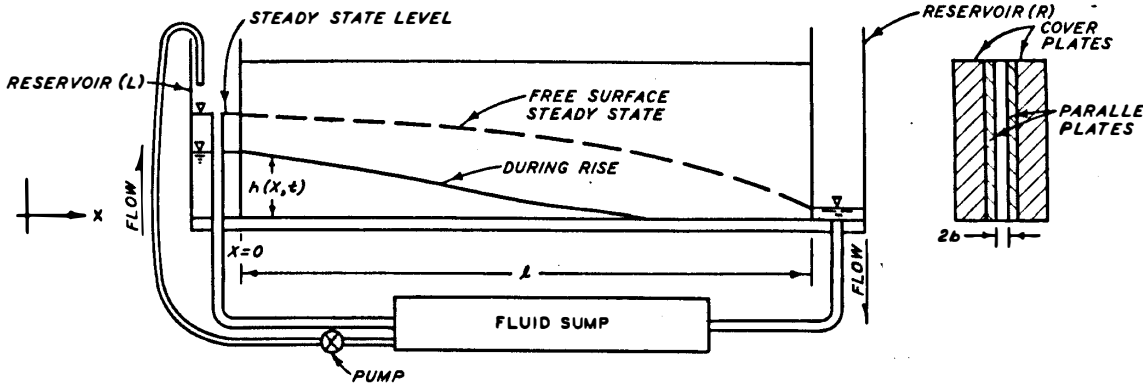

a. Rise in external fluid level

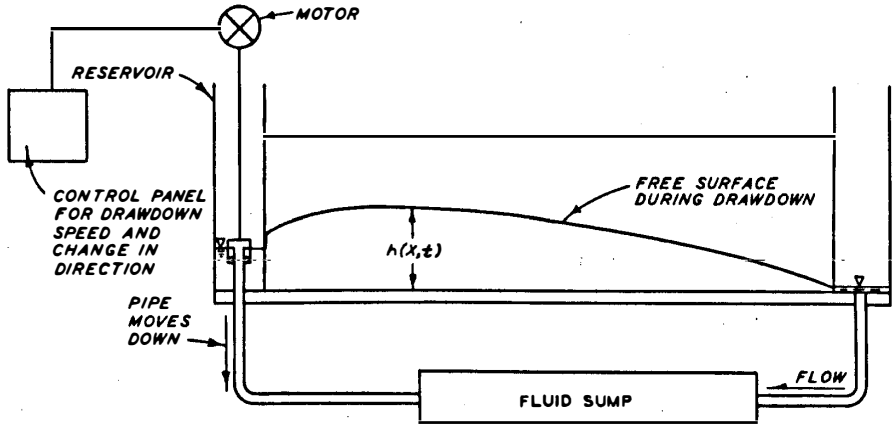

b. Drawdown in external fluid level

Fig. 4. Schematic diagram of rise and fall (drawdown) in the viscous-flow model

under the steady head until no significant changes occurred in its movements.

17. Drawdown at a preset rate was also achieved by setting a selected rate on the electronic control panel (fig. 4b). The control system was connected to the model by a motor and gear system that actuated the adjustable pipe either to rise or to fall. The falling case simulated a gradual drawdown situation by permitting the fluid to flow out as the pipe was lowered.

18. Fig. 4 schematically shows typical stages during rising, steady-state, and drawdown conditions. A record of the changing external levels and the free surface was obtained by still photographs, manual measurements, and motion pictures of typical cases. The entire front face of the model was divided into a grid of 1-in. squares which permitted measurements of free-surface heads and interpretations of photographs.

Theory of Flow Through the Viscous-Flow Model

Governing equations of flow in porous media

19. General governing equations for the motion of a fluid are expressed as a system of differential equations. These equations satisfy the three basic physical conditions: continuity, rheological equation of state, and Newton's laws of motion. Together with a set of initial and boundary conditions, these equations define a given problem. The best known of these equations are those of Navier and Stokes[1,6,14,19] which are applicable to incompressible viscous fluids. The Navier-Stokes equations may be expressed as

$$X - \frac{1}{\rho}\frac{\partial p}{\partial x} + \frac{\nu}{3}\frac{\partial}{\partial x}\left(\frac{\partial u}{\partial x} + \frac{\partial v}{\partial y} + \frac{\partial w}{\partial z}\right) + \nu\nabla^2 u = \frac{Du}{\partial t} \qquad (1a)$$

$$Y - \frac{1}{\rho}\frac{\partial p}{\partial y} + \frac{\nu}{3}\frac{\partial}{\partial y}\left(\frac{\partial u}{\partial x} + \frac{\partial v}{\partial y} + \frac{\partial w}{\partial z}\right) + \nu\nabla^2 v = \frac{Dv}{\partial t} \qquad (1b)$$

$$Z - \frac{1}{\rho}\frac{\partial p}{\partial z} + \frac{\nu}{3}\frac{\partial}{\partial z}\left(\frac{\partial u}{\partial x} + \frac{\partial v}{\partial y} + \frac{\partial w}{\partial z}\right) + \nu\nabla^2 w = \frac{Dw}{\partial t} \qquad (1c)$$

where

x,y,z = spatial coordinates

u,v,w = velocity components in x , y , and z directions, respectively

X,Y,Z = body forces in x , y , and z directions, respectively

$\rho = \gamma/g$, mass density of fluid

g = gravitational constant

$\nu = \mu/\rho$, kinematic viscosity

$\nabla^2 = \partial^2/\partial x^2 + \partial^2/\partial y^2 + \partial^2/\partial z^2$

$D/\partial t = \partial/\partial t + u(\partial/\partial x) + v(\partial/\partial y) + w(\partial/\partial z)$

Application to viscous-flow model

20. Hele-Shaw[16,17] developed the first parallel-plate, viscous-flow model. The Hele-Shaw viscous-flow model (figs. 1 and 5) consists of two closely spaced, parallel plates. The narrow gap between the plates forms a channel through which the fluid flows. The channel represents a two-dimensional cross section of an unconfined homogeneous and isotropic aquifer. Regulating reservoirs are provided at each end of the model. A regulating reservoir can be considered as any body of open water that the aquifer intersects. One of the major advantages of the Hele-Shaw model is its clearly defined free surface, which eliminates the broad capillary zone of partial saturation that complicates the use of sand models.[18]

21. In the sketch of the model shown in fig. 5, if the distance $2b$ between the two plates is small, the flow between the plates can be considered as two-dimensional, with coordinate axes as shown, and the velocity component w can be assumed as zero. The gravitational forces are the only body forces acting on the system. The gravitational force can be replaced by a potential function $\Omega = gH$, where H is the elevation head. Thus,

$$X = -\frac{\partial}{\partial x}(gH) \tag{2a}$$

$$Y = -\frac{\partial}{\partial y}(gH) \tag{2b}$$

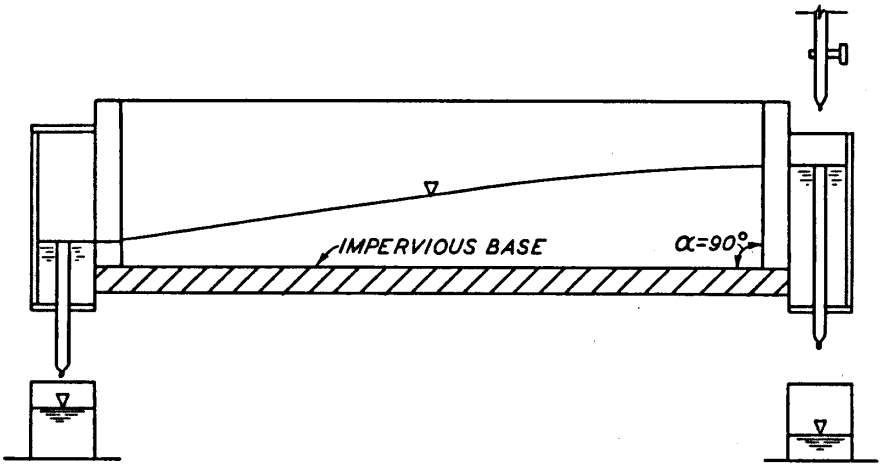

a. Elevation

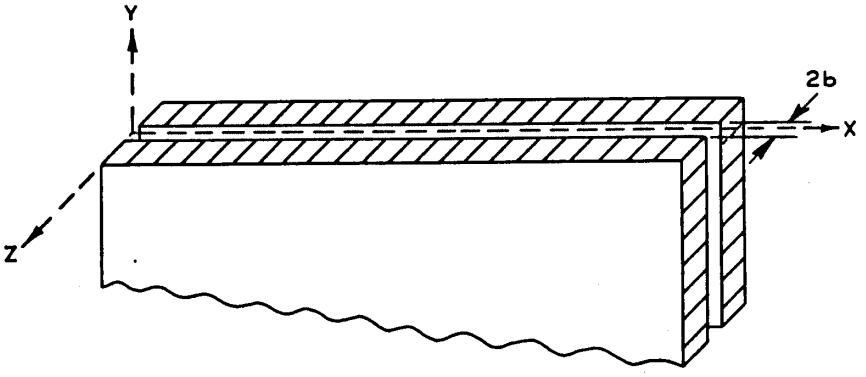

b. Isometric view of parallel plates

Fig. 5. Details of viscous-flow model

$$Z = -\frac{\partial}{\partial z}(gH) \qquad (2c)$$

22. For an incompressible fluid, there is no volume change; hence, the third term in equation 1, representing the rate of volume dilation, can be ignored. Assuming the flow to be laminar, the fluid velocities at the plates must be zero (fig. 5b); hence, the change in the velocity components u and v with respect to z will be much greater than the changes with respect to the x and y directions. Therefore, the derivatives $\partial u/\partial x$, $\partial u/\partial y$, $\partial v/\partial x$, and $\partial v/\partial y$ and their second derivatives can be neglected.

23. Introducing the above assumptions in equation 1,

$$\frac{\partial}{\partial x}(\rho g H + p) - \mu \frac{\partial^2 u}{\partial z^2} = -\rho \frac{\partial u}{\partial t} \tag{3a}$$

$$\frac{\partial}{\partial y}(\rho g H + p) - \mu \frac{\partial^2 u}{\partial z^2} = -\rho \frac{\partial v}{\partial t} \tag{3b}$$

$$\frac{\partial}{\partial z}(\rho g H + p) = 0 \tag{3c}$$

For the special case of steady-state flow, equation 3 will reduce to

$$\frac{\partial}{\partial x}(\rho g H + p) - \mu \frac{\partial^2 u}{\partial z^2} = 0 \tag{4a}$$

$$\frac{\partial}{\partial y}(\rho g H + p) - \mu \frac{\partial^2 v}{\partial z^2} = 0 \tag{4b}$$

$$\frac{\partial}{\partial z}(\rho g H + p) = 0 \tag{4c}$$

24. Equation 4c shows that the total head at any point within the flow domain will depend upon the x and y coordinates only. Hence, equations 4a and 4b can be integrated with respect to z to yield

$$z \frac{\partial}{\partial x}(\rho g H + p) = \mu \frac{\partial u}{\partial z} + c_1 \tag{5a}$$

$$z \frac{\partial}{\partial y}(\rho g H + p) = \mu \frac{\partial v}{\partial z} + c_2 \tag{5b}$$

Now, $\partial u/\partial z = \partial v/\partial z = 0$ when $z = 0$; therefore, from equation 5,

$$c_1 = c_2 = 0$$

Integrating, once again with respect to z ,

$$\frac{z^2}{2} \frac{\partial}{\partial x}(\rho g H + p) = \mu u + c_3 \tag{6a}$$

and

$$\frac{z^2}{2}\frac{\partial}{\partial y}(\rho g H + p) = \mu v + c_4 \tag{6b}$$

Here, $u = v = 0$ when $z = \pm b$; therefore,

$$c_3 = \frac{b^2}{2}\frac{\partial}{\partial x}(\rho g H + p)$$

and

$$c_4 = \frac{b^2}{2}\frac{\partial}{\partial y}(\rho g H + p)$$

$$u = \frac{z^2 - b^2}{2\mu}\frac{\partial}{\partial x}(\rho g H + p) \tag{6c}$$

$$v = \frac{z^2 - b^2}{2\mu}\frac{\partial}{\partial y}(\rho g H + p) \tag{6d}$$

25. Equation 6 shows that the distribution of velocity components is parabolic. The maximum velocity at the center of the gap, i.e., at $z = 0$, is

$$u = -\frac{b^2}{2\mu}\frac{\partial}{\partial x}(\rho g H + p) \tag{7a}$$

$$v = -\frac{b^2}{2\mu}\frac{\partial}{\partial y}(\rho g H + p) \tag{7b}$$

and the mean velocity is 2/3 of the maximum, thus,

$$\bar{u} = -\frac{b^2}{3\mu}\frac{\partial}{\partial x}(\rho g H + p) \tag{8a}$$

$$\bar{v} = -\frac{b^2}{3\mu}\frac{\partial}{\partial y}(\rho g H + p) \tag{8b}$$

Multiplying and dividing by ρg on the right-hand side of equation 8 and substituting h for $H + p/\rho g$ yields

$$\bar{u} = -\frac{b^2 \rho g}{3\mu}\frac{\partial h}{\partial x} \tag{9a}$$

$$\bar{v} = -\frac{b^2 \rho g}{3\mu} \frac{\partial h}{\partial y} \tag{9b}$$

or

$$\bar{u} = -m \frac{\partial h}{\partial x} \tag{9c}$$

$$\bar{v} = -m \frac{\partial h}{\partial y} \tag{9d}$$

where m designates the coefficient of permeability of the gap.

Relationship between
model and prototype

26. Darcy's law, which represents a linear relationship between the hydraulic gradient and the discharge velocity, is given by

$$v = -k \frac{\partial h}{\partial s} \tag{10a}$$

Using the relationship between the permeability and the coefficient of permeability[19]

$$k = k_o \frac{\rho g}{\mu} \tag{10b}$$

equation 10a is transformed to

$$v = -\frac{k_o \rho g}{\mu} \frac{\partial h}{\partial s} \tag{10c}$$

where

k = coefficient of permeability, L/T

k_o = permeability, L^2

s = coordinate direction along the stream line

27. Now, writing equation 9b for the model and equation 10c for the prototype yields

$$V_m = V_{model} = -\frac{b^2 \rho_m g}{3\mu_m} \frac{\partial h}{\partial s} \tag{11a}$$

and

$$V_p = V_{proto} = -\frac{k_o \rho_p g}{\mu_p} \frac{\partial h}{\partial s} \tag{11b}$$

28. The velocity ratio between the model and prototype for the same gradients is given by

$$V_r = \frac{v_m}{v_p} = \frac{b^2}{3} \frac{\rho_r}{k_o \mu_r} = \frac{b^2 \rho_m g}{3k\mu_m} \tag{12}$$

Selection of model scales

29. The properties of the Silicone fluid SF-96-1000 at 24 C are given by

$$\rho_m = 0.97 \text{ g/cm}^3$$

$$\mu_m = 9.7 \text{ poises}$$

Therefore,

$$V_r = \frac{0.97 \times 980}{3 \times 9.7} \times \frac{b^2}{k} = 33 \frac{b^2}{k} \tag{13}$$

Now,

$$V_r = \frac{L_r}{T_r}$$

where L_r = length scale ratio and T_r = time scale ratio. Thus, sample calculations for model dimensions for certain numerical values of prototype conditions are given by the following:

a. For a flood of 75 ft, simulated by 1.25 ft in the model,

$$L_r = \frac{1.25}{75} = 0.0167$$

b. For a flood of one week ($\simeq$605,000 sec), simulated in the model by approximately 8 min (480 sec),

$$T_r = \frac{480}{605,000} = \frac{1}{1,260}$$

Therefore

$$V_r = \frac{0.0167}{1/1260} = 21.00 \qquad (14)$$

c. Equating equations 13 and 14 yields

$$33 \frac{b^2}{k} = 21$$

where

b = half width, cm

k = permeability, cm/sec

or

$$b^2 = 0.636k$$

If

$$k = 100 \times 10^{-4} \text{ cm/sec}$$

$$b^2 = 0.636 \times 100 \times 10^{-4}$$

and

$$b = 0.08 \text{ cm}$$

Then the model width $W = 2 \times b = 0.16$ cm or approximately 1/16 in.

30. Values of T_r for different combinations of b and k are as follows:

W	b	k , cm/sec	$T_r = \frac{0.0167}{33} \frac{k}{b^2}$
1/8 in.	1/16 in. (0.16 cm)	100×10^{-4}	1/5000
		500×10^{-4}	1/1000
		1000×10^{-4}	1/500

(Continued)

W	b	k , cm/sec	$T_r = \frac{0.0167}{33} \frac{k}{b^2}$
1/16 in.	1/32 in. (0.08 cm)	100×10^{-4}	1/1250
		500×10^{-4}	1/250
		1000×10^{-4}	1/125

For a given L_r , the following relationship can be written

$$33 \frac{b^2}{k} = \frac{0.0167}{T_r} \tag{15}$$

PART III: THE FINITE DIFFERENCE APPROACH

Background

31. The basic equations governing transient, unconfined fluid flow through rigid porous media are nonlinear; no closed-form solutions are available that can adequately account for the complexities posed by this phenomenon. Some of the closed-form solutions that can handle simplified boundary conditions and material properties are described in Appendix A. It can be seen from the descriptions in Appendix A that even a linearized form of the governing equation is difficult to solve in closed form for arbitrary and variable boundary conditions. Probably the most suitable course of action under these conditions would be to adopt numerical techniques for approximate solutions of the problem. With the availability of high-speed computers and such efficient procedures as the finite difference and finite element methods, it is now possible to obtain satisfactory numerical solutions.

32. The finite difference technique was used in the first phase of investigations involving numerical methods. In certain situations, the finite difference method could provide adequate solutions economically. The second phase of the numerical study consisted of the use of the finite element method. An evaluation of the two techniques is presented in Part V.

33. The finite difference method has been used for the solution of the equations governing fluid flow in rigid porous media.[14,15,20-29] Most of the previous work is based on the solution of the Laplace or Poisson's equations. In the case of unconfined seepage with a free surface, it usually becomes necessary to adopt an approximate form of the governing equation, employ an iterative technique for satisfaction of the Laplace equation, or solve the nonlinear equation directly. In the finite difference solution presented herein, an approximate nonlinear form of the governing equation was adopted.

Governing Equations

Two-dimensional flow

34. The following nonlinear equation is assumed to govern the two-dimensional fluid flow.[5]

$$n \frac{\partial h}{\partial t} = \frac{k_x}{2} \frac{\partial^2 h^2}{\partial x^2} + \frac{k_y}{2} \frac{\partial^2 h^2}{\partial y^2} \tag{16a}$$

where

h = head at point (x,y) at time t

n = porosity

k_x and k_y = horizontal and vertical permeability, respectively

Equation 16a is based on such assumptions as laminar flow, incompressible fluid, rigid soil, and no change in k_x, k_y, and n with time. Moreover, Dupuit assumption is made in deriving equation 16a, and the function h^2 satisfies only approximately the basic Laplace equation governing the flow.[19]

35. If a mean head $\bar{h}$ is assumed, a linearized equation can be obtained as[2,14,15,22]

$$n \frac{\partial h}{\partial t} = \bar{h} \left(k_x \frac{\partial^2 h}{\partial x^2} + k_y \frac{\partial^2 h}{\partial y^2} \right) \tag{16b}$$

The boundary conditions (fig. 6) associated with equation 16a are

$$\left.\begin{aligned} &\text{i.} && h(x,y,0) = 0 \text{ for an initially dry bank} \\ &\text{ii.} && h(x,y,t) = f(t) \text{ on the entrance face} \\ &\text{iii.} && \frac{\partial h}{\partial y} = 0 \text{ at the impervious base} \\ &\text{iv.} && h(x,y,t) = Y \text{ elevation head at free surface} \end{aligned}\right\} \tag{16c}$$

One-dimensional flow

36. One-dimensional equations corresponding to equations 16a and 16 b are

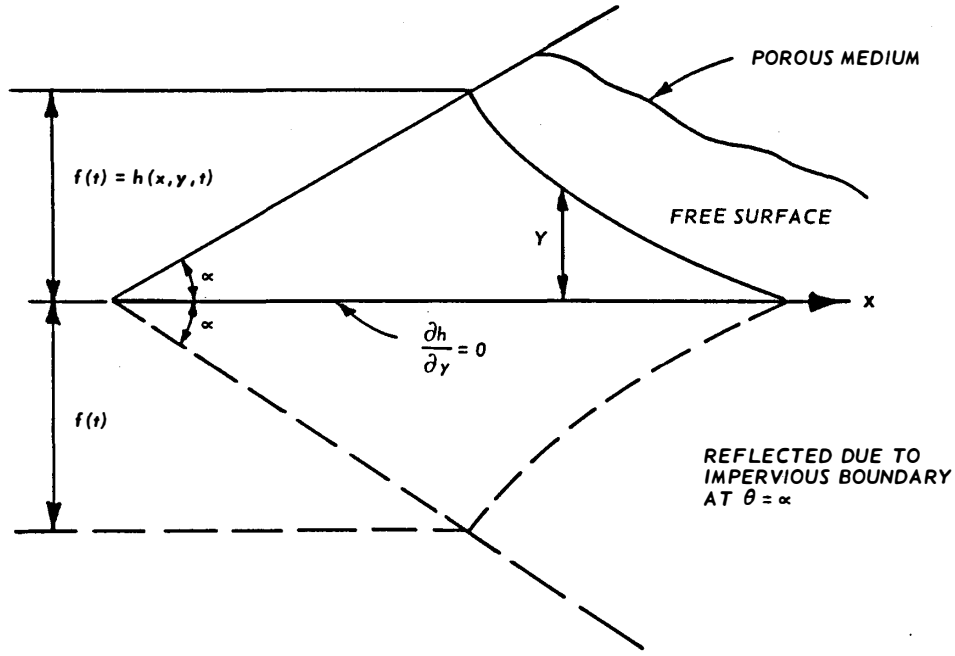

Fig. 6. Section of earth bank subjected to time-dependent external heads

$$n \frac{\partial h}{\partial t} = \frac{k_x}{2} \frac{\partial^2 h^2}{\partial x^2} \tag{17a}$$

and

$$n \frac{\partial h}{\partial t} = k_x \bar{h} \frac{\partial^2 h}{\partial x^2} \tag{17b}$$

37. The above equations of free-surface flow through porous media were considered analogous to the equations governing the flow through the narrow gap of a parallel-plate model.[14,16,18,19] The parallel-plate model used in the experiments had a uniform gap throughout (fig. 5b). This configuration simulated an isotropic and homogeneous soil mass. It is possible, however, to simulate a nonhomogeneous and anisotropic soil mass by appropriately varying the gap between the plates. The permeability of the model for use in equations 16 and 17 was obtained from the relationship[14,18,19]

$$k_m = k_x = k_y = \frac{b^2 \rho g}{3\mu} \tag{17c}$$

where b = half width of the gap, with porosity equal to unity.

Alternative linearization

38. The linearization in equation 17 essentially yields solutions of the form

$$h(x,t) = \alpha_1 x + \alpha_2 \tag{18}$$

where α_1 and α_2 are constants. Equation 18 is a linear function and indicates that the equation of the free surface is obtained in the form of a straight line.[5]

39. An alternative linearized form for equation 17a can be obtained by adopting h^2 as an unknown and writing the equation as

$$n \frac{\partial u}{\partial t} = k_x \sqrt{u} \frac{\partial^2 u}{\partial x^2} \tag{19}$$

where $u = h^2$ and $\sqrt{u}$ represents the mean height of the external level of fluid. This approach can yield a parabolic variation of the free-surface head.[5,14]

Finite Difference Procedures

Alternating direction explicit procedure scheme

40. A special scheme, the alternating direction explicit procedure (ADEP),[30-32] of the finite difference procedure can be employed (fig. 7) to derive the finite difference analogue of equation 16a,

$$h_{i,j,t+1} = h_{i,j,t} + \beta_x \left(\frac{h^2_{i-1,j,t+1} - h^2_{i,j,t+1}}{\Delta x_1} - \frac{h^2_{i,j,t} - h^2_{i+1,j,t}}{\Delta x_2} \right)$$

$$+ \beta_y \left(\frac{h^2_{i,j+1,t+1} - h^2_{i,j,t+1}}{\Delta y_1} - \frac{h^2_{i,j,t} - h^2_{i,j-1,t}}{\Delta y_2} \right) \tag{20a}$$

where $\beta_x = k_x \Delta t / n(\Delta x_1 + \Delta x_2)$ and $\beta_y = k_y \Delta t / n(\Delta y_1 + \Delta y_2)$.

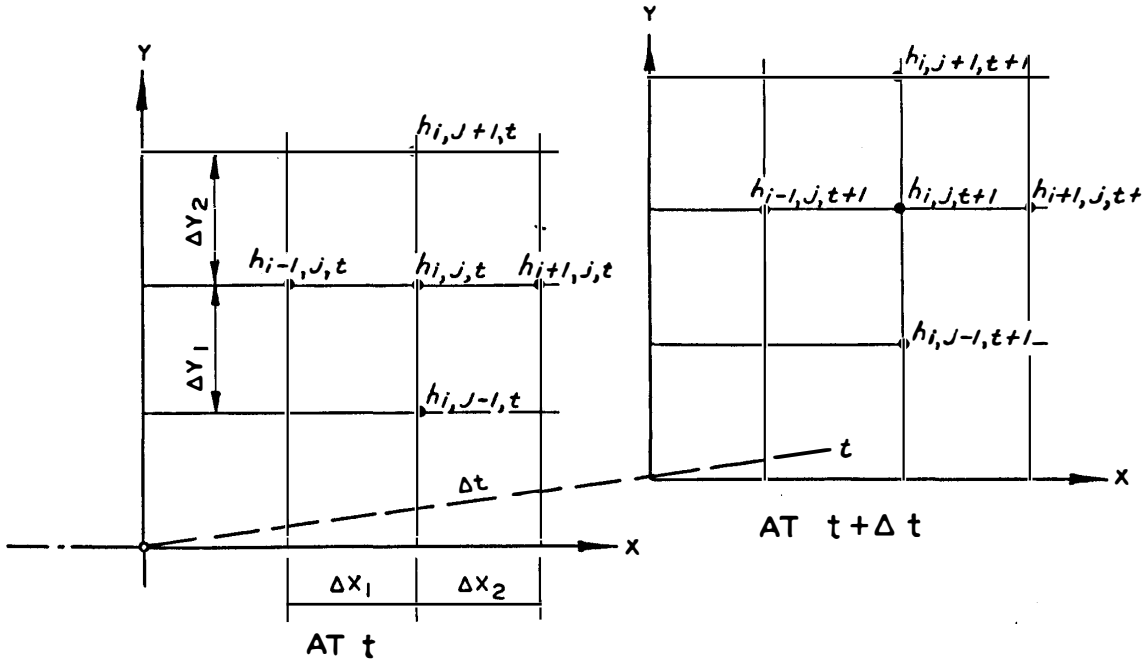

Fig. 7. Finite difference approximation for ADEP

Equation 20a, at time level $t + 1$, reduces to the quadratic form

$$Ah^2_{i,j,t+1} + Bh_{i,j,t+1} + C = 0 \qquad (20b)$$

where

Δx and Δy = spatial intervals

Δt = time interval

A , B , C = known constants at $(t + 1)$, and are functions of β_x , β_y , and known heads at t and $(t + 1)$

and the index symbols are shown in fig. 7.

41. The finite difference form corresponding to the linearized equation 1b is

$$h_{i,j,t+1} = h_{i,j,t} + \bar{\beta}_x \left(\frac{h_{i-1,j,t+1} - h_{i,j,t+1}}{\Delta x_1} - \frac{h_{i,j,t} - h_{i+1,j,t}}{\Delta x_2} \right)$$

$$+ \bar{\beta}_y \left(\frac{h_{i,j+1,t+1} - h_{i,j,t+1}}{\Delta y_1} - \frac{h_{i,j,t} - h_{i,j-1,t}}{\Delta y_2} \right) \qquad (21)$$

where $\bar{\beta}_x = k_x \bar{h}/0.5n\,(\Delta x_1 + \Delta x_2)$, and $\bar{\beta}_y = k_y \bar{h}/0.5n\,(\Delta y_1 + \Delta y_2)$.

42. For the equation governing one-dimensional flow, equation 17a, the ADEP forms are

$$h_{i,j,t+1} = h_{i,j,t} + \beta_x \left(\frac{h^2_{i-1,j,t+1} - h^2_{i,j,t+1}}{\Delta x_1} - \frac{h^2_{i,j,t} - h^2_{i+1,j,t}}{\Delta x_2} \right) \quad (22a)$$

and

$$h_{i,j,t+1} = h_{i,j,t} + \bar{\beta}_x \left(\frac{h_{i-1,j,t+1} - h_{i,j,t+1}}{\Delta x_1} - \frac{h_{i,j,t} - h_{i+1,j,t}}{\Delta x_2} \right) \quad (22b)$$

43. Alternatively, simple explicit forms of the finite difference scheme can be used; however, this scheme[14] is only conditionally stable.

Steps in the numerical scheme

44. In equations 20-22, two time levels are used. At each of the two time levels, only one head from each direction is included. If a proper choice of an initial starting point is made, e.g., at the upstream face where $f(t)$ is prescribed for all times, then $h_{i,j,t+1}$ is the only unknown and can thus be computed explicitly. Equation 20 or 21 is sequentially applied point by point, either in the x or y directions. The accuracy of this procedure is improved by adopting the point-by-point sequence in the alternate directions. It has been found that the ADEP is more suitable and computationally stable, compared to some other finite difference schemes, and can also be extended for three-dimensional flow.[31,32]

45. The solution usually starts at time $t = 0$ when the head distribution in the flow domain is specified, as in the boundary condition i of equation 16c. The solutions for increasing times are then propagated by using one of the recurrence equations, 20, 21, or 22. These equations are easy to program for the computer.

Solution for rise of external water level

46. The solution for a rise of external water level proceeds as described above, with the applied heads at the entrance known at all time levels according to the boundary condition ii, equation 16c. The

approximate location of the free surface at a given time is obtained on the basis of the known heads at that time. This solution is achieved by locating those points in the flow domain at which the computer head is equal to the elevation head. A linear interpolation scheme is used to satisfy this condition as stated in the boundary condition iv, equation 16c. Thus, the free surface can be located at any selected time level.

Solution for fall (or drawdown) of external water level

47. The solution for a drawdown in the external water level involves additional complexities due to the occurrence of the surface of seepage (fig. 8). The surface of seepage arises because the fall of the free surface lags behind the fall of the external water level. Consequently, the surface exits the entrance face at a point higher than the external water level. Since the seepage forces near the entrance are influenced by the location of the exit point, it is necessary to compute the point for all time levels. Furthermore, this location is necessary for imposing the appropriate modified upstream heads.

48. Pavlovsky's method of fragments[5,15,19,22,33] or the method of permeable membrane[34] may be used to locate the point of exit. The method of fragments, which also has been recently used by Dvinoff,[22] is employed herein. Fig. 8 shows a section of the bank at a typical instant of time $t + 1$ during drawdown. To apply the method, the time interval Δt from t to $t + 1$ is divided into a number of small time intervals $\Delta\tau$. For instance, $\Delta t = 100$ sec used in this study was divided into 5000 small $\Delta\tau$'s. The quantity of fluid out of the upstream face is equal to the amount of fluid contained between the free surfaces at two time levels $\Delta\tau$ apart. Hence, the outflow per unit length, assuming it to be essentially horizontal, is

$$\Delta Q = -k_x \left[h_e(t + \Delta\tau) - h_d(t + 1)\right] \tan\alpha \, (1 + \log\lambda)\Delta\tau \qquad (23a)$$

where $\lambda = \dfrac{h_e(t + \Delta\tau)}{h_e(t + \Delta\tau) - h_d(t + 1)}$.

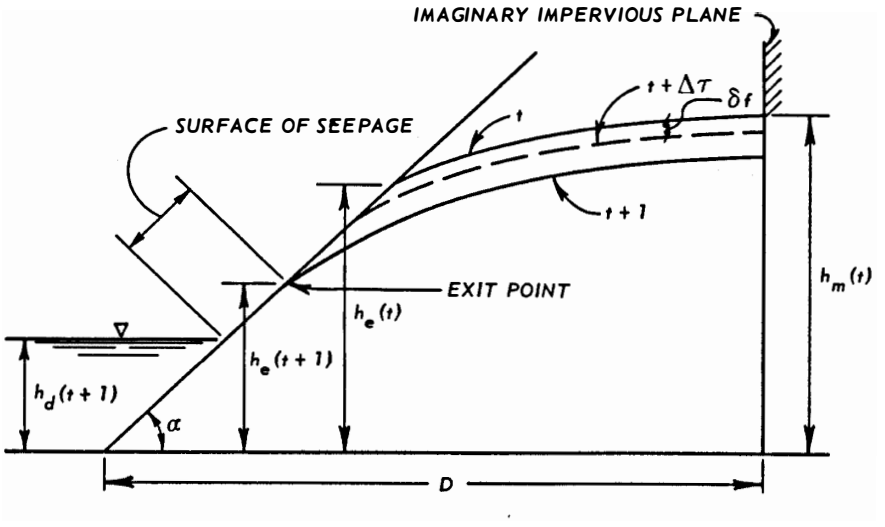

a. Inclined entrance face

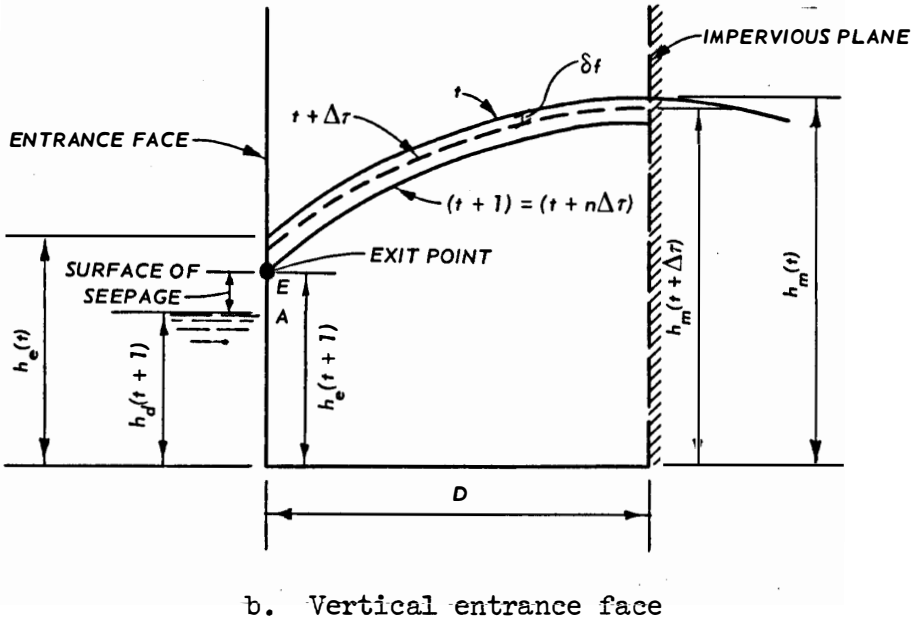

b. Vertical entrance face

Fig. 8. Location of the surface of seepage

The corresponding volume change is

$$\Delta V = n\left[h_m(t) - h_e(t + \Delta\tau)\cot\alpha\,\delta f + n\cot\alpha\,(\delta f)^2\right] \qquad (23b)$$

where δf denotes the fall of the free surface in time $\Delta\tau$. Equating ΔQ and ΔV yields an expression for δf,

$$\delta f = \frac{-p + \sqrt{p^2 + 4r}}{2} \tag{23c}$$

where $p' = h_m(t) - h_e(t + \Delta\tau)$, and $r = \Delta Q \tan \alpha / n$. For $\alpha = 90$ deg, the above equations reduce (fig. 8b) to[5]

$$\Delta Q = k_x \left[\frac{h_m^2(t) - h_d^2(t + 1)}{2D} \right] \Delta\tau \tag{24a}$$

$$\Delta V = nD\, \delta f \tag{24b}$$

and

$$\delta f = \frac{\Delta Q}{nD} \tag{24c}$$

in which D denotes the distance between the entrance toe and the location of the maximum head (fig. 8). An impervious boundary is needed in using the above procedure. For the model that represents a long riverbank, no such physical boundary is generally available. Hence, an imaginary impervious boundary is established at each time level. This boundary is established by locating the point of maximum head $h_m(t)$ at the previous time and using the vertical plane through that point as the required impervious boundary.

49. Once the fall of the surface δf corresponding to $\Delta\tau$ is computed, the location of the exit point is obtained from the recurrence relation

$$h_e(t_i + \Delta\tau) = h_e(t_i) - \delta f_i \tag{25}$$

where t_i assumes values from t to $t + 1$, which include, for instance, 5000 iterations for $\Delta t = 100$ sec. The last value in equation 25, $h_e(t + 1)$, gives the exit head for the current time $t + 1$.

50. The entrance boundary heads are now imposed as

$$
\left.
\begin{aligned}
&\text{i.} \quad h(x, x\tan\alpha, t+1) = h_d(t+1) \quad \text{for points below} \quad h_d(t+1) \\
&\text{ii.} \quad h(x, x\tan\alpha, t+1) = \text{elevation head along the surface of seepage} \\
&\text{iii.} \quad h(x, x\tan\alpha, t+1) = \frac{h_e(t+1) + h_m(t)}{2} \quad \text{for points above} \\
&\qquad\qquad\qquad\qquad\qquad\qquad h_e(t+1)
\end{aligned}
\right\} \quad (26)
$$

Condition iii is arbitrarily chosen.

51. Equation 20, 21, or 22 is now applied, and the procedure is repeated until the desired drawdown level is attained.

52. For the constant-head time zone between the time of maximum rise and the time when the fall starts (fig. 9), equation 20, 21, or 22 is used in the same manner as for the rising condition.

Approximation for boundary conditions at the downstream face

53. The level of fluid at the tail or exit end was always maintained at zero. The above procedure for locating the surface of seepage was not employed for the exit face, since the variations in the exit point for a model of this length were very slow. Instead, an approximation was made according to which zero head was assumed at a distance of one Δx outside the exit face with a linear head variation from this point to the point one Δx inside from the exit face.

Experimental Results

54. A number of experiments were conducted by the WES with a viscous-flow model that was about 350 cm long and 50 cm high.[14] Results from four tests are reported herein. Silicone fluid, which is stable under the influence of temperature, was used in these tests; the level in the reservoir of the model was varied by pumping the fluid at desired rates. After a desired height was reached, the free surface was studied under a constant head until the surface was relatively stable. Then the fluid level was allowed to fall. Typical photographs taken during the experiments are shown in photos 1-4. Typical variations,

interpreted from photographic and manually obtained data, are plotted in figs. 9-12.

55. In the first test (fig. 9), the length of the rectangular plates (α = 90 deg) was about 190 cm, with an average width of gap of 0.2 cm. One-dimensional equations were used for this case. Three different plates with upstream slopes of 45, 30, and 18.5 deg (1:3), lengths of 300 cm, and an average gap width of 0.17 cm were used for the other three tests, figs. 10-12. The permeability of the model was computed from equation 17c, with the following values for the various quantities: ρ = 0.97 g/cm^3, g = 980 cm/sec^2, μ = 9.7 poises. The porosity of the model n was assumed as equal to unity.

Comparison and assessment of results

56. Typical experimental results for the four tests are plotted in figs. 9-12, in comparison with the numerical solutions. Each of these figures contains three typical plots: the first, during the rising water level; the second, at the steady-state condition; and the third, during the drawdown. The results from the linearized equations gave satisfactory comparison at earlier times but generally only in the regions in the vicinity of the entrance face. These results showed poor correlation with the experiments in the majority of the flow domain at higher time levels and for the fall (drawdown) conditions. Dvinoff[22] used the linearized equation and compared the numerical results with experiments from two viscous-flow models with upstream slopes of 45 deg and 22.5 deg and lengths equal to 24 in. and 30 in., respectively. The linearized solutions gave satisfactory comparison in the flow zones in the vicinity of the entrance face. In a previous study,[2] closed-form analytical solutions for the linearized equation were compared with experiments from models with upstream slopes of 90, 45, and 22.5 deg and with similar lengths. Satisfactory comparisons were obtained in the vicinity of the entrance face, but the two results showed significant differences in other regions of the flow domain.

57. In the case of long riverbanks and embankments, it is desirable that the solutions be satisfactory for the entire flow domain. Particularly, the designer is interested in seepage forces near both the

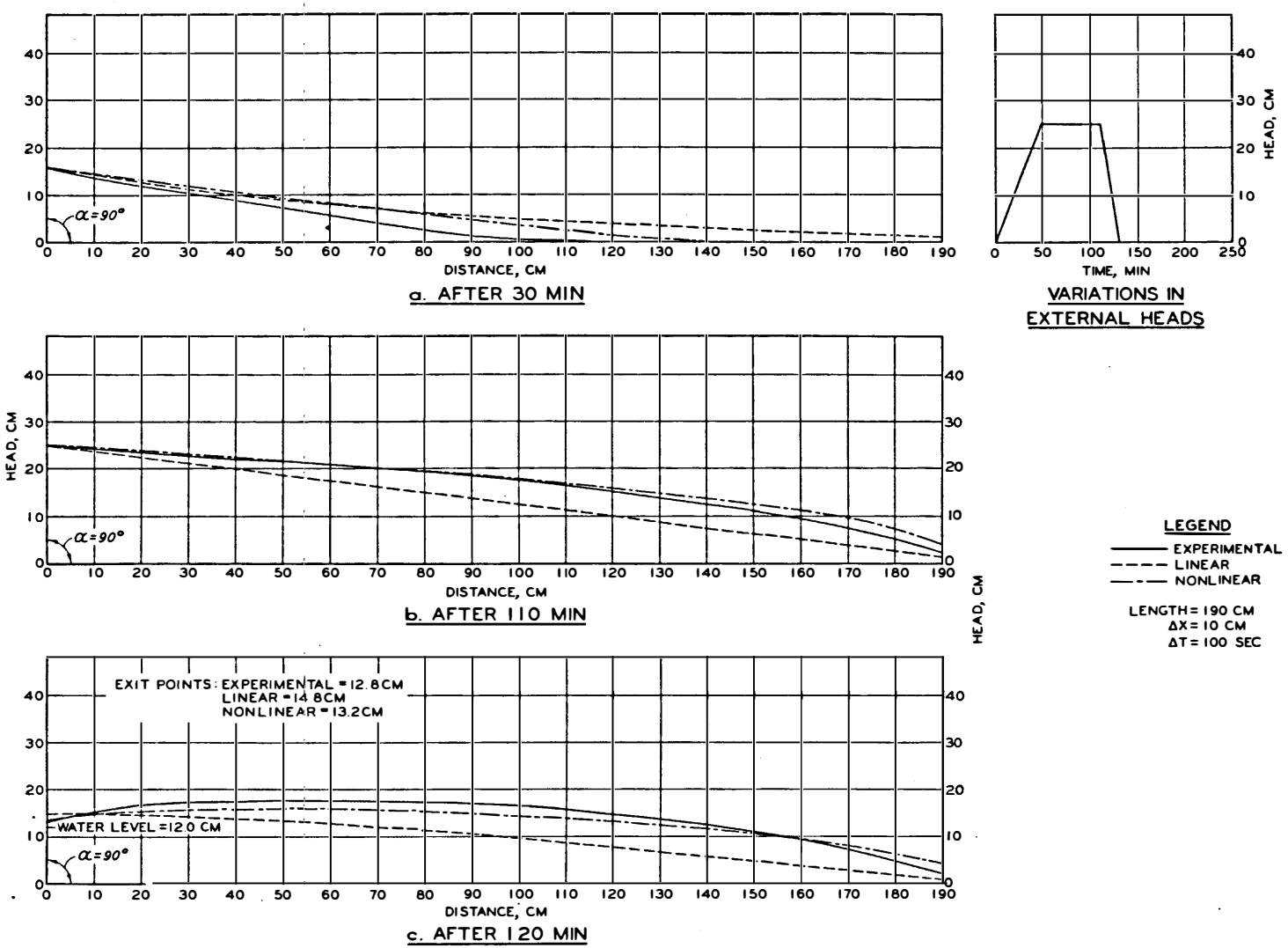

Fig. 9. Free surface at various times: α = 90 deg

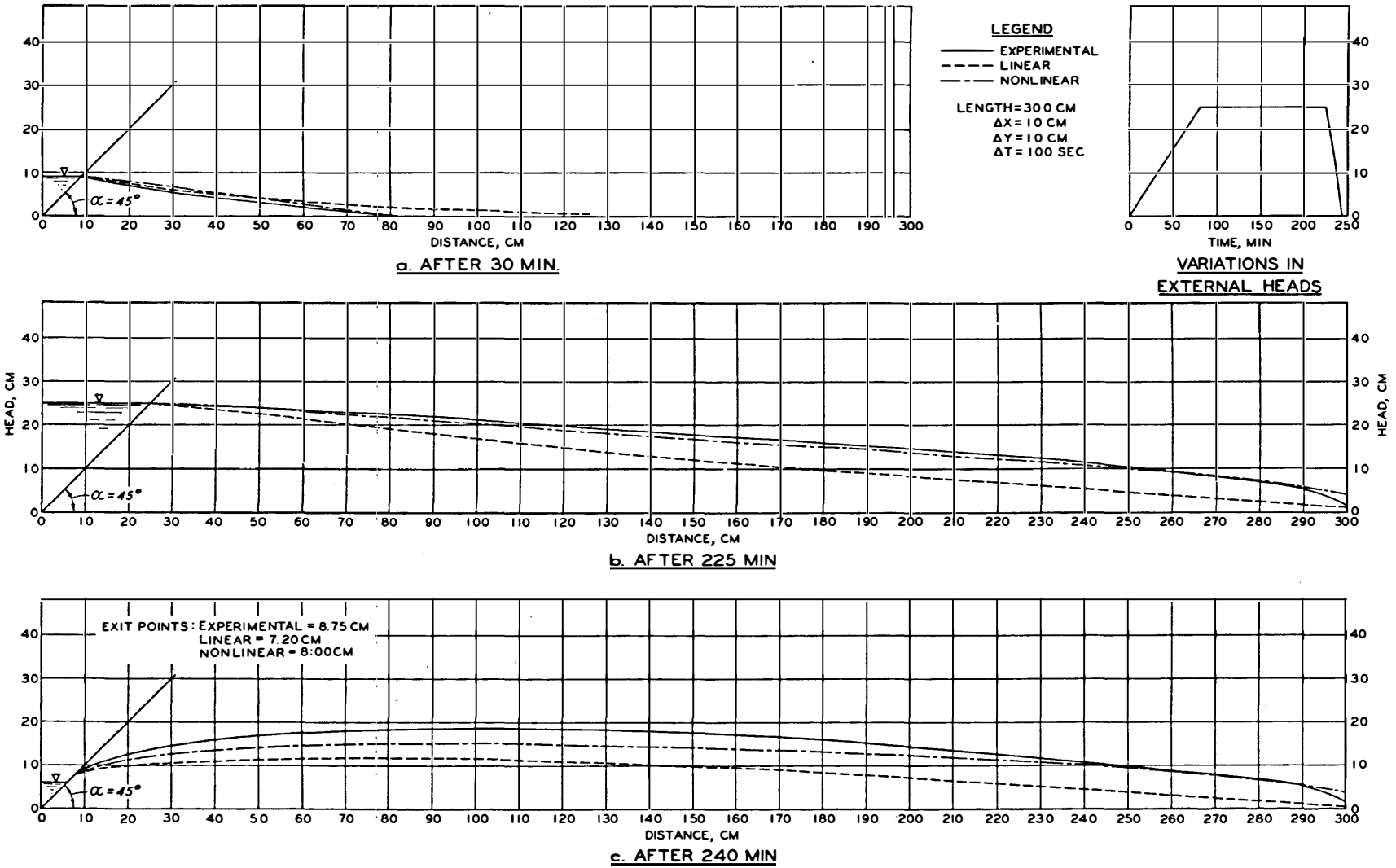

Fig. 10. Free surface at various times: α = 45 deg

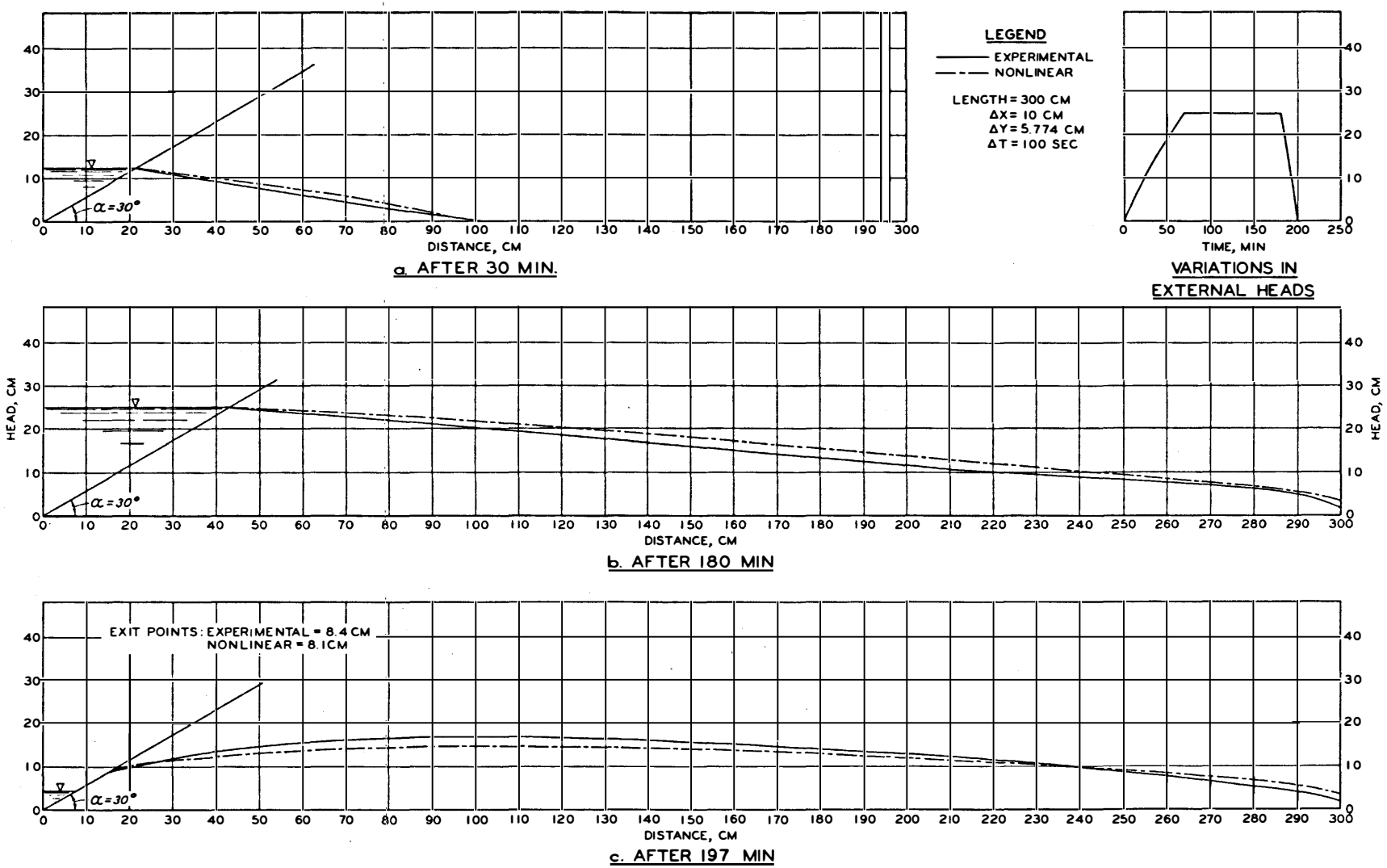

Fig. 11. Free surface at various times: α = 30 deg

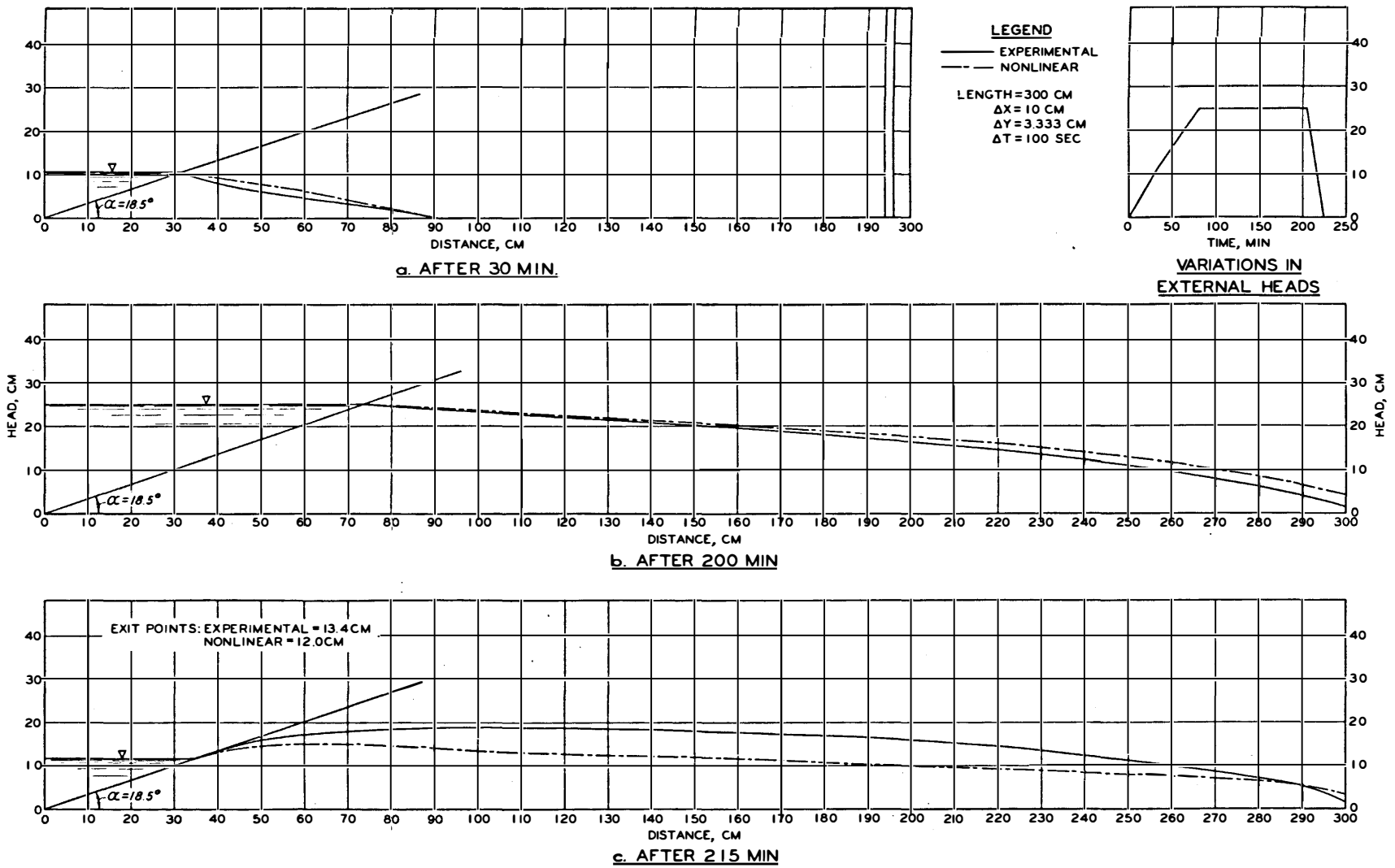

Fig. 12. Free surface at various times: α = 18.5 deg (1:3)

entrance and the exit faces. The nonlinear form of the equation used in this report showed improved agreement with the experiments for the entire flow domain and for all times. The main reasons for the improvements compared with the linearized solutions may be due to the higher order nature of the head distributions inherent in the nonlinear solution[5] and the reduced influence of the impervious boundary.[14]

58. Figs. 9 and 10 for $\alpha = 90$ and $\alpha = 45$ deg, respectively, are plotted to show comparisons between nonlinear and linearized solutions and the experimental results. Since the nonlinear solutions were found to be better, figs. 11 and 12 for $\alpha = 30$ and 18.5 deg slopes are plotted to show only the nonlinear and the experimental results.

Numerical discretization and
its effects on the solutions

59. The finite difference mesh size for the results reported in figs. 9-12 was $\Delta x = 10$ cm, $\Delta y = \Delta x \tan \alpha$, and $\Delta t = 100$ sec. The extent of the vertical domain included as a flow region was determined on the basis of the magnitudes of the head h developed in the flow domain. When the computed h at a node point was very small, the cycle of analysis was terminated, and the next cycle was started. The heads became negligible at a distance from the base of approximately four to six times the maximum head in the reservoir.

60. A Time-Sharing system connected to a GE 400 computer system was used for all computations reported herein. The numerical solutions gained accuracy as the time interval was reduced. For example, for the same Δx and Δy, the solution gained about 5 to 10 percent accuracy with a reduction in Δt from 100 to 50 sec. For $\Delta t = 10$ sec, the numerical solution gained further accuracy and showed very close agreement with the experiments. The computation time, however, increased with a decreasing Δt. For instance, the computation times for $\Delta t = 100$, 50, and 10 sec for the same $\Delta x = 10$ cm were in approximate ratios of 1:2:10. The approximate time for computing the free surface for six time levels, for $\Delta x = 10$ cm and $\Delta t = 100$ sec, was 30 sec. No significant increase in accuracy was observed for a decrease in the spatial subdivision, and it required much higher computer times. Often the

results from finer space subdivisions became less accurate. For instance, $\Delta x = 2.5$ cm and $\Delta t = 50$ sec were attempted, but these values required so long a time in the Time-Sharing system that the computations were terminated. Plots of comparison between various discretization schemes and experiments for $\alpha = 90$ deg and for two typical times are shown in fig. 13.

61. The numerical results described in this report were for $\Delta x = 10$ cm, $\Delta y = \Delta x \tan \alpha$, and $\Delta t = 100$ sec. It should be noted that these numerical results can be considerably improved by reducing the size of the time interval and that such a reduction is recommended for field applications, which will necessitate use of a larger computer device.

Nonhomogeneous Media

62. Soils usually occur as nonhomogeneous materials. A soil medium can consist of different layers of soils separated by vertical, horizontal, or inclined interfaces. It can also contain pockets of different materials. The latter possibility was not considered in these analyses. Consideration of a highly nonhomogeneous system can be accomplished by obtaining statistical values of the soil parameters. Only the general case of an inclined interface is considered to derive modified finite difference equations. Fig. 14 shows an inclined interface between two soils with different permeabilities. For convenience, an inclined interface is treated as a combination of horizontal and vertical interfaces.[14,22,35]

Vertical interface v-v

63. As shown in fig. 14, the vertical interface v-v can occur either to the left or to the right of the node point (i,j). Linear head variation is assumed between nodes (i - 1,j), (i,j), and (i + 1,j). It is necessary, as a numerical expedient, to establish a fictitious head h^* that represents head at node points (i - 1,j), fig. 14b, or (i + 1,j), fig. 14c, as if soil 2 and soil 1 were extending, respectively, into soil 1 and soil 2. An expression for h^* can then be

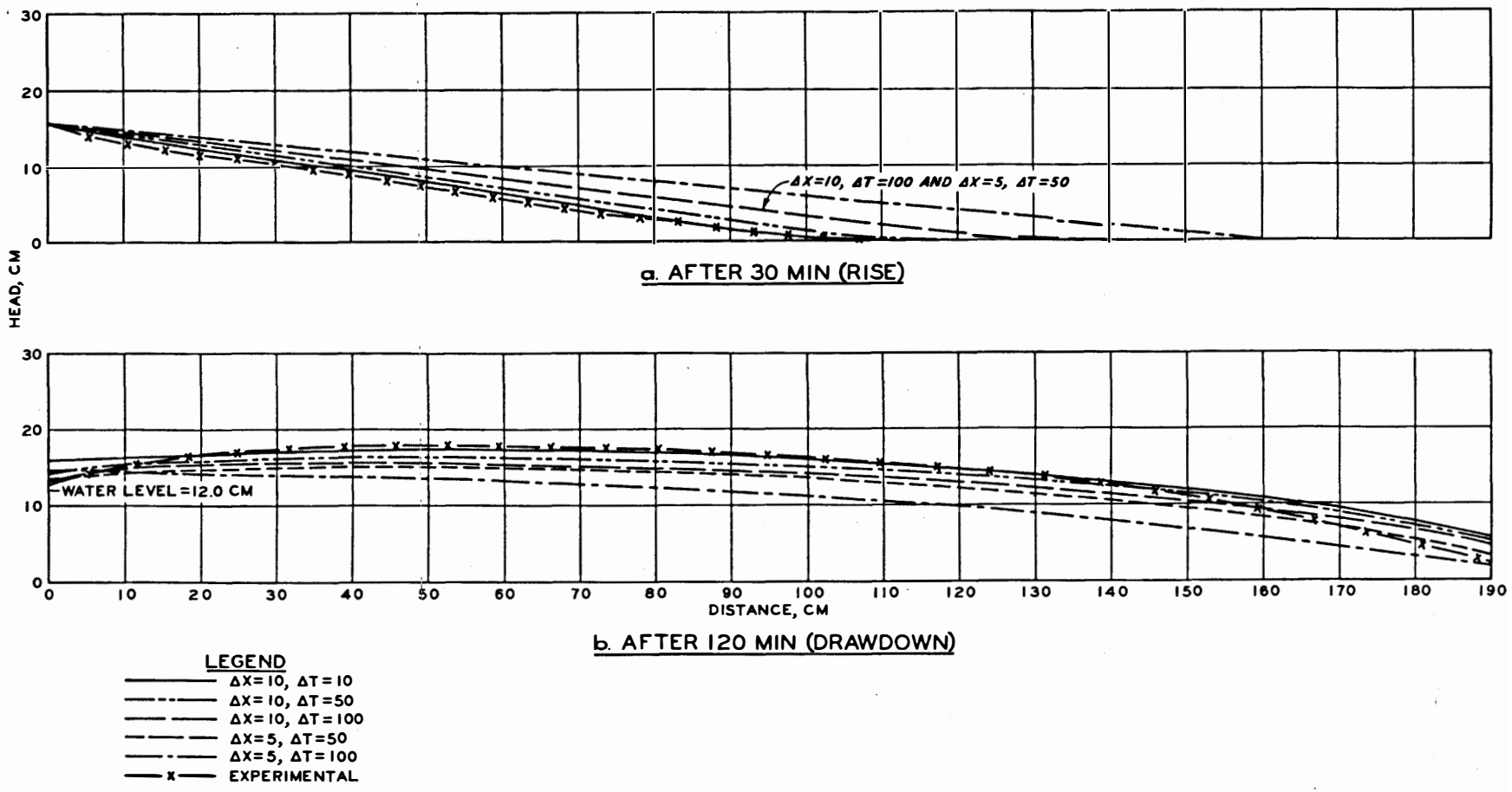

Fig. 13. Effect of discretization on numerical solutions

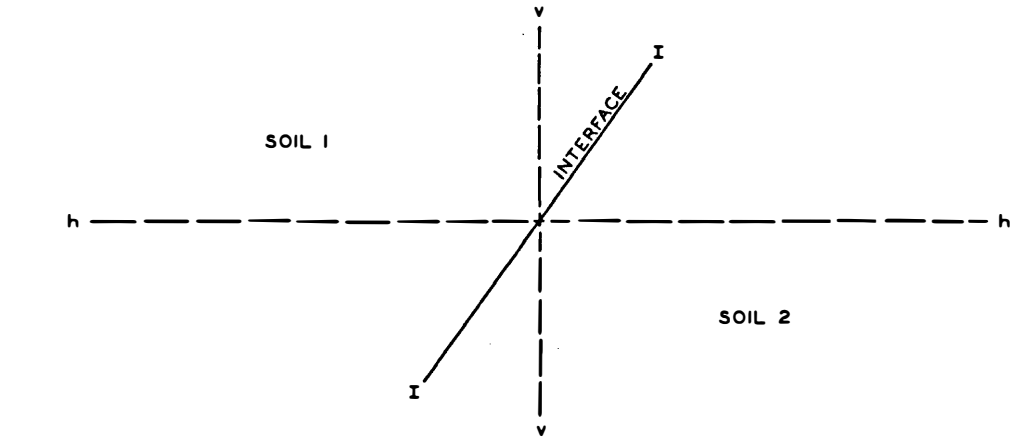

a. INCLINED INTERFACE

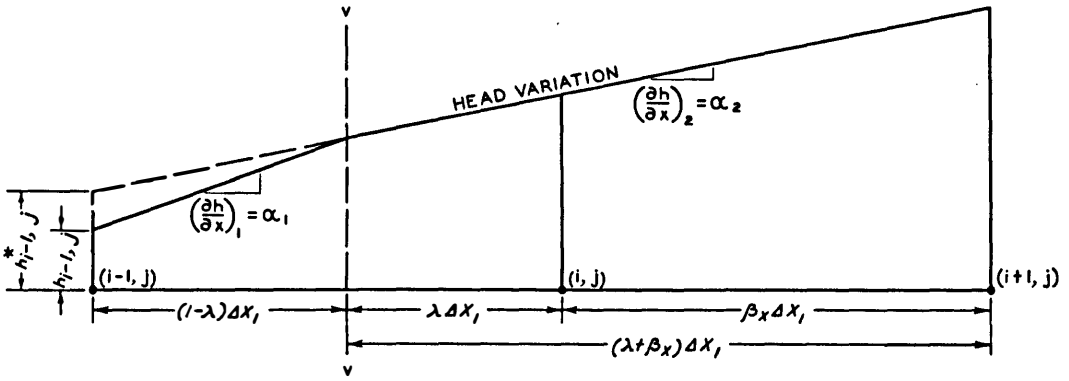

b. V-V TO LEFT OF (i, j)

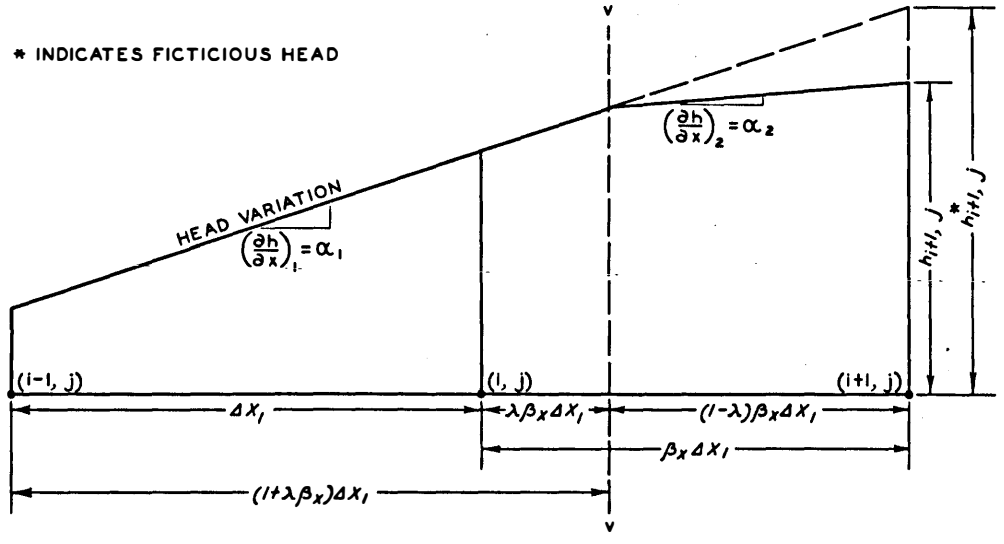

c. V-V TO RIGHT OF (i, j)

Fig. 14. Nonhomogeneous material

substituted into the ADEP scheme as if the soils were homogeneous at the interface.

64. For a v-v to the left of (i,j), fig. 14b, continuity of flow across v-v gives

$$k_{x1}\alpha_1 = k_{x2}\alpha_2 \tag{27}$$

where $\alpha_1 = (\partial h/\partial x)_1$ and $\alpha_2 = (\partial h/\partial x)_2$. Also, from the linear head variation (the time subscript is dropped for convenience),

$$\alpha_1(1 - \lambda)\Delta x_1 + \alpha_2(\lambda + \beta_x)\Delta x_1 = h_{i+1,j} - h_{i-1,j} \tag{28}$$

Substitution of equation 27 into equation 28 gives

$$\alpha_1 = (h_{i+1,j} - h_{i-1,j}) \times \frac{1}{\Delta x_1\left[(1 - \lambda) + k_{rx}(\lambda + \beta_x)\right]} \tag{29}$$

where $k_{rx} = k_{x1}/k_{x2}$. Now,

$$h^*_{i-1,j} = h_{i-1,j} + (\alpha_1 - \alpha_2)(1 - \lambda)\Delta x_1 \tag{30}$$

Substituting for α_1 and α_2, equation 30 becomes

$$h^*_{i-1,j} = h_{i-1,j} + (h_{i+1,j} - h_{i-1,j})\gamma_{x1} \tag{31}$$

where $\gamma_{x1} = \left[(1 - k_{rx})(1 - \lambda)\right]\Big/\left[(1- \lambda) + k_{rx}(\lambda + \beta_x)\right]$. In a similar manner, for v-v to the right of (i,j), fig. 14c, the fictitious head is

$$h^*_{i+1,j} = h_{i+1,j} + (h_{i+1,j} - h_{i-1,j})\gamma_{x2} \tag{32}$$

where $\gamma_{x2} = \left[(1 - k_{rx})(1 -\lambda)\right]\Big/\left[(1 + \lambda\beta_x) + k_{rx}(1 - \lambda)\beta_x\right]$.

Horizontal interface h-h

65. Following a similar procedure for the horizontal interface h-h above and below the node point (i,j), the fictitious heads are, respectively,

$$h^*_{i,j-1} = h_{i,j-1} + (h_{i,j+1} - h_{i,j-1})\gamma_{y1} \tag{33}$$

and

$$h^*_{i,j+1} = h_{i,j+1} + (h_{i,j+1} - h_{i,j-1})\gamma_{y2} \tag{34}$$

where

$$\gamma_{y1} = \frac{(1 - k_{ry})(1 - \lambda)}{(1 - \lambda) + k_{ry}(\lambda + \beta_y)}$$

$$\gamma_{y2} = \frac{(1 - k_{ry})(1 - \lambda)}{(1 + \lambda\beta_y) + k_{ry}(1 - \lambda)\beta_y}$$

and

$$k_{ry} = \frac{k_{y1}}{k_{y2}}$$

66. The expressions for h* can now be substituted in the ADEP scheme (equations 20-22) to account for an interface between two materials.

Comments

67. The finite difference procedure developed herein could provide satisfactory and economical solutions for the transient, unconfined fluid flow in porous, anisotropic, and nonhomogeneous media. The solutions are straightforward for simple geometries and material variations but may become cumbersome for complex geometries and severe nonhomogeneities.

PART IV: THE FINITE ELEMENT APPROACH

68. The second phase of the numerical solutions for the seepage problem constituted development of the finite element procedures. A general, two-dimensional finite element solution presented later in this report can be used for fluid flow in porous media, idealized as both one- and two-dimensional. However, a finite element formulation based on a governing equation directly representing one-dimensional flow can yield simplified and economical solutions. Such an approximate solution is developed in this part of the report, and the results therefrom are compared with experimental results from the viscous-flow model with rectangular entrance face.

One-Dimensional Seepage

69. Certain situations involving flow of fluids through porous media can be approximated as one-dimensional. Some examples of engineering interest are flow in and out of earthen banks with vertical faces, such as in the case of long, parallel drains or ditches, quay walls, and sheet-pile walls. In this part of the report, attention is directed toward a simplified and approximate finite element solution of a linearized equation governing such one-dimensional transient fluid flow. Both rise and drawdown in the external water level are considered. The case of sudden or gradual drawdown conditions is solved by an indirect scheme. This scheme is based on Pavlovsky's method of fragments described in Part III.

70. Since this approach requires only one-dimensional elements, it would provide significant savings in the formulation of and computational efforts for the above class of problems, compared with numerical solutions for such problems based on two- and three-dimensional idealizations. Moreover, it is somewhat difficult to establish a changing finite elements mesh for a rising phreatic surface for two- and three-dimensional solutions[36-39] when the external water level rises at a given rate. The approximate solutions presented could avoid such a

difficulty for the problems idealized as one-dimensional. The economy and the usefulness of the procedure for approximate solutions are illustrated by obtaining an example of satisfactory comparison with experimental solutions for free-surface flow in and out of the rectangular, parallel-plate, viscous-flow model, simulating a vertical bank subjected to rise and fall (gradual drawdown) in the external water level. An additional use of the procedure for seepage analysis in parallel drains or ditches under sudden drawdown conditions is given in reference 37.

71. The effects on the solutions of the proposed procedure of spatial and temporal discretizations were examined. Consideration was given to material nonhomogeneities introduced by vertical separations in the one-dimensional medium. Effects on the solution of higher order approximating models were also briefly examined.

Finite element formulation

72. Flow through a porous medium with vertical faces (α = 90 deg, fig. 6) is assumed to be one-dimensional. As stated in Part III, this idealization is based on such simplifications as the Dupuit assumption and Darcy's law. A linearized version of the equation governing such flow is given by equation 17b as

$$k_x \bar{h}(t) \frac{\partial^2 h}{\partial x^2} = n \frac{\partial h}{\partial t} \qquad \text{(17b bis)}$$

where

h = fluid head

k_x = permeability in x direction

n = porosity

t = the space and time coordinates

$\bar{h}(t)$ = the mean external fluid head given by

$$\bar{h}(o,t) = \frac{h(o,t) + h(o,t + \Delta t)}{2} \qquad (35)$$

in which Δt denotes the time increment. The boundary conditions are

$$h = \bar{h}(x,t) \text{ prescribed on boundary } S_1 \qquad (36a)$$

$$k_x \frac{\partial h}{\partial x} = \bar{q}(x,t) \quad \text{prescribed on boundary} \quad S_2 \tag{36b}$$

and the initial conditions are

$$h = h_o(x,o) \quad \text{in the domain} \quad D \tag{36c}$$

Formulation by the
Galerkin residual method

73. The Galerkin method of weighted residuals is used to derive the finite element equations.[36,37,40-42] The approximating function for h is written as

$$h(x,t) = \sum_{j=1}^{r} N_j(x) h_j(t) \tag{37}$$

where

N_j = interpolating functions for the finite elements, which vanish elsewhere in the domain D

h_j = nodal values of h in the subdivided domain

r = number of degrees of freedom

74. The Galerkin method requires that the weighted averages of the residual R over the domain should vanish. By using the interpolating functions N_j as the weighting functions, this method yields

$$\int_D R N_m \, dD = 0 \; ; \quad m = 1, 2, \ldots r \tag{38a}$$

For equation 17b, the residual R is

$$R = \left[\lambda(t) \frac{\partial^2}{\partial x^2} - n \frac{\partial}{\partial t}\right] \sum_1^r N_j h_j \tag{38b}$$

where $\lambda(t) = k_x \bar{h}(o,t)$. Hence,

$$\int_D \left[\lambda(t) \frac{\partial^2}{\partial x^2} - n \frac{\partial}{\partial t}\right] \sum_1^r (N_j h_j) N_m \, dD = 0 \tag{38c}$$

which will yield r equations for r unknowns. By applying Green's theorem, equation 38c can be modified to

$$\int_D \left[\lambda(t)\,\frac{\partial N_m}{\partial x}\sum_1^r \frac{\partial N_j}{\partial x}\right]h_j\,dD + \int_D nN_m \sum_1^r N_j \dot{h}_j\,dD - \int_{S_2} N_m\left(k_x \sum_1^r \frac{\partial N_j}{\partial x}\,\ell_x\right)h_j\,dS = 0 \qquad (39)$$

in which ℓ_x = direction cosine of the normal to the boundary and the overdot denotes the derivative with respect to time. Equation 39 leads to a system of equations than can be expressed as

$$\left[K\right]\left\{h\right\} + \left[P\right]\left\{\dot{h}\right\} = \left\{R\right\} \qquad (40a)$$

where

$$K_{mi} = \sum \int_E \left[\lambda(t)\,\frac{\partial N_m}{\partial x} \times \frac{\partial N_j}{\partial x}\right]dx \qquad (40b)$$

$$P_{mi} = \sum \int_E nN_m N_j\,dx \qquad (40c)$$

and

$$R_m = -\sum \int_E N_m \bar{q}\,dS \qquad (40d)$$

Here, $\left[K\right]$, $\left[P\right]$, and $\left\{R\right\}$ can be called permeability matrix, porosity matrix, and forcing parameter vector, respectively; E denotes an element; and the summation is carried for all elements in the domain.

Approximating models

75. The linear-, quadratic-, and cubic-interpolating function

models (fig. 15) used in the study are, respectively,

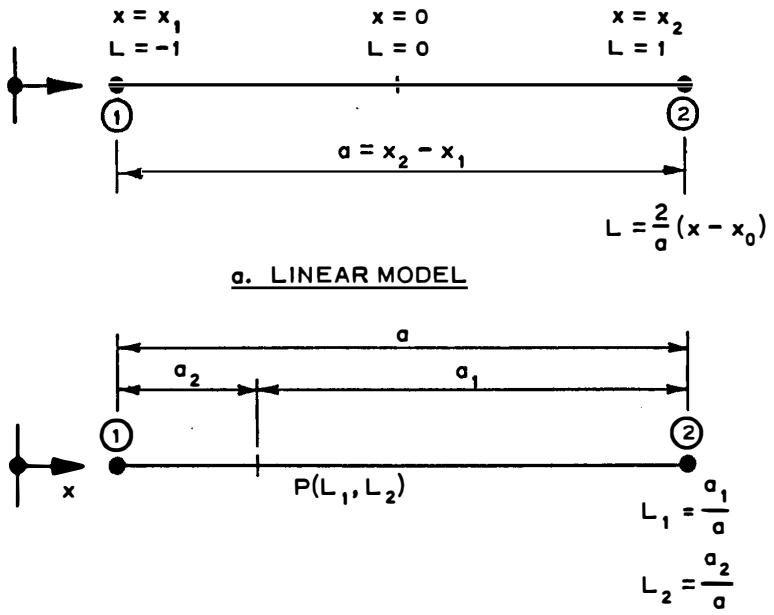

Fig. 15. One-dimensional finite elements and local coordinate systems

$$h = \left[\frac{1}{2}(1 - L) \quad \frac{1}{2}(1 + L)\right] \begin{Bmatrix} h_1 \\ h_2 \end{Bmatrix} \tag{41a}$$

$$h = \left[\frac{1}{2}L(L - 1) \quad \frac{1}{2}L(L + 1) \quad (1 - L^2)\right] \begin{Bmatrix} h_1 \\ h_2 \\ h_o \end{Bmatrix} \tag{41b}$$

where h_o = head at the internal node, and

$$h = \left[L_1^2(3 - 2L_1) \quad L_1^2L_2a \quad L_2^2(3 - 2L_2) \quad -L_1L_2^2a\right] \begin{Bmatrix} h_1 \\ \theta_1 \\ h_2 \\ \theta_2 \end{Bmatrix} \tag{41c}$$

where θ = gradient of h .

76. Integration in time. Initial heads $h(x,o)$ are prescribed; hence, equation 40a can be expressed by a finite difference integration

scheme for solution at the subsequent time level Δt and so on. The following difference scheme is employed herein.[37,42,43]

$$[K]\left\{h_{t-(\Delta t/2)}\right\} + [P]\left(\frac{\left\{h_t\right\} - \left\{h_t\right\}}{\Delta t}\right) = \left\{R_t\right\} \qquad (42a)$$

where $\left\{h_{t-(\Delta t/2)}\right\} = \left\{h_t\right\} + \left\{h_{t-\Delta t}\right\}/2$. Finally, equation 40 reduces to

$$\left([K] + \frac{2[P]}{\Delta t}\right)\left\{h_{t-(\Delta t/2)}\right\} = \left\{R_t\right\} + \frac{2[P]}{\Delta t}\left\{h_{t-\Delta t}\right\} \qquad (42b)$$

77. Rise in external heads. Values of the fluid head at the nodal points are obtained by a straightforward application of equation 42b, with prescribed heads at the nodes at $x = o$ and at $x = \ell$. For impervious plane or plane of symmetry at $x = \ell$, the natural boundary condition of $\partial h/\partial x = 0$ is automatically satisfied. Equation 42b is also applicable for periods beyond the time by which the maximum head, point B (fig. 16), is reached and until the steady-state condition is approached, point C. The steady state is assumed to have been approached when the phreatic surface does not change appreciably.

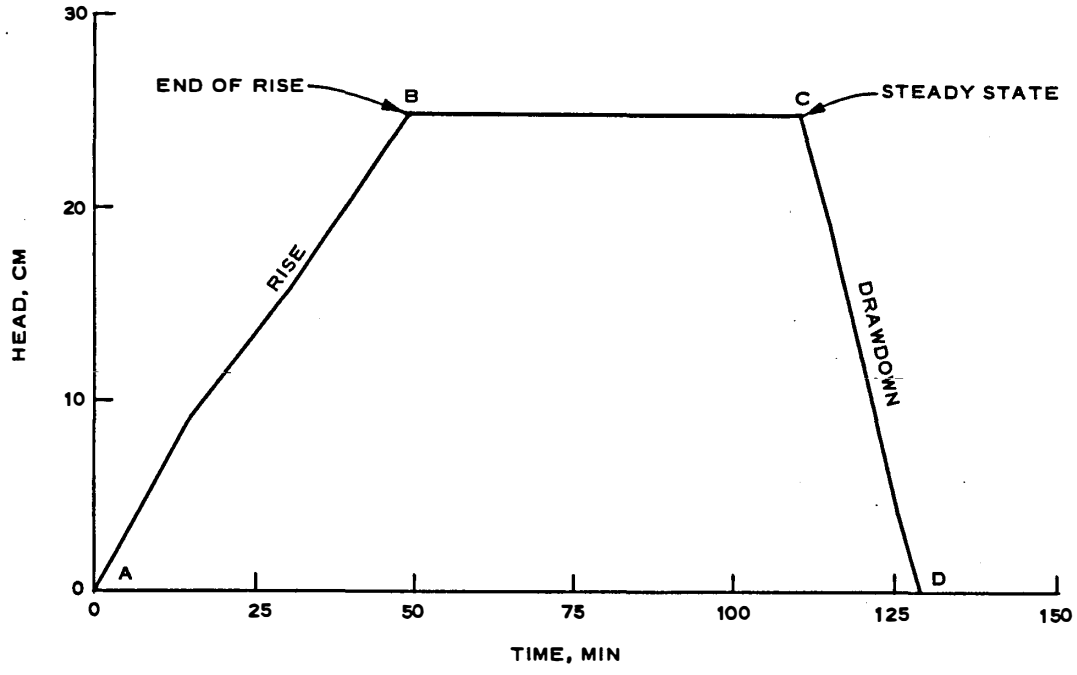

Fig. 16. Variations in external heads

78. Drawdown (fall) of external fluid level. During drawdown conditions, the free surface lags behind the level of water in the reservoir (fig. 8b). Consequently, the applied entrance head at any time should be modified to account for the surface of seepage A-E and the exit head $h_e(t + \Delta t)$. In this study, the entrance boundary nodal head is adopted as equal to $h_e(t + \Delta t)$. Determination of the exit point E requires a special procedure in addition to the solution of equation 42b. Such a procedure is introduced as an iterative scheme that is based on Pavlovsky's method of fragments, described in Part III, equation 24.

Applications

79. A computer code was prepared on the basis of the foregoing finite element formulation. For the results reported herein, the linear approximating model, equation 41a, was used. The example problem described below was solved by using the code.

80. Description of example. The example represents the transient flow in a viscous-flow model with linear rise and gradual linear drawdown. As described in Part III, a number of experiments were conducted with the parallel-plate, viscous-flow model at the WES. For the one-dimensional case, the experimental results with the vertical-face model were adopted. The average gap between the parallel plates was about 0.20 cm. The permeability of the model k_m was computed by using the equation

$$k_m = \frac{b^2 \rho g}{3\mu} \qquad \text{(17c bis)}$$

where

ρ = density of the fluid (0.97 g/cm^3)

g = gravitational constant (980 cm/sec^2)

μ = viscosity of the fluid (9.7 poises)

b = half width of gap (0.1 cm)

These values yield k_m = 0.323 cm/sec. A value of $n = 1$ was adopted for the model. The position of the free surface at various time levels was recorded photographically.

81. Figs. 17 and 18 compare the experimental results and the

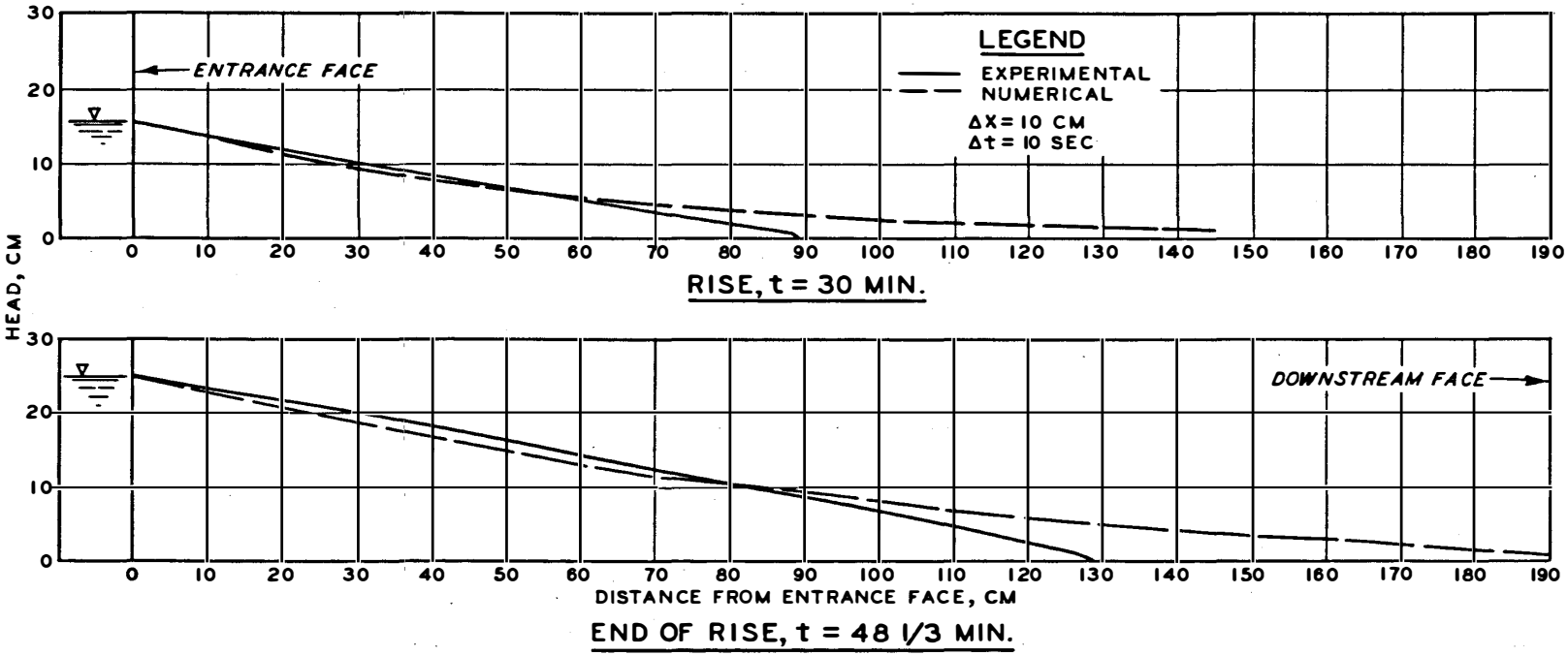

Fig. 17. Comparisons between numerical and experimental results for rise

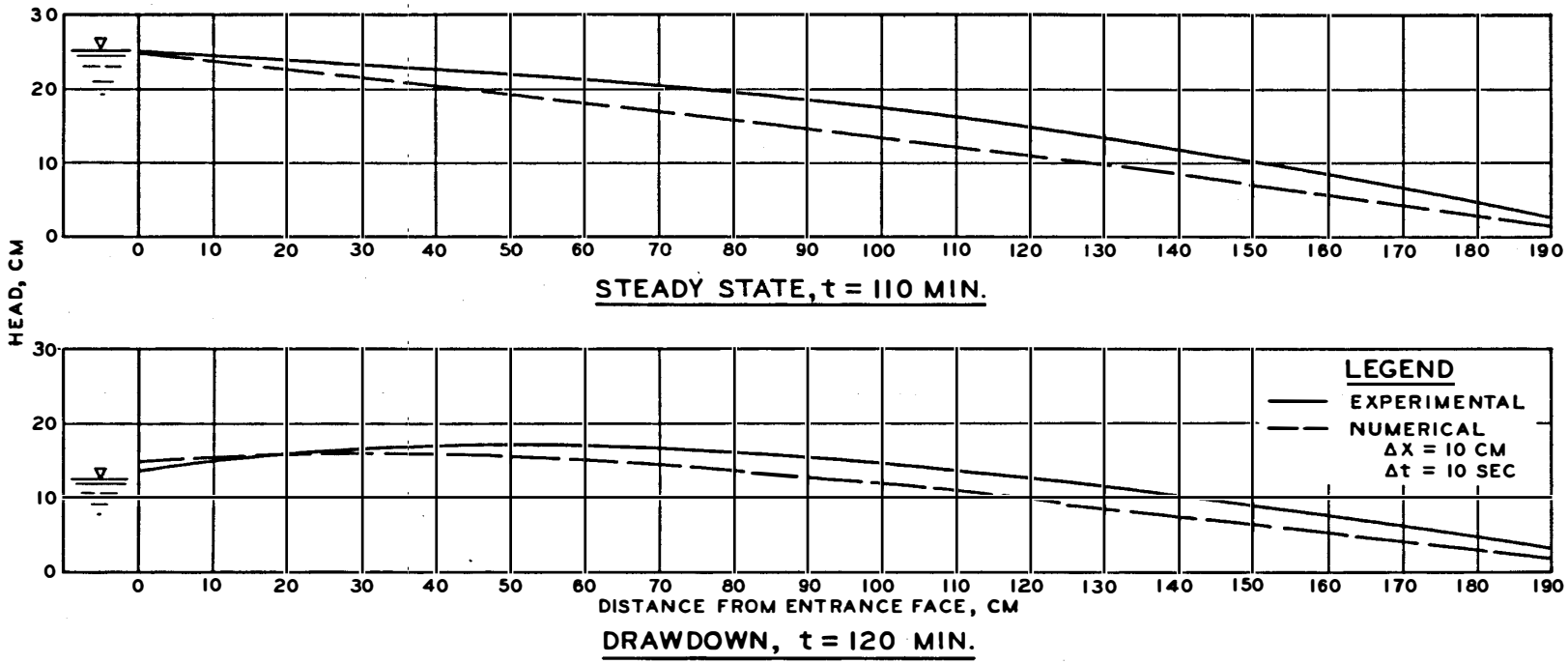

Fig. 18. Comparisons between numerical and experimental results at steady and drawdown states

numerical solutions at various time levels during rise, steady-state, and drawdown conditions. Time levels of 30 and 48-1/3 min represent typical times during rise. Time level of 110 min denotes a steady-state condition; 120 min is a typical time during drawdown. The results for both rise and drawdown conditions show good agreement near the entrance face. The agreement away from the entrance is fair. The discrepancy may be due to the linearization of the governing equation. Such experimental sources of errors as nonuniform gap between the plates, leakage of fluid, friction at the base, some variations in the properties of the fluid, and capillary effects may also have contributed to the discrepancy.

82. Since the variation in head at the downstream end was very small, the iterative scheme for locating the exit point was not used for that end. Instead, linear head variation was assumed between an inside node distance a from the downstream face and a zero head at a node distance a outside that face.

83. Details of computer analysis. The solution was programmed on the General Electric 430 Time-Sharing system. The equation set was obtained in the form of a banded matrix and was solved by using the symmetric Gauss-Doolittle procedure. Twenty elements, each with a length $a = 10$ cm, were used. The time increment $\Delta t = 10$ sec was used for the results reported in figs. 17 and 18. Computations for each time increment, including the iterative scheme for locating the exit point, took about 0.30 sec on the Time-Sharing system.

84. General use. The formulation developed herein can be applied to such other problems as flow toward sheet-pile walls and parallel drains or ditches.[37]

Analysis of factors affecting the solution

85. Improvement of accuracy. A quadratic field variable model, equation 41b, with an internal node in the element in fig. 15 was used. This model was found to affect the numerical solution only to a small extent. A cubic model, equation 41c, was also tried. This model included the gradients of the heads at the nodes as unknowns in addition

to the nodal heads. Thus, there were four unknowns per element. The solutions from the cubic model formulation improved the solution to a small extent. It seems that, due to the linearization and the Dupuit assumption, increasing the order of the field variable model does not improve the solution to a great extent.

86. Spatial and temporal discretizations. Three different meshes, Δx = 20, 10, and 5 cm , were adopted with time intervals of Δt = 100, 10, and 5 sec in order to examine their effects on the solutions for the foregoing problem. It was found, as in the case of the finite difference method, that with the present formulation and the linear model no significant improvements occurred by refining the spatial mesh. However, refining the timewise mesh did improve the solutions. Typical results for Δx = 10 cm and Δt = 100 and 5 sec are shown in fig. 19 in comparison with the test results. The results for Δt = 10 sec lie in between the results for Δt = 100 and 5 sec.

87. Nonhomogeneous materials. Any number of material properties can be incorporated if they happen as nonhomogeneities introduced by vertical interfaces. A typical result for the free surface with three different permeabilities is shown in fig. 20. Distinct changes occur in the free surface with the changes in material properties.

Comments

88. The solution described herein is intended for a special class of problems and is based on an approximate linearized version of the flow equation. The solutions obtained are approximate; however, it is believed that they could provide adequate accuracy for engineering solutions with considerable savings and simplifications in the computational and formulation efforts.

Two-Dimensional Seepage

89. Insofar as the stability of an earthen bank is concerned, the seepage forces induced during drawdown are more severe and critical than those induced by the rising river level. Hence, attention in this phase of the study was directed toward drawdown conditions. A finite element

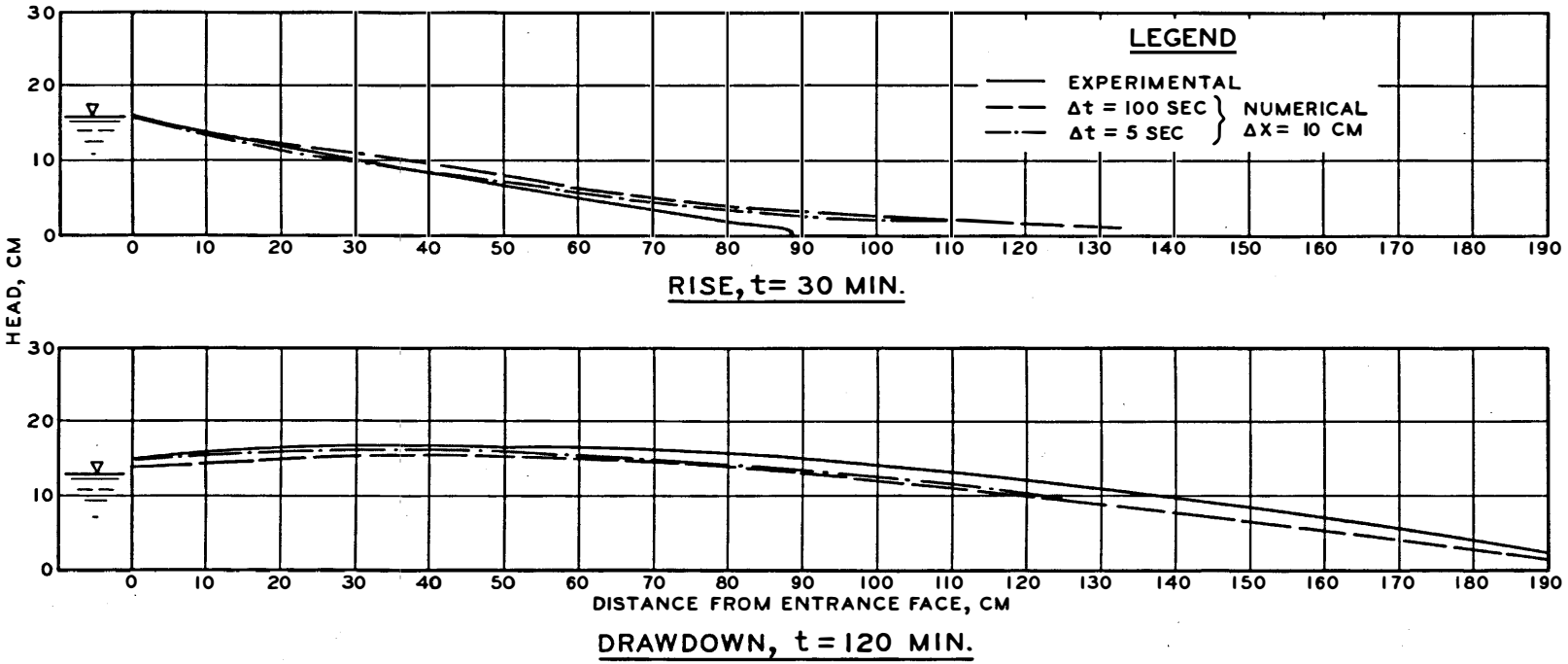

Fig. 19. Effects of timewise discretization on numerical solutions

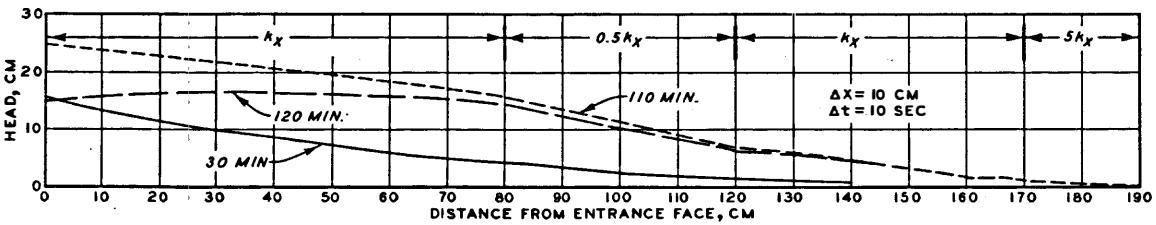

Fig. 20. Seepage in nonhomogeneous media

procedure was developed and applied to two-dimensional seepage during drawdown.

90. There are a number of publications available regarding application of the finite element method to various categories of seepage.[36-39,42,44-52] Only those works directly related to the category treated herein are referenced in further detail. Although the formulation developed is general, it was used for solution of free-surface seepage in long riverbanks (or dams) subjected to gradual drawdown conditions in the external water levels. This situation has significant applications for stability analyses and computations of fluid flow from banks and dams. Specifically, the procedure was used for seepage analyses in the pervious banks of the Mississippi River.

91. Three examples were solved by using the proposed finite element procedure. In the first example, the numerical solutions were compared with a typical result from laboratory experiments with the parallel-plate viscous-flow model. The second and the third examples involved actual field observations at two sections along the banks of the Mississippi River. The LMVD has installed a number of piezometer stations along the banks, and periodic readings of river stages and the corresponding piezometric heads are recorded. The field observations at the sections were compared with the solutions from the finite element method.

92. In dealing with an infinite medium such as a riverbank, the inherent nature of a numerical technique requires that only a significant portion of the infinite medium be included in the analysis as the discretized assemblage.[36] The selection of the significant portion requires adequate study and is influenced by various factors. Some criteria for discretization of such infinite media are suggested herein on the basis of the experimental observations and a number of numerical solutions.

Finite element formulation

93. Governing differential equation. The differential equation governing two-dimensional steady flow in a long riverbank or a dam, shown schematically in fig. 21, is expressed as

$$\frac{\partial}{\partial x}\left(k_x \frac{\partial \psi}{\partial x}\right) + \frac{\partial}{\partial y}\left(k_y \frac{\partial \psi}{\partial y}\right) = 0 \qquad (43)$$

where k_x and k_y = the coefficients of permeability in the x and y directions, respectively, and ψ = the total fluid head . Equation 43 is based on Darcy's law, expressed in matrix form as

$$\{v\} = -[R]\{g\} \qquad (44)$$

and on the fulfillment of the continuity conditions in the flow domain. In equation 44,

$\{v\}^T$ = the velocity vector $[v_x \; v_y]$

$[R]$ = the matrix of permeabilities = $\begin{bmatrix} k_x & 0 \\ 0 & k_y \end{bmatrix}$

$\{g\}^T$ = the vector of gradients $[(\partial\psi/\partial x) \; (\partial\psi/\partial y)]$

94. The boundary conditions associated with the free-surface flow, as shown in fig. 21, are

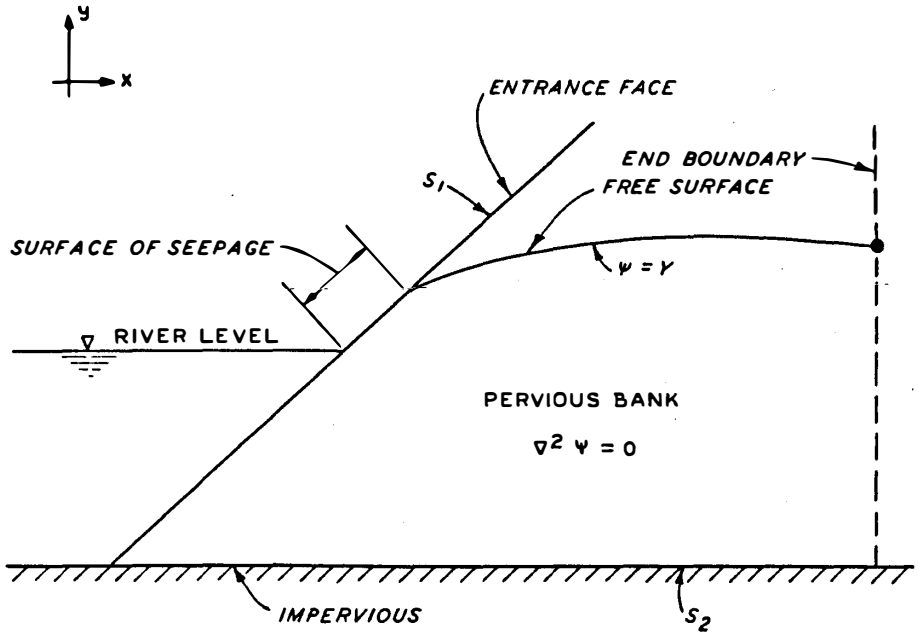

Fig. 21. Schematic representation of two-dimensional flow

$$\psi = \overline{\psi}(t) \quad \text{on} \quad S_1 \tag{45a}$$

$$k_x \frac{\partial \psi}{\partial x} \frac{\partial x}{\partial \eta} + k_y \frac{\partial \psi}{\partial y} \frac{\partial y}{\partial \eta} = \overline{Q} \quad \text{on} \quad S_2 \tag{45b}$$

and

$$\psi = Y(x,y,t) \tag{45c}$$

on the free surface and on the surface of seepage. Here, S_1 is that part (entrance face) of the boundary on which ψ is prescribed, S_2 is that part on which flow $\overline{Q}$ is prescribed, and Y represents the elevation head.

95. The variational function corresponding to governing equation 1 is[36,40-42]

$$A = \iiint_V \frac{1}{2} \left[k_x \left(\frac{\partial \psi}{\partial x} \right)^2 + k_y \left(\frac{\partial \psi}{\partial y} \right)^2 \right] dV \tag{46}$$

96. Finite element and field variable model. A four-node, isoparametric, quadrilateral element (fig. 22) was used.[36,51,53,54] The field variable model describing an approximate variation of ψ within the element is

$$\psi(s,t) = \left\{ N \right\}^T \left\{ q \right\} \tag{47a}$$

where

s,t = the natural coordinates of the element

$\left\{ N \right\}^T = \left[N_1 \; N_2 \; N_3 \; N_4 \right]$ is the vector (or matrix) of interpolation functions, and

$\left\{ q \right\}^T = \left[\psi_1 \; \psi_2 \; \psi_3 \; \psi_4 \right]$ is the vector of nodal heads

The values of N_i for the system shown in fig. 22 are

$$N_i = \frac{1}{4} (1 + ss_i)(1 + tt_i) \; ; \quad i = 1,2,3,4 \tag{47b}$$

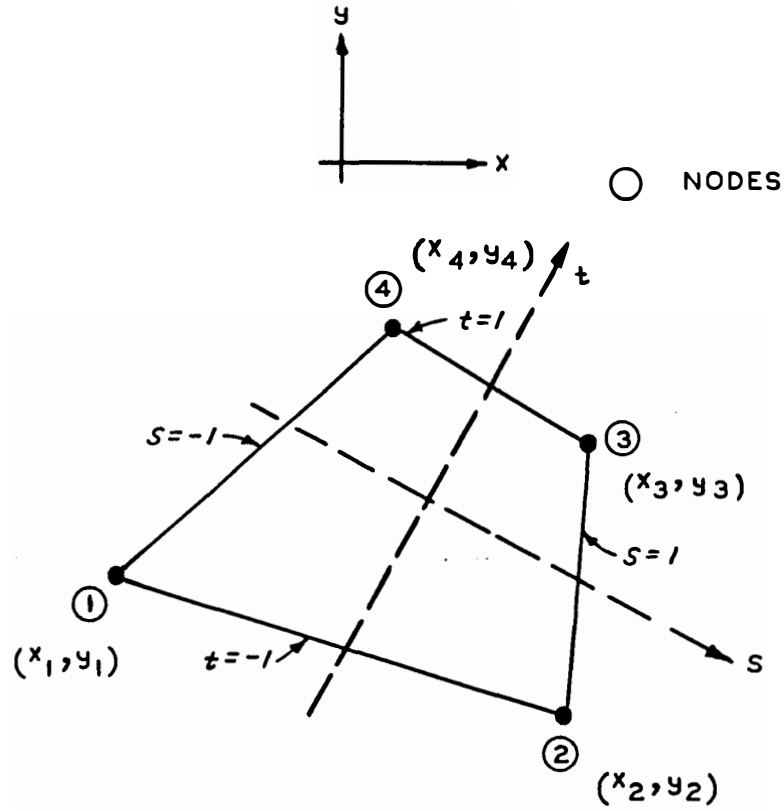

Fig. 22. Quadrilateral finite element

The coordinates x,y of the element are also expressed by using the same interpretation functions

$$\begin{Bmatrix} x \\ y \end{Bmatrix} = \begin{bmatrix} \{N\}^T & 0 \\ 0 & \{N\}^T \end{bmatrix} \begin{Bmatrix} x_n \\ y_n \end{Bmatrix} \tag{48}$$

where $\{x_n\}^T = [x_1\ x_2\ x_3\ x_4]$ and $\{y_n\}^T = [y_1\ y_2\ y_3\ y_4]$. The gradient vector can be computed from equation 47a as

$$\{g\} = \begin{Bmatrix} \frac{\partial \psi}{\partial x} \\ \frac{\partial \psi}{\partial y} \end{Bmatrix} = \left[[B_1][B_2][B_3][B_4] \right] \{q\} \tag{49a}$$

where the submatrices $[B_i]$ are given by

$$[B_i]^T = \begin{bmatrix} \frac{\partial N_i}{\partial x} & \frac{\partial N_i}{\partial y} \end{bmatrix} \tag{49b}$$

and

$$\begin{Bmatrix} \frac{\partial \psi}{\partial x} \\ \frac{\partial \psi}{\partial y} \end{Bmatrix} = \left[J\right]^{-1} \begin{Bmatrix} \frac{\partial \psi}{\partial s} \\ \frac{\partial \psi}{\partial t} \end{Bmatrix} \tag{49c}$$

in which $\left[J\right]$ is the Jacobian matrix.

97. Element equations. Substitution of equations 47-49 into equation 46 yields

$$A = \left\{q\right\}^T \iiint_V \left[B^T\right]\left[R\right]\left[B\right] \det\left(\left[J\right]\right)\left\{q\right\} ds\, dt \tag{50}$$

Extremization of A in equation 50 gives the element equations for steady-state seepage

$$\left[k\right]\left\{q\right\} = 0 \tag{51}$$

where $\left[k\right] = \iiint_V \left[B^T\right]\left[R\right]\left[B\right] \det\left(\left[J\right]\right) ds\, dt$, and is referred to as element permeability matrix, and $\left\{q\right\}$ = vector of element nodal heads. The assemblage equations are obtained by adding element equations, using the direct stiffness method. Such assemblage equations, after the introduction of boundary conditions such as $\psi = \bar{\psi}(t)$ (equation 45a), can be written as

$$\left[K\right]\left\{r\right\} = \left\{R\right\} \tag{52}$$

where

$\left[K\right]$ = assemblage permeability matrix

$\left\{r\right\}$ = assemblage nodal head vector

$\left\{R\right\}$ = assemblage nodal forcing parameter vector

Natural boundary conditions such as equation 45b are automatically satisfied in the variational formulation.

98. Determination of changing free surface. Under a small change in the external head (fig. 23), the free surface experiences corresponding movements. In the solution scheme, the transient problem is divided

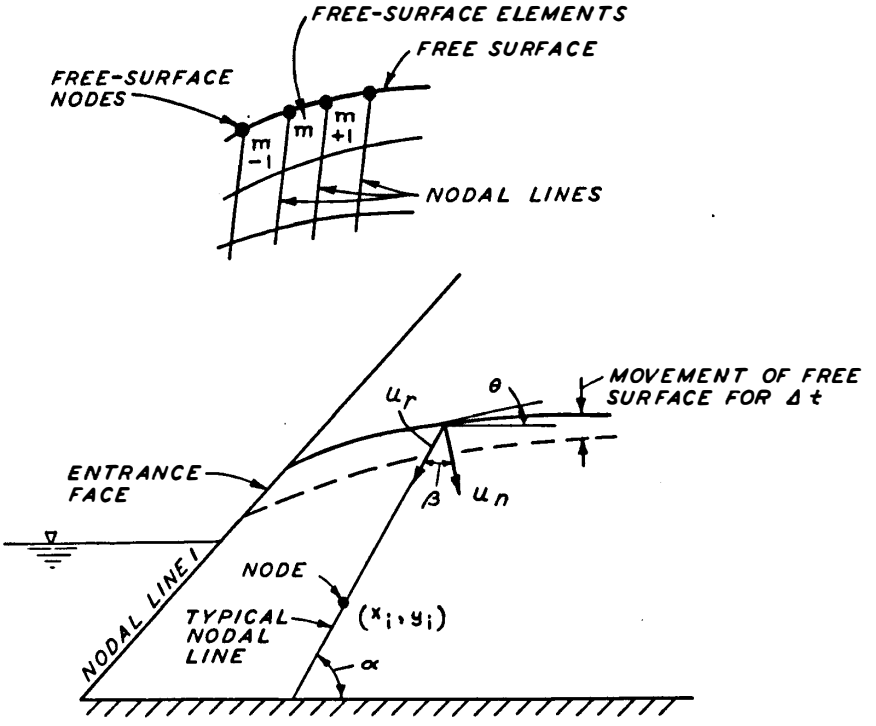

Fig. 23. Movement of free surface

into a number of steady-state problems, and equation 52 is solved to obtain values of nodal heads and velocities for a given time level. The domain of flow for such a solution is defined by the free surface at that time and by the impervious boundaries (fig. 21). Since the problem is actually transient, the conditions of null normal flow and velocity across the free surface are not satisfied. The nonzero values of the velocities at the nodes on the free surface are computed from the computed heads at the nodes of the elements along the free surface. The velocities are evaluated by using equation 44. Since the velocities thus computed are those based on Darcy's law, the actual particle velocities need to be computed.[39,51,52,55] The particle velocity vector $\{v_p\}$ is obtained as

$$\{v_p\} = \frac{1}{n}\{v\} \tag{53}$$

in which n = porosity of the medium. A similar procedure has also been recently reported by France et al.[39] for steady, unconfined, and sudden drawdown analyses.

99. The normal movements of the particles at the free-surface nodes are computed by multiplying the normal component of the velocity, equation 54 below, by a given time increment Δt . This permits evaluation of the new coordinates of the free-surface nodes. A new finite element mesh is thus generated by modifying the coordinates of the nodes in the flow domain. To facilitate such modifications, a number of nodal lines (fig. 23) are fixed by assigning angles α , which the lines subtend, with a bottom boundary. These lines retain their orientation during the drawdown. Further simplification is obtained by locating the nodes along a nodal line at equal vertical and horizontal distances. The following equations summarize the process of modification of the mesh:

$$\left.\begin{aligned} \bar{v}_x &= \frac{v_x^m + v_x^{m+1}}{2} \\ \bar{v}_y &= \frac{v_y^m + v_y^{m+1}}{2} \end{aligned}\right\} \text{ for all free-surface nodes except at entrance and end faces}$$

$$\bar{v}_x = v_x^m \quad \text{and} \quad \bar{v}_y = v_y^m \quad \text{at entrance and end faces}$$

$$v_n = \frac{(\bar{v}_x \sin\theta + \bar{v}_y \cos\theta)}{n} \qquad (54)$$

$$u_n = v_n \times \Delta t$$

$$u_r = \frac{u_n}{\cos\beta}, \quad \beta = \frac{\pi}{2} - \alpha + \theta$$

$$u_x = u_r \cos\alpha$$

$$u_y = u_r \sin\alpha$$

The revised coordinates are then computed as

$$\begin{aligned} x_i^j &= x_i^{j-1} + u_x \\ y_i^j &= y_i^{j-1} + u_y \end{aligned} \qquad (55)$$

where i denotes a nodal point and j denotes a time level. (Other symbols are explained in fig. 23.) Since the field variable model, equation 47a, yields discontinuous velocities at a node between two elements, an average of the velocities at that node is adopted for computing the foregoing movements (first two equations of equation 54). A number of iterations can be performed at each time increment in order to improve satisfaction of the conditions at the free surface (equation 45c).[36,45,46] If the time interval is small, one to three iterations are sufficient for an acceptable solution.

Applications

100. Example 1: Comparisons with laboratory tests. As described in Part II, a number of experiments were performed with a large, parallel-plate, viscous-flow model. A typical result for a slope angle equal to 45 deg is included herein. The approximate length and height of this model were 300 and 50 cm, respectively (fig. 24). The level of fluid in the reservoir in the model was raised at a certain rate, allowed to stabilize at 25-cm height of fluid, and then allowed to fall as shown in fig. 25a. Equivalent permeability of the model was computed by using

$$k_m = \frac{b^2 \rho g}{3\mu} \qquad \text{(17c bis)}$$

in which

b = half width of gap

ρ = the density of the fluid (0.97 g/cm^3)

g = the gravitation constant (980 cm/sec^2)

μ = viscosity of the fluid (9.7 poises)

The average value of b was found equal to 0.085 cm, which yields k_m = 0.236 cm/sec. A value of unity was adopted for the porosity n of the model.

101. Equivalent field permeability. Details of derivation of the procedure for computing the field permeability equivalent to a given model dimensions and fluid properties were described previously and are given in reference 14. Only brief computations for equivalent field

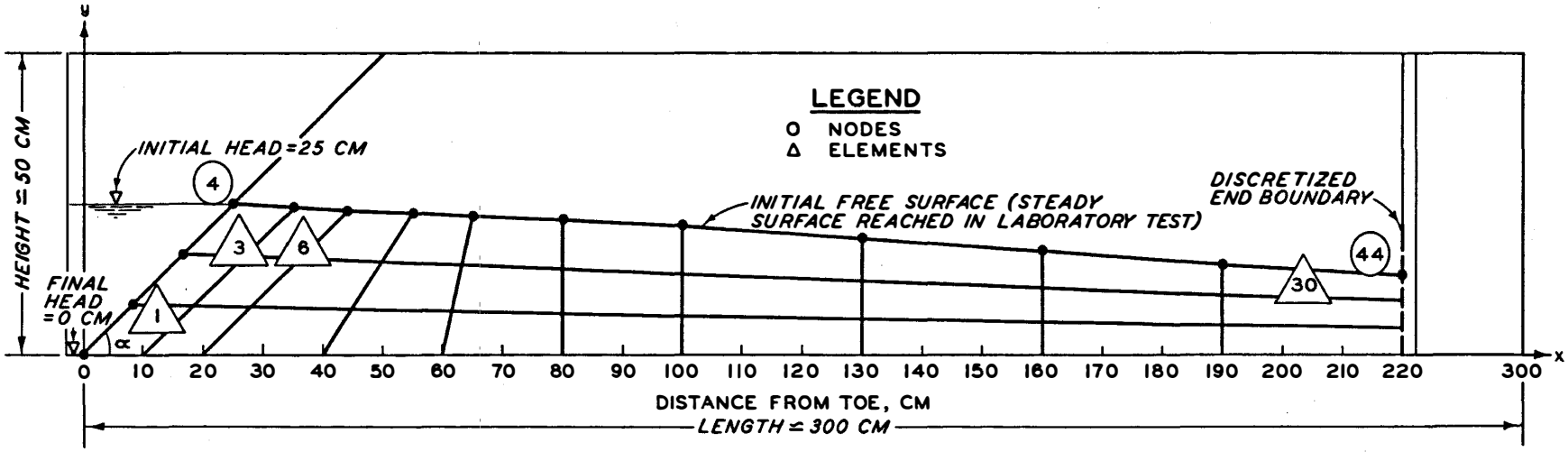

Fig. 24. Finite element mesh for viscous-flow model; α = 45 deg

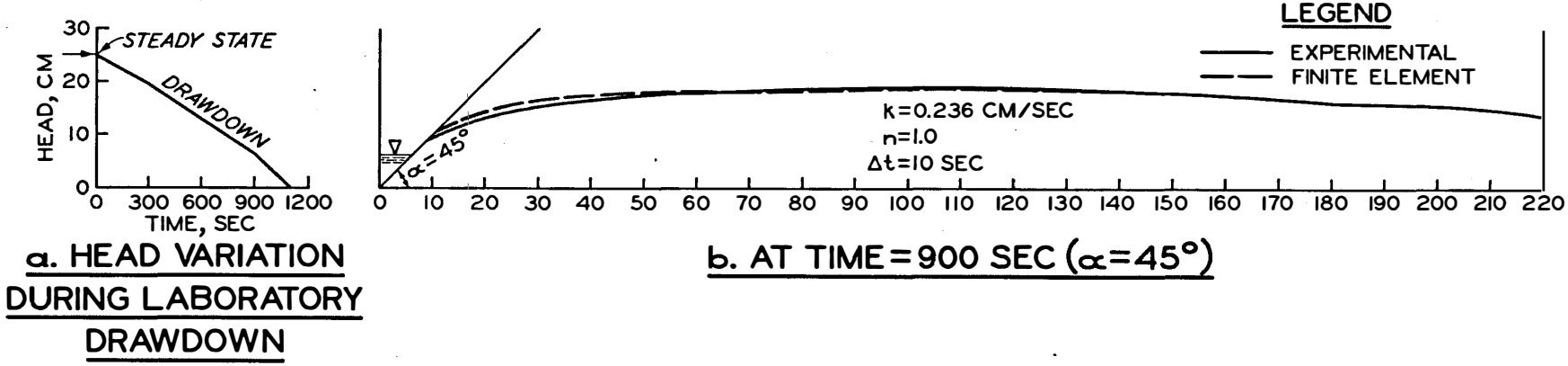

Fig. 25. Comparisons and variations in head

permeability are described herein. The ratio of mean model velocity $\bar{v}_m$ and field velocity v from equation 12 is

$$V_r = \frac{\bar{v}_m}{v} = \frac{b^2 \rho_m g}{3k\mu_m}$$

The fluid in the field is assumed to be water, and the same gradients are assumed in the model and in the field. For the properties of the fluid given above,

$$V_r = \frac{0.97 \times 980}{3 \times 9.7} \frac{b^2}{k} \simeq 33 \frac{b^2}{k} \tag{56}$$

As an illustration, assume a flood of 20-ft height simulated in the model by 10 in.; then, the ratio of heights is $L_r = 1/24$. For a flood of 4 weeks ($4 \times 605{,}000$) duration, simulated in the model by about 20 min, the ratio of time $T_r = 1{,}200/(4 \times 605{,}000)$. Therefore,

$$V_r = \frac{L_r}{T_r} = 84 \tag{57}$$

Equating equations 56 and 57

$$33 \frac{b^2}{k} = 84 \tag{58}$$

which, for $b = 0.085$ cm, yields an approximate field permeability of

$$k \simeq 25 \times 10^{-4} \text{ cm/sec} \tag{59}$$

which is representative of the permeability of fine sands in the Mississippi River banks under consideration.

102. Finite representation of infinite media. An important question arises as to what extent of the flow region should be discretized for the finite element solution. During the laboratory tests, the changes in the reservoir head did not affect significantly the movements of the points in regions at a distance of about 10 times the total magnitude of change in the external level. In other words, for the model

test, the total change in external head was 25 cm. Around distances of about 200 cm measured from the final point reached after drawdown (in this case the toe of the model), the free surface did not experience significant movements during drawdown. In order to further examine this observation, numerical results from the finite element analysis for three different distances, 190, 220, and 250 cm, were obtained. On the basis of the experimental and numerical results, it seems that acceptable solutions can be obtained by placing the end boundary at a distance of about 8H-12H from the final point of drawdown (fig. 26), where H = total drawdown .

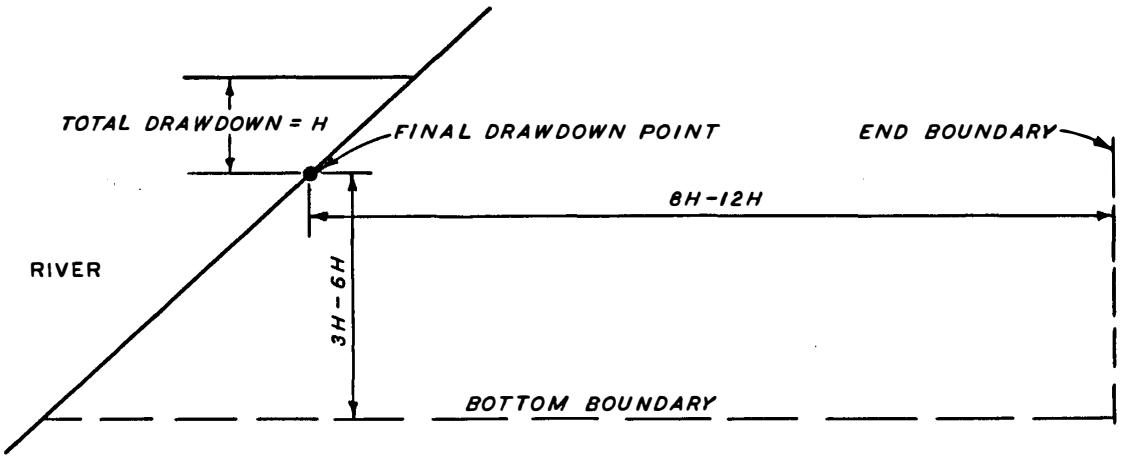

Fig. 26. Discretization of infinite porous media

103. An impervious bottom boundary is physically available for the viscous-flow model. However, for deep porous media in the field, it is necessary to select adequate location for the bottom boundary, which is assumed to be impervious in the formulation. On the basis of the numerical solution, it was observed that at a depth of about 4H from the final drawdown point, the computed heads along vertical sections showed little change. Hence, if the bottom boundary is located in the range of about 3H-6H, it would provide an approximate impervious boundary (fig. 26).

104. Finite element analysis. The end boundary was placed at 220 cm from the toe. The finite element mesh (fig. 24) contains 30 elements and 44 nodes. Since, in a problem of this nature, the variation

of gradients in the zones away from the entrance face is not severe, a rather coarse mesh was adopted in those zones. The time interval Δt = 10 sec was adopted for the results in fig. 25b. The external drawdown history is shown in fig. 25a.

105. The question of boundary assumptions at the discretized end boundary is analyzed subsequently. For the viscous-flow model, the nodes on the end boundary were fixed, but the heads at those nodes were permitted to vary. Fixing of the nodes on the end boundary was guided by the fact that the free-surface points around that distance did not move significantly during the drawdown.

106. Fig. 25b shows a comparison between the finite element solution and the experimental results for a typical time level of 900 sec during drawdown. The correlation between the two results is considered to be good.

107. Example 2: Comparisons with field observations. The histories of river stages and the corresponding heads of water in the piezometers were recorded over periods of time at Walnut Bend 6 section. A typical history at this section, for a part of 1965, is shown in fig. 27.

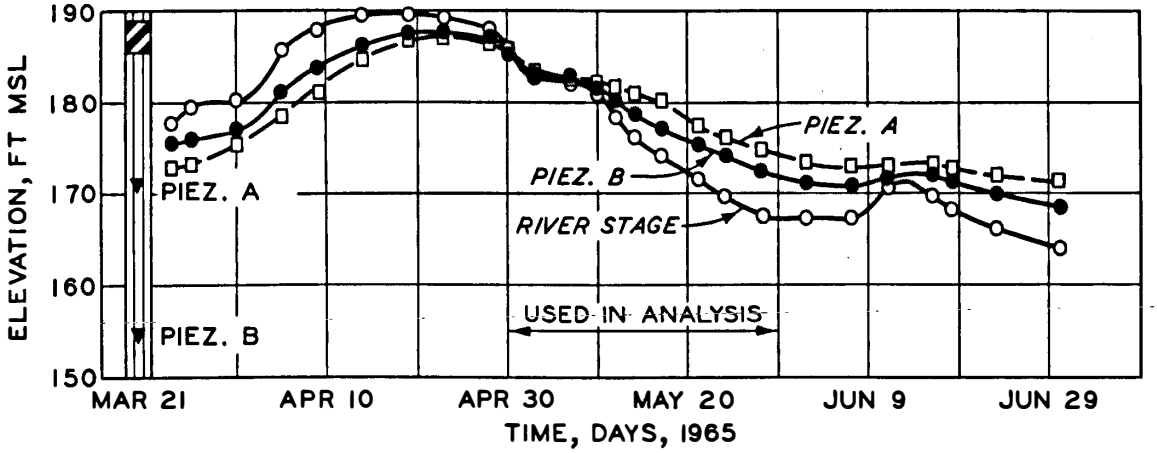

Fig. 27. History of river stages and piezometer heads at Walnut Bend 6

This figure indicates the variation in river level and the corresponding heads in two piezometers, A and B, installed in a well at a distance of about 30 ft from the top of the bank. Fig. 28 shows the location of the piezometers, the cross section of the river at Walnut Bend 6, and the

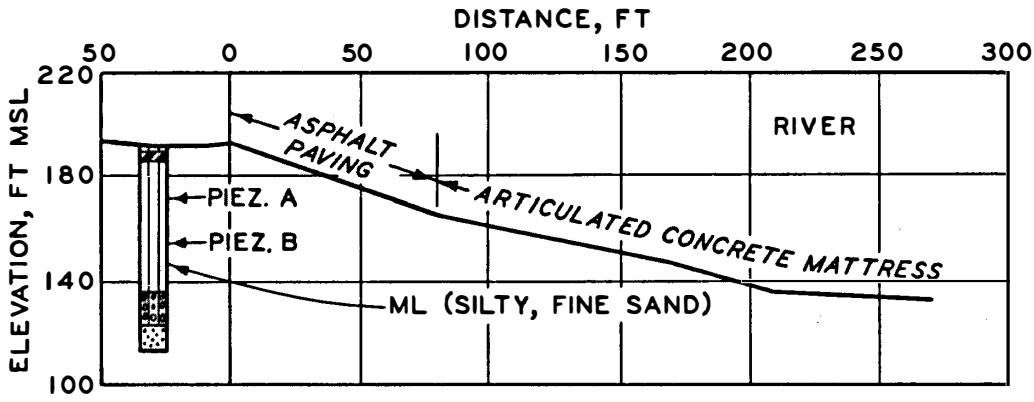

Fig. 28. Cross section at Walnut Bend 6 and boring log

boring log at the section. The bank at this section consists of predominantly silty fine sand (ML). The LMVD has performed investigations for evaluating the permeabilities and porosities of the soils in the regions in the vicinity of the Mississippi River.[56-59] The coefficient of permeability and the porosity of the soil at Walnut Bend 6 section were estimated to be of the order of 10×10^{-4} to 20×10^{-4} cm/sec (2.84 to 5.68 ft/day) and 0.4, respectively.

108. The drawdown in the river level from April 30-May 30 1965 (fig. 27) was considered for the analysis herein. In this time period of 30 days, the river level fell from about elevation 187.5 to 167.5, at an average rate of about 0.67 ft/day. Assuming that the section was porous for a large distance across the river and assuming that the flood stayed long enough for the free surface to develop, the steady free surface was estimated as shown in fig. 29. Such a steady free surface can

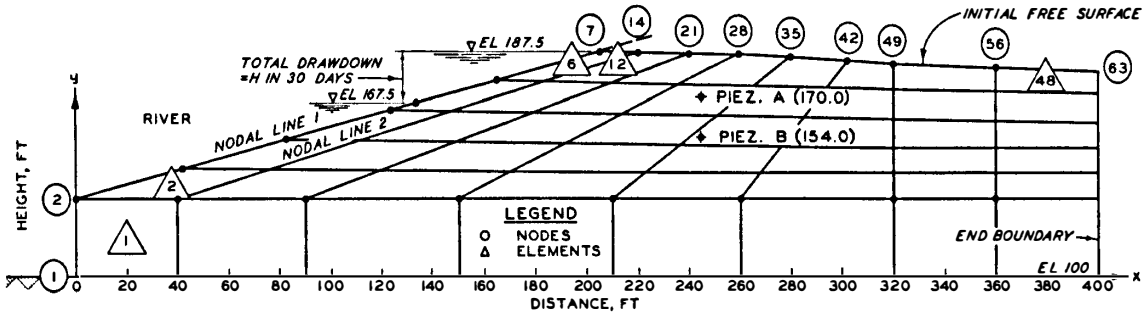

Fig. 29. Finite element mesh for idealized Walnut Bend 6 section

be estimated either on the basis of experimental observations,[14] from a conventional analysis,[19] by using the finite element method,[45,46,51] or by using other numerical techniques.[15]

109. The section in fig. 28 was idealized as shown in fig. 29, and the mesh contained 48 elements and 63 node points. On the basis of the observation of the model tests stated above, the infinite bank was represented by a finite region (fig. 29) which was terminated at 400 ft from the toe of the bank. This distance was about 13 times the maximum fall $H = 20$ ft in the river level as measured from the final point of drawdown. The bottom boundary was placed at a distance of about 4H measured from the final drawdown point. At the end boundary, the nodes were fixed, but the nodal heads were permitted to vary. A time interval $\Delta t = 0.25$ day was adopted.

110. Correlations. Fig. 30 shows the location of the free surface at typical time levels of 20 and 30 days during drawdown for $k = 10 \times 10^{-4}$ and 20×10^{-4} cm/sec. The piezometers A and B are located at approximate elevations of 174.0 and 154.0, respectively. Their locations are marked in fig. 29. Fig. 30 shows the computed values of heads in the piezometers in comparison with the field observations. The computed values were averaged from the heads at the nodes in the vicinity of a piezometer at a certain time level. The computed values of heads for the foregoing range of permeability at the Walnut Bend section show good correlation with the field observations. The correlation between the numerical and field results is better in the initial times during drawdown than in the final times. Also, for the field permeabilities of 10 to 20×10^{-4} cm/sec, the movement of the free surface seems to be faster compared with the observed piezometer heads. The movement slowed down as the permeability decreased; this change is indicated from the computed heads (fig. 30) for $k = 1 \times 10^{-4}$ cm/sec. Overall, in view of the precision that can be obtained in estimating k and n values and in field measurements of heads, the correlation is considered to be good.

111. Effect of end-boundary assumptions on the numerical solution. Depending upon the geological and geotechnical properties of a given

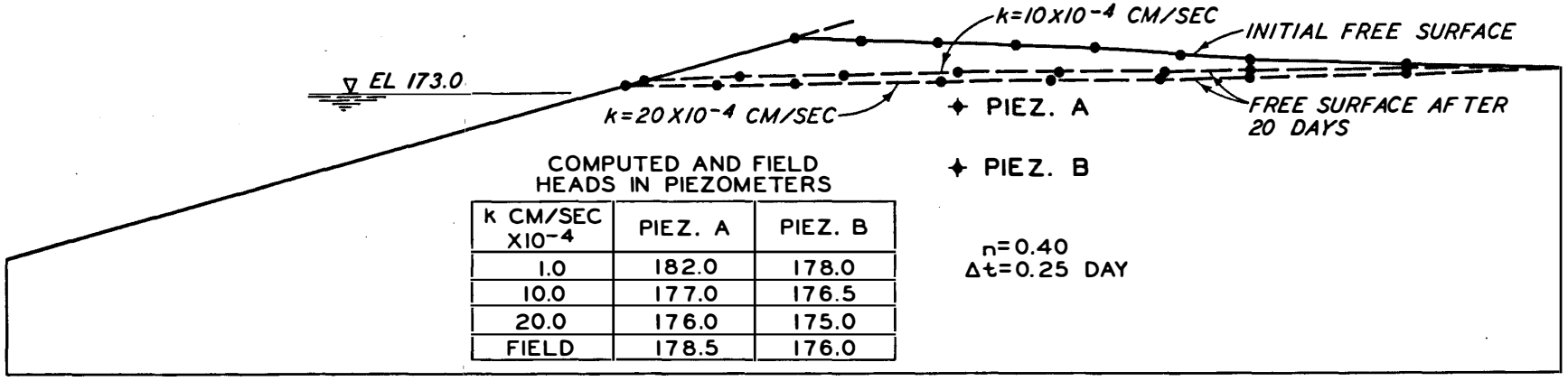

COMPUTED AND FIELD HEADS IN PIEZOMETERS

k CM/SEC X10⁻⁴	PIEZ. A	PIEZ. B
1.0	182.0	178.0
10.0	177.0	176.5
20.0	176.0	175.0
FIELD	178.5	176.0

a. AFTER 20 DAYS

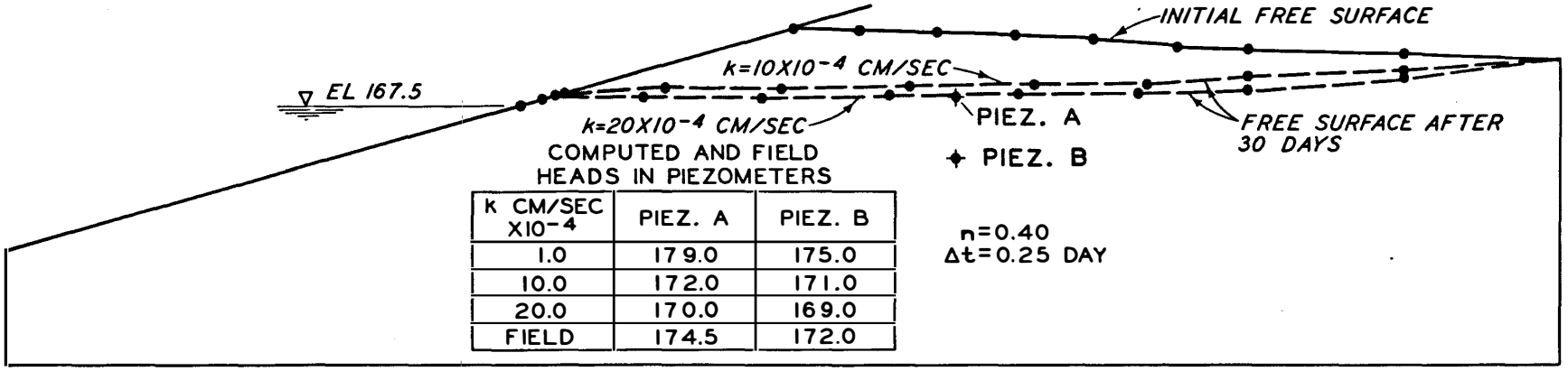

COMPUTED AND FIELD HEADS IN PIEZOMETERS

k CM/SEC X10⁻⁴	PIEZ. A	PIEZ. B
1.0	179.0	175.0
10.0	172.0	171.0
20.0	170.0	169.0
FIELD	174.5	172.0

b. AFTER 30 DAYS

Fig. 30. Comparisons of computed and field heads, Walnut Bend 6

site, the flow situation at the assumed finite boundary at the end section will differ. Three different types of boundary assumptions are delineated as: (a) variable nodes with variable heads, (b) fixed nodes with variable heads, and (c) fixed nodes with fixed heads. These three categories are shown schematically in fig. 31. The first condition

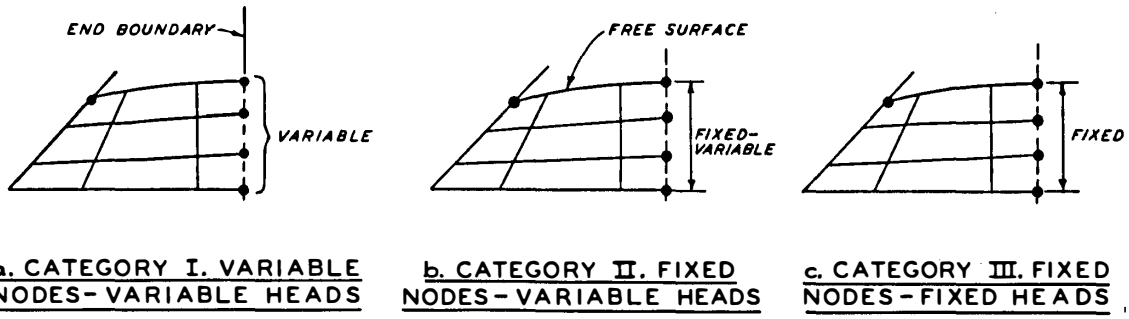

Fig. 31. Various end-boundary assumptions in discretized pervious banks

implies that the free surface extends beyond the end section, the second condition could imply an impervious end with fixed location of the nodes, and the third category implies an equipotential at the end section and the possibility of continuous recharge at the end section.

112. Fig. 32 compares the solutions for the mesh shown in fig. 24 for the three different categories. The results shown are for a typical time level of 20 days, $k = 5.64$ ft/day, and $n = 0.4$. The figure shows the movement of typical nodes 14, 28, and 80 for the three categories. The vertical coordinates or heights of the nodes for various time levels are plotted; the horizontal coordinates are shown in the parentheses.

113. The results for the first two categories show no significant differences. The results for the third category are significantly different from the other two. Both the first and second category seem to be suitable for long, pervious banks. In the foregoing analysis, the second category was adopted. This assumption also permitted some reduction in computations. The assumption in the third category would be suitable for analysis of drawdown on a face of a dam when the water level at the other face remains constant and provides an equipotential.

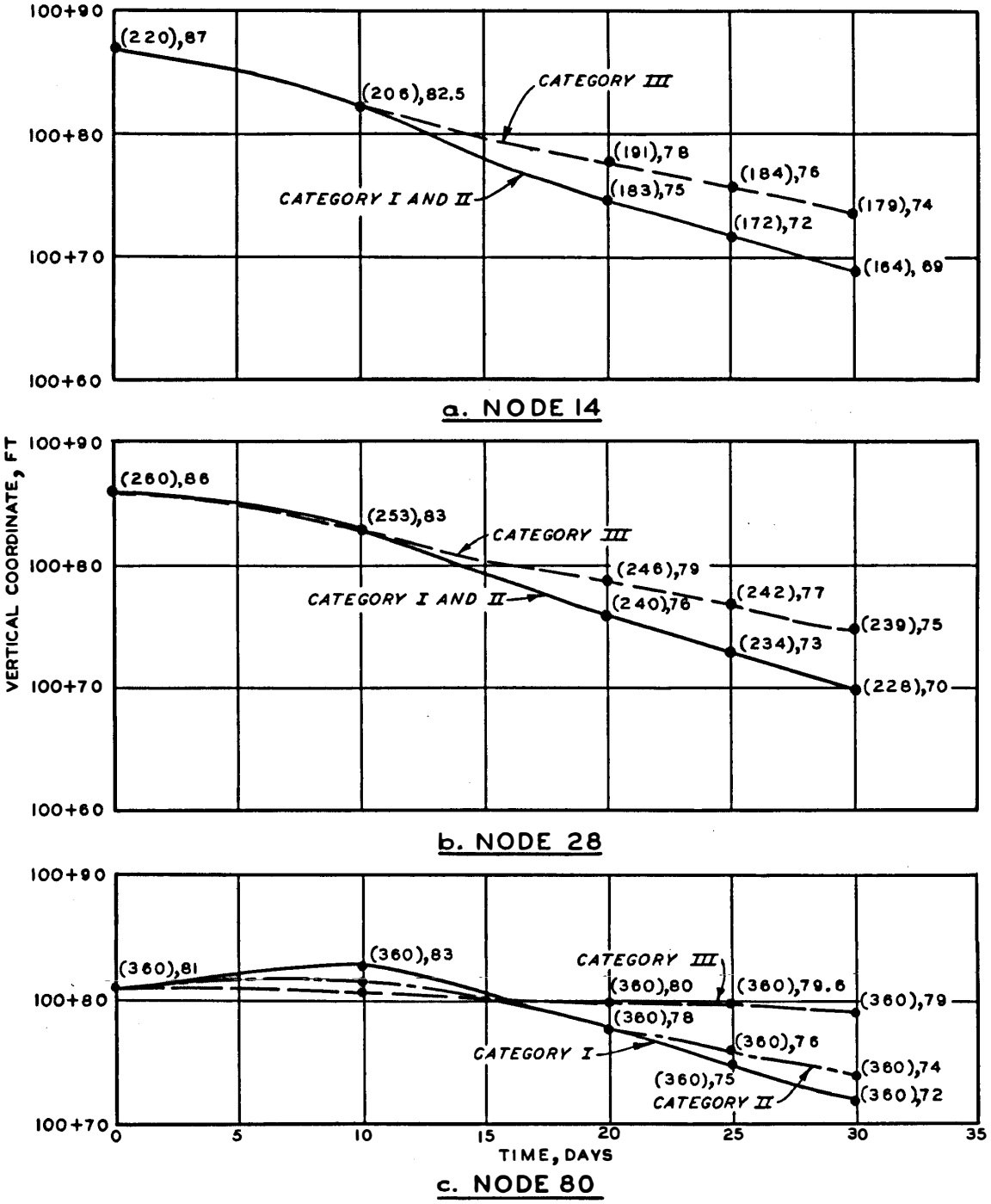

Fig. 32. Comparisons of movements of typical free-surface nodes for various categories (fig. 31)

114. Analysis for different permeabilities. The banks of the Mississippi River in the zones of interest usually contain fine sands, silty sands, and sandy silts. The coefficients of permeability for these sands are assumed to fall in the range of 1×10^{-4} cm/sec (0.284 ft/day) to 100×10^{-4} cm/sec (28.4 ft/day). Fig. 33 shows the locations of free surface for the mesh in fig. 29 at typical time levels of 20 and 30 days for different coefficients of permeability (0.284, 2.84, 5.68, 16.4, and 28.4 ft/day). The results for $k = 2.84$ ft/day are between those for $k = 1.44$ and 7.2 ft/day. The porosity was assumed to be equal to 0.4. It can be seen that the free surface moves faster with increasing permeability.

115. Nonhomogeneities in a bank. For nonhomogeneities posed by vertical and near-vertical interfaces and in the cases where the free surface does not cross an interface between different soils in a bank, the proposed procedure could be directly applied. Certain modifications would be required in the event of layered soil systems in a bank in which the free surface traverses an element made up of two or more different materials. In this event, a simple procedure would be to assign an equivalent permeability to an element in proportion to the areas of different materials contained in the element.

116. Example 3: Comparisons with field observations, King's Point section. Fig. 34 shows the cross section at King's Point Revetment. Fig. 35b shows the histories of heads in piezometers A and B and in the river during the months of April-June, 1964. The properties of soils in the bank are also shown in fig. 35b. The values of the coefficients of permeability, indicated in fig. 35b, were obtained from reference 59 on the basis of the D_{10} values indicated in fig. 35a. The value of $n = 0.4$ was adopted for all soils.

117. The drawdown condition, as shown in fig. 35b, was introduced in the finite element analysis. During this period of about 17 days, the river fell by about 23 ft (i.e., at the rate of about 1.35 ft/day). This rate was about twice that for Walnut Bend 6 considered in the previous example.

118. Fig. 36 shows the finite element mesh for the river section

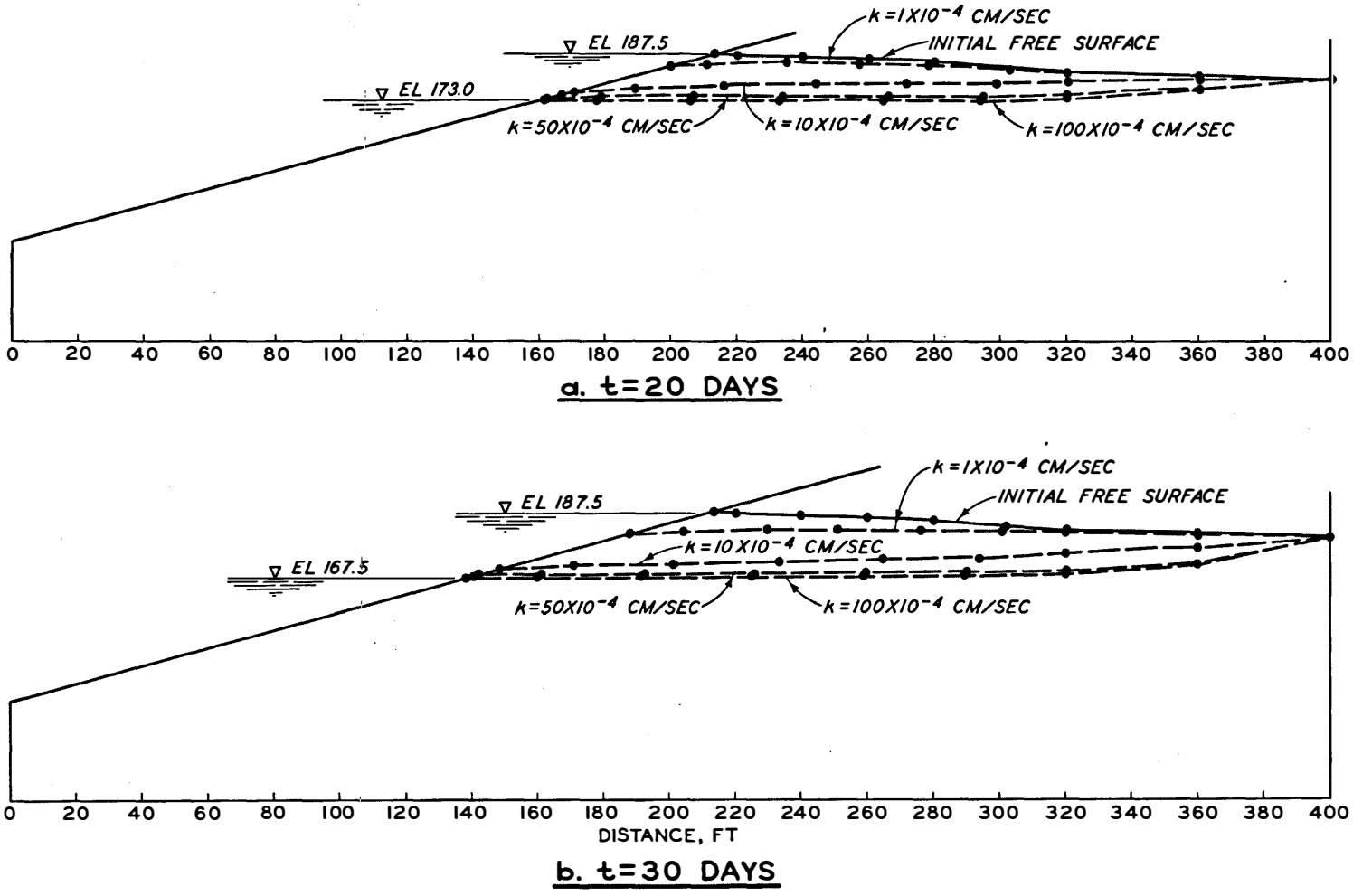

Fig. 33. Free-surface movements for various permeabilities

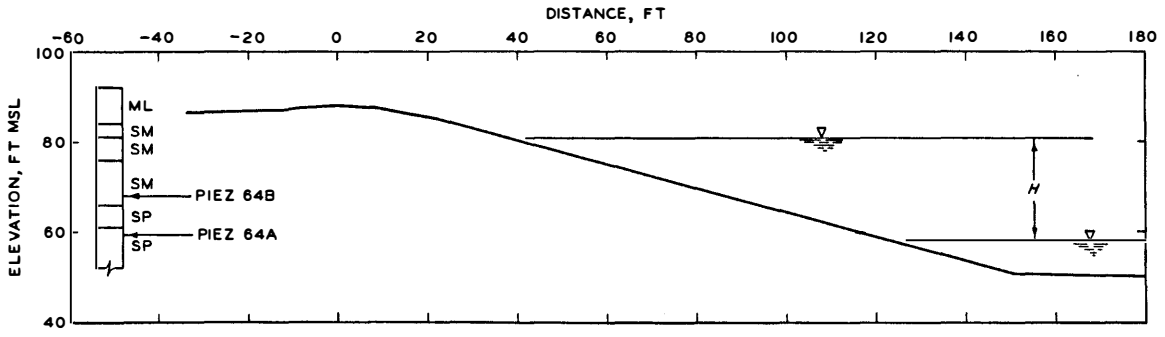

Fig. 34. Cross section at King's Point Revetment

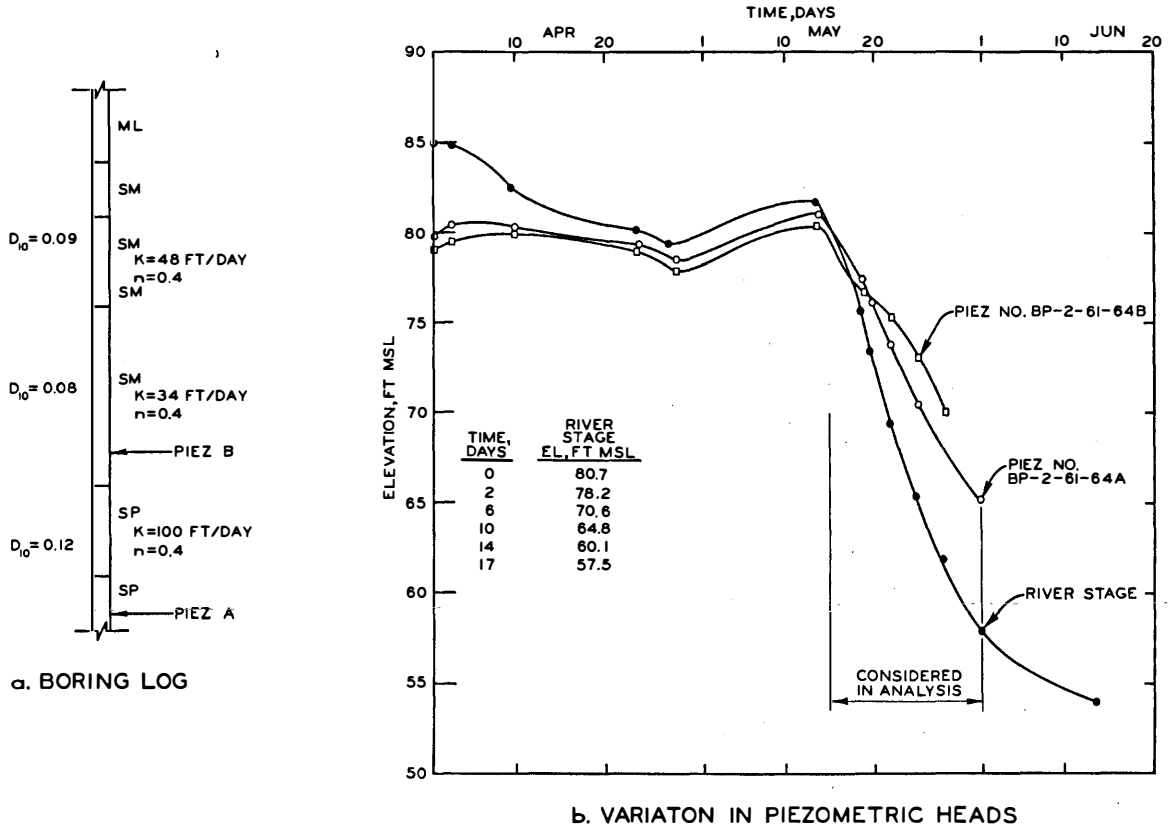

Fig. 35. History of heads and soil properties, King's Point Revetment

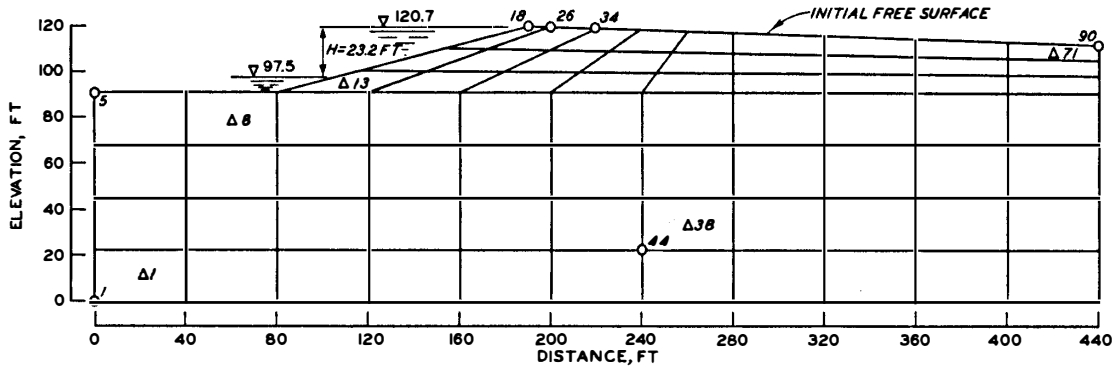

Fig. 36. Finite element mesh

shown in fig. 34. The drawdown H = 23 ft took place from a modified elevation of 120.7 (actual height = 120.7 - 40.0 = 80.7, fig. 35) to el 97.5 (actual height = 97.5 - 40.0 = 57.5, fig. 35).

119. Analysis for various permeabilities. As shown in fig. 35b, three different layers existed with three different permeabilities. The middle layer was most affected by the drawdown history under consideration. An average permeability for the bank was computed to be about 50 ft/day .

120. A number of finite element analyses were performed by using the average values of $k_x = k_y = 50$ ft/day and $k_x = k_y = 40$ ft/day . Figs. 37 and 38 show variations of free surface with time for $k = 40$ and $k = 50$, respectively. Table 1 shows a comparison between the computed and measured piezometer heads for the two permeabilities for $\Delta t = 0.025$ day. It can be seen that the correlations between the measured and computed values are good and that an increase of ten in the magnitude of permeability does not affect significantly the computed values.

121. Effect of magnitudes of time interval. The time integration scheme indicated in equation 54 is essentially the forward difference procedure. Numerical stability of this procedure was dependent upon the magnitude of the time interval Δt . Figs. 38, 39, and 40 show finite element solutions for three different values of $\Delta t = 0.025$, 0.05, and 0.1 day, respectively. Although the results for $\Delta t = 0.025$ day and $\Delta t = 0.05$ day do not show much difference, the solutions seemed to

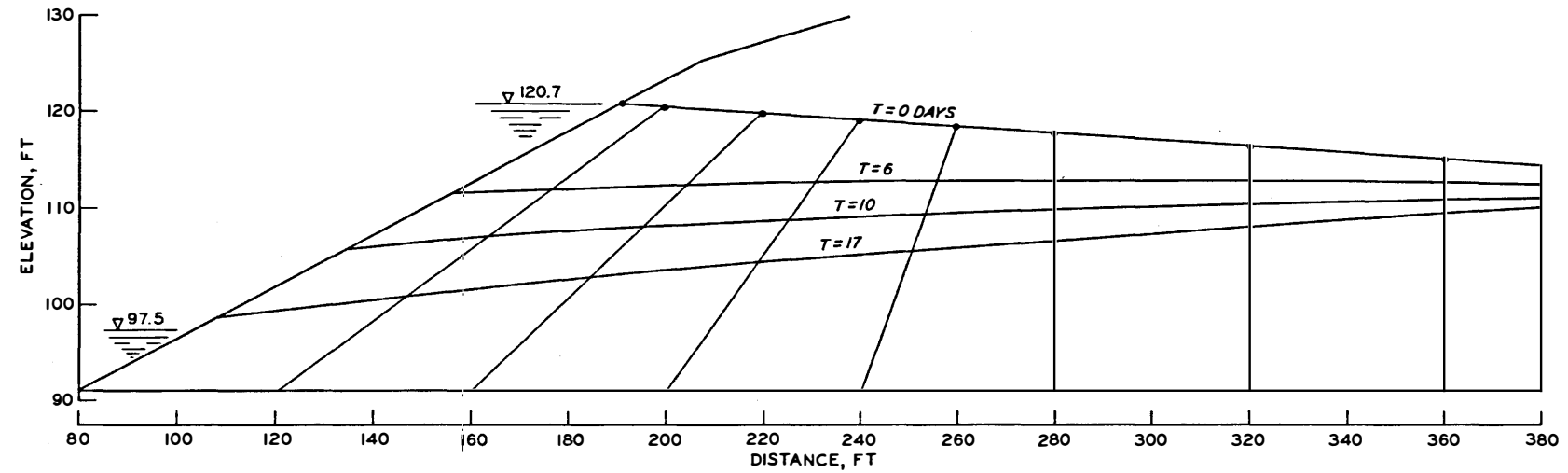

Fig. 37. Computed variations of free surface, $k_x = k_y = 40$ ft/day, $\Delta t = 0.025$ day (fixed end boundary)

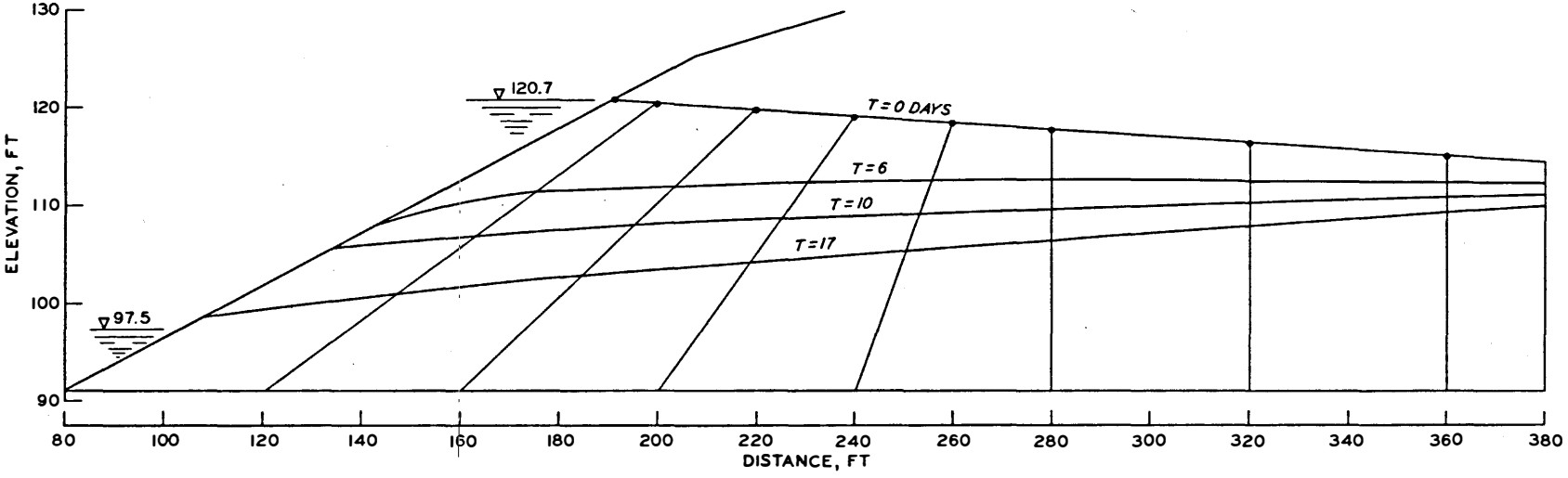

Fig. 38. Computed variations of free surface, $k_x = k_y = 50$ ft/day, $\Delta t = 0.025$ day (fixed end boundary)

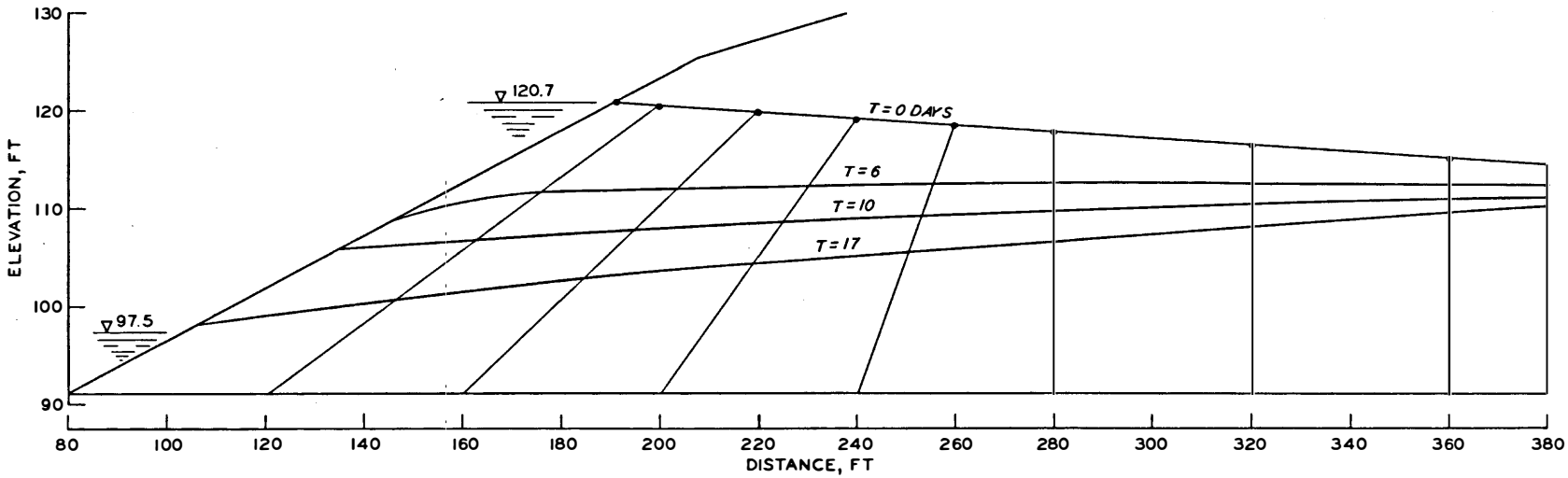

Fig. 39. Computed variations of free surface, $k_x = k_y = 50$ ft/day, $\Delta t = 0.05$ day (fixed end boundary)

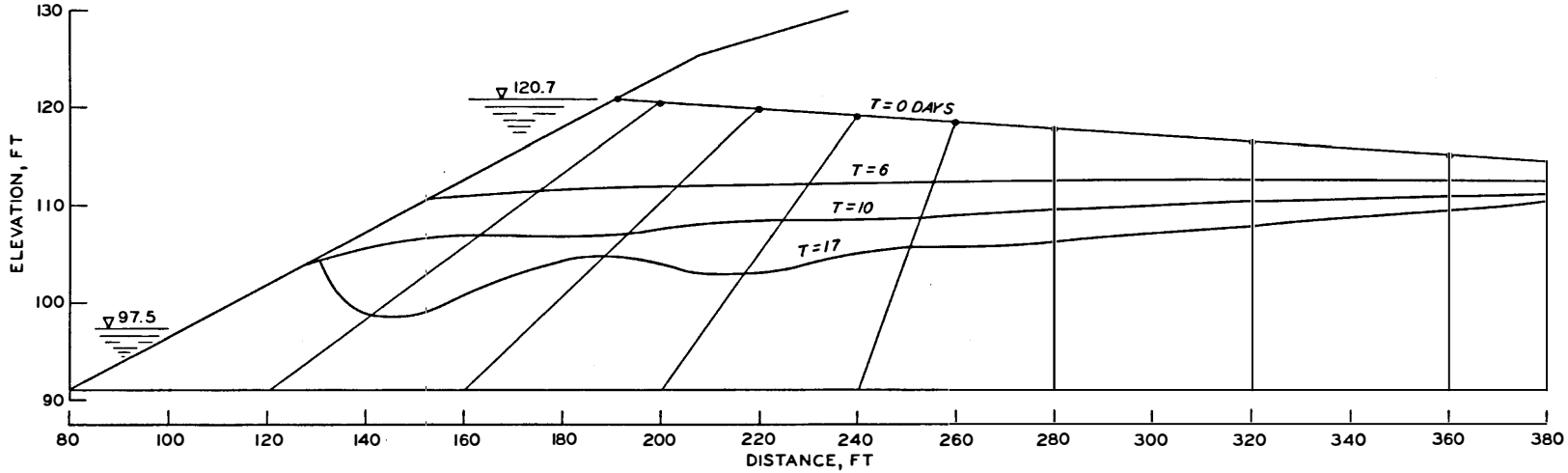

Fig. 40. Computed variations of free surface, $k_x = k_y = 50$ ft/day, $\Delta t = 0.10$ day (fixed end boundary)

become unstable for $\Delta t = 0.1$, fig. 40. The subject of numerical stability and its practical implications will be presented in Report 2.

122. Effect of anisotropy. Very often, soils in the Mississippi River banks exhibit different permeabilities in different directions. To study these effects, a number of finite element analyses were performed with $k_x = k_y = 30$ ft/day, $k_x = 30$ and $k_y = 3$ ft/day, and $k_x = 3$ and $k_y = 30$ ft/day. Table 2 shows comparisons between the measured piezometric heads and the computed heads for the three foregoing sets of permeabilities. Although the solutions thus obtained differ in magnitudes, the differences did not seem great. The most probable situation would be one in which the horizontal permeability is higher than the vertical permeability.

123. Effect of end-boundary assumption. Three flow and head boundary conditions (fig. 31) were considered for the King's Point Revetment. Figs. 39, 41, and 42 show free-surface solutions for $k_x = k_y = 50$ ft/day, $\Delta t = 0.05$ day, and for the three boundary conditions, respectively. Fig. 43 shows the effects of the boundary assumptions on the movements of nodes 26, 50, and 82 (fig. 36). The trends of these effects were found to be similar to those for Walnut Bend 6 analyses (fig. 32).

124. Example 4: Comparisons with laboratory observations, sudden drawdown in a viscous-flow model simulating a dam with core. Dvinoff[22] conducted a number of experiments on viscous-flow models. A schematic diagram of a typical model with an entrance angle of 45 deg used by Dvinoff is shown in fig. 44a. The model was made of plexiglas, with the spacing between the parallel plates equal to about 1/8 in. The fluid used in the experiments was glycerin. The permeability of the model was computed as equal to 0.846 in./sec.

125. A trap door at the bottom of the reservoir permitted "instantaneous" drawdown. The right end of the model was closed to simulate an impervious core. The movements of the free surface with time were recorded photographically.

126. The finite element mesh for the model (fig. 44a) is shown in fig. 44b. The results from the finite element analysis are shown in fig. 45, in comparison with the experimental results. Also shown in

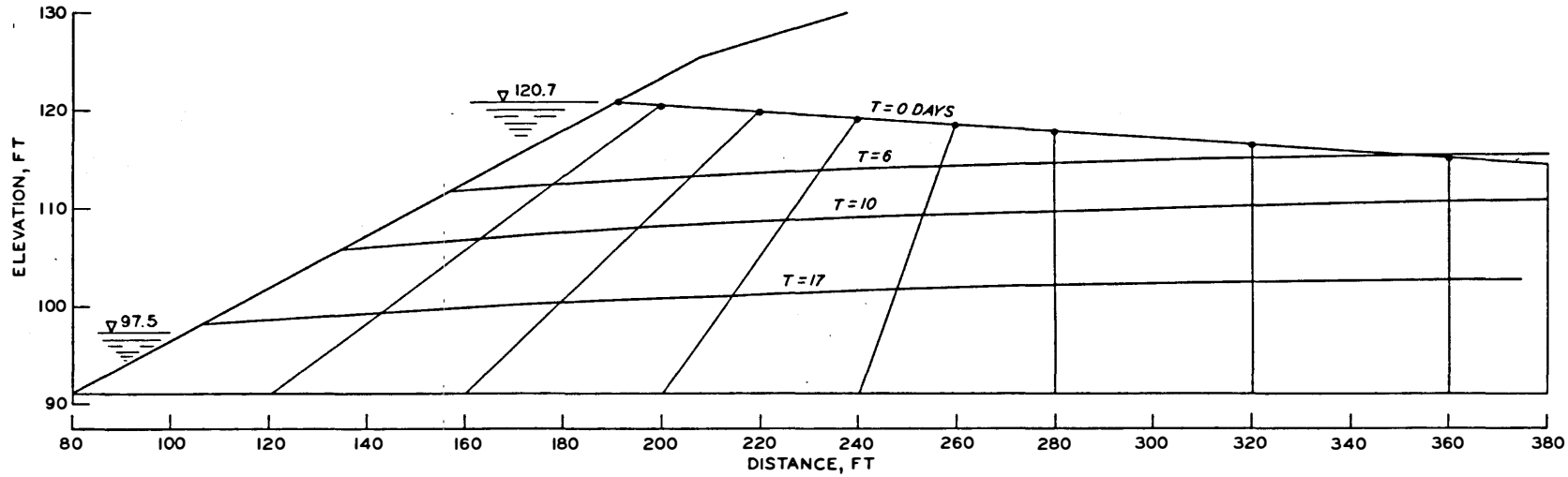

Fig. 41. Computed variations of free surface, $k_x = k_y = 50$ ft/day , $\Delta t = 0.05$ day (variable end boundary)

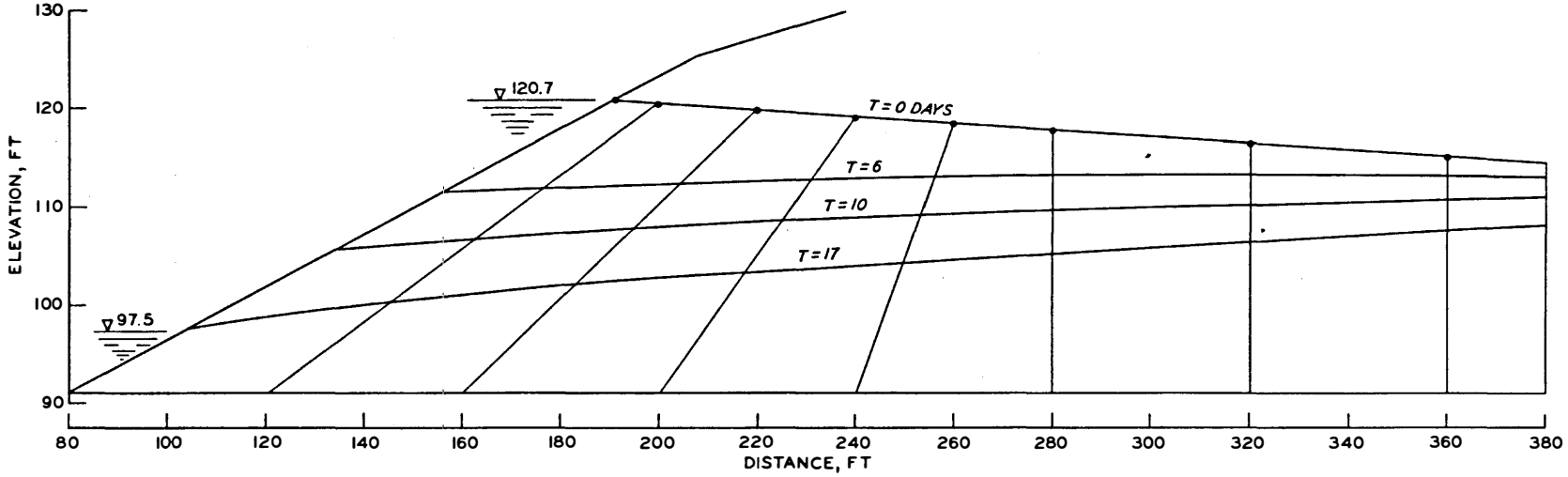

Fig. 42. Computed variations of free surface, $k_x = k_y = 50$ ft/day , $\Delta t = 0.05$ day (fixed-variable end boundary)

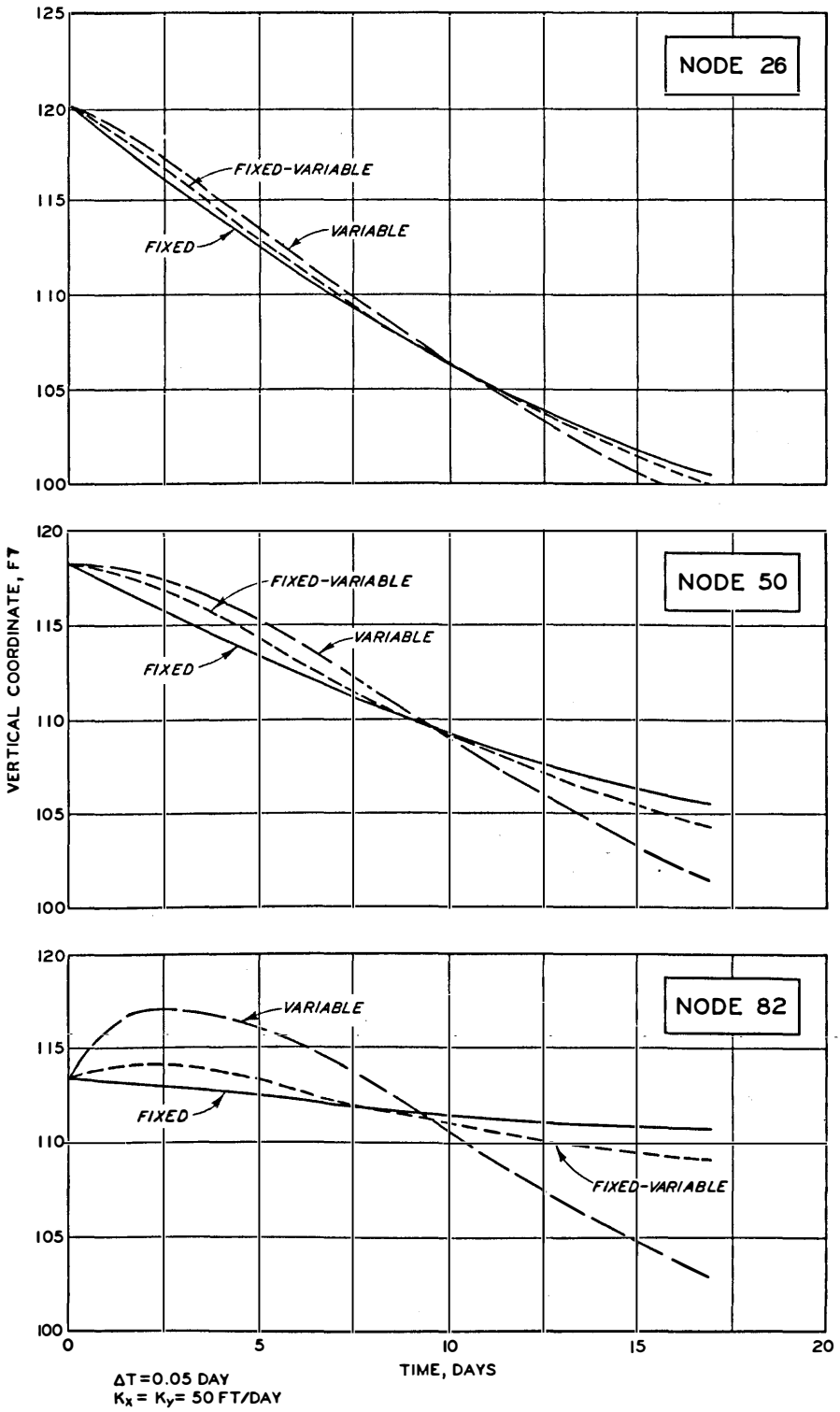

Fig. 43. Variations of heads at typical nodes for different end boundary assumptions

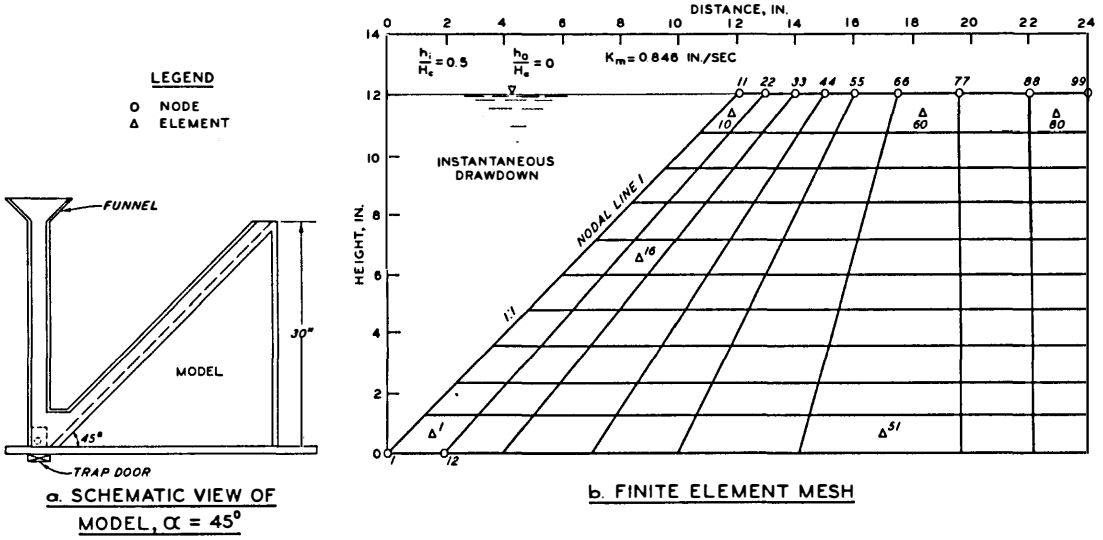

Fig. 44. Sudden drawdown in a viscous-flow model (from Dvinoff[22])

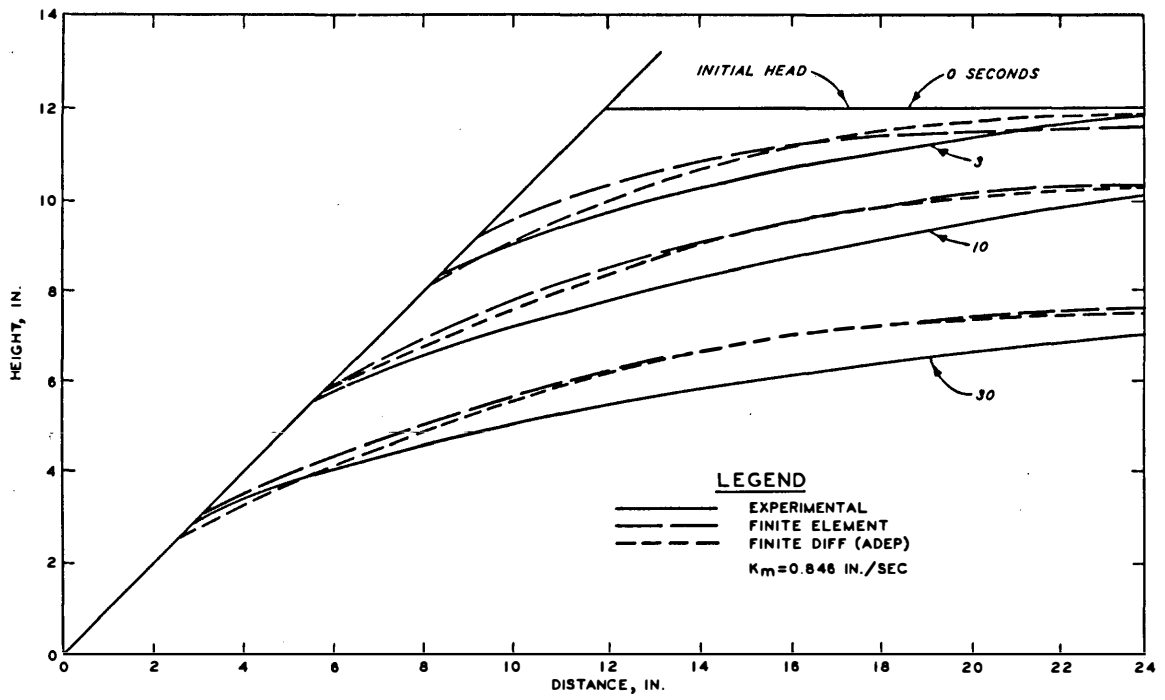

Fig. 45. Variation of free surface under sudden drawdown

this figure are the numerical results from the alternating direction, explicit finite difference procedure. There are no substantial differences between the results of the finite difference and the finite element procedures.

127. The agreement between the measured and the computed values is considered satisfactory. A point of interest is the movement of the exit (nodal) point at higher time levels during drawdown, when the exit point approaches zero height (fig. 45). According to the finite element computations, the exit point moves much faster at higher time levels. This movement may be due to the fact that the point of zero height poses mathematical singularity, whereas, in physical measurements, such mathematical singularity does not make a difference. In other words, during laboratory observations, a film of fluid could hang along the entrance face and show a nonzero elevation for the exit point for a long period of time.

PART V: SUMMARY, CONCLUSIONS, AND PROJECTIONS

128. A number of procedures based on the finite difference and the finite element methods have been proposed, and corresponding computer codes have been developed. The results from the numerical procedures were compared with those from laboratory experiments with viscous-flow models and from a number of field observations along the Mississippi River. The correlations between the numerical and observed data have been satisfactory.

129. On the basis of the satisfactory correlations, it is believed that the numerical techniques proposed herein can be used for design analysis of many problems in transient, free-surface seepage, including analyses for stability of Mississippi River banks. The procedures can also be used for seepage towards wells in layered soils.

130. It can be possible to obtain design curves for certain common situations along the river, which may include sets of curves for such variables as typical cross sections, rates of drawdown, and permeabilities. Investigations toward this end are in progress and will be included in a future report. Factors such as numerical stability criteria and representation of the movements of free surface by mathematical functions will also be considered in these investigations.

131. Other topics that are under investigation and that will be included in the next report are:

a. Comments on comparisons of the finite difference and the finite elements developed herein.

b. Formulations and codes based on quadratic and cubic approximating models and the corresponding isoparametric elements have been obtained. Results from these formulations will be compared with those from the formulation based on the bilinear model used in this report. This comparison will yield estimations of trade-offs in accuracy and computational efforts in using higher order models.

132. The proposed finite difference and the finite element procedures can be easily extended for situations requiring three-dimensional analyses. Some examples of such problems are an earthen bank with severe changes in material and geometric properties in the direction of the

river, multiple wells in layered media, and seepage near intersections of two structures made up of porous soil media.

133. A number of computer codes developed under the project will also be included in Report 2.

LITERATURE CITED

1. Carslow, H. S. and Jaeger, J. H., Conduction of Heat in Solids, 2d ed., Clarendon Press, Oxford, 1959.

2. Brahma, S. P. and Harr, M. E., "Transient Development of Free Surface in Homogeneous Earth Dam," Geotechnique, Vol 12, No. 4, Dec 1962, pp 283-302.

3. Cooper, H. H. and Rorabaugh, M. I., "Groundwater Movements and Bank Storage Due to Flow Stages in Surface Stream," Water Supply Paper 1536-J, 1963, U. S. Geological Survey, Washington, D. C.

4. Hantush, M. S., Discussion of paper "An Equation for Estimating Transmissibility and Coefficient of Storage from River-Level Fluctuations," by P. P. Rowe, Journal of Geophysical Research, Vol 66, No. 4, Apr 1961, pp 1310-1311.

5. Polubarinova-Kochina, P. Ya., Theory of Ground Water Movement, Princeton University Press, Princeton, N. J., 1962; Translated from Russian by J. M. Roger DeWiest.

6. Scheidegger, A. E., The Physics of Flow Through Porous Media, Macmillan, New York, 1960.

7. Douglas, J., "On the Numerical Integration by Implicit Methods," Journal, Society for Industrial and Applied Mathematics, Vol 3, No. 1, 1955.

8. Peaceman, D. W. and Rachford, H. H., "The Solution of Parabolic and Elliptic Differential Equations," Journal, Society for Industrial and Applied Mathematics, Vol 3, No. 1, 1955.

9. Varga, R. S., Matrix Iterative Analysis, Prentice-Hall, Englewood Cliffs, N. J., 1962.

10. Aronfsky, J. S. and Jenkins, R., "Unsteady Flow of Gas Through Porous Media, One-Dimensional Case," Proceedings, First U. S. National Congress on Applied Mechanics, 1951.

11. Schnitter, G. and Zeller, J., "Sickerstrumungen als Folge von Strauspiegel-Schwankungen in Erddammen," Schweizrische Bauzeitung, Vol 75, No. 52, Dec 1957.

12. Casagrande, A. and Shannon, W. L., "Base Course Drainage for Airport Pavements," Transactions, American Society of Civil Engineers, Vol 117, Paper No. 2516, 1952, pp 792-814.

13. Newlin, C. W. and Rossier, S. C., "Embankment Drainage After Instantaneous Drawdown," Journal, Soil Mechanics and Foundations Division, American Society of Civil Engineers, Vol 93, No. SM6, Nov 1967, pp 79-95.

14. Desai, C. S., "Seepage in Mississippi River Banks; Analysis of Transient Seepage Using Viscous Flow Model and Numerical Methods," Miscellaneous Paper S-70-3, Report 1, Feb 1970, U. S. Army Engineer Waterways Experiment Station, CE, Vicksburg, Miss.

15. Desai, C. S. and Sherman, W. C., Jr., "Unconfined Transient Seepage in Sloping Banks," Journal, Soil Mechanics and Foundations Division, American Society of Civil Engineers, Vol 97, No. SM2, Feb 1971, pp 357-373.

16. Hele-Shaw, H. S., "Experiments on the Nature of Surface Resistance of Water and of Streamline Motion Under Certain Experimental Conditions," Transactions, Institution of Naval Architects, Vol 40, 1898.

17. _____, "Streamline Motion of a Viscous Film," Report, British Association for the Advancement of Science, 1899.

18. Todd, D. K., "Unsteady Flow in Porous Media by Means of a Hele-Shaw Viscous Fluid Model," Transactions, American Geophysical Union, Vol 35, No. 6, Dec 1954, pp 905-916.

19. Harr, M. E., Groundwater and Seepage, McGraw-Hill, New York, 1962.

20. Brakensiek, D. L., "Finite Differencing Methods," Water Resources Research, Vol 3, No. 3, 1967, pp 847-860.

21. Bredehoeft, J. D., "Finite Difference Approximations to the Equations of Ground-Water Flow," Water Resources Research, Vol 5, No. 2, Apr 1969.

22. Dvinoff, A., Response of the Phreatic Surface in Earthen Dams Due to Headwater Fluctuations, Ph. D. Dissertation, Purdue University, Lafayette, Ind., 1970.

23. Dvinoff, A. and Harr, M. E., "Phreatic Surface Location After Drawdown," Journal, Soil Mechanics and Foundations Division, American Society of Civil Engineers, Vol 97, No. SM1, Jan 1971, pp 47-58.

24. Finnermore, E. J. and Perry, B., "Seepage Through an Earth Dam Computed by the Relaxation Technique," Water Resources Research, Vol 4, No. 5, Oct 1968, pp 1059-1067.

25. Karadi, G., Krizek, R. J., and Elnaggar, H., "Unsteady Seepage Flow Between Fully Penetrating Trenches," Journal of Hydrology, Vol 6, 1968, pp 417-430.

26. Rubin, J., "Theoretical Analysis of Two-Dimensional, Transient Flow of Water in Unsaturated and Partly Saturated Soils," Proceedings, Soil Science Society of America, Vol 32, 1968.

27. Taylor, G. S. and Luthin, J. N., "Computer Methods for Transient Analysis of Water-Table Aquifers," Water Resources Research, Vol 5, No. 1, Feb 1969, pp 144-152.

28. Terzidis, G., "Computational Schemes for the Boussinesq Equation," Journal, Irrigation and Drainage Division, American Society of Civil Engineers, Vol 94, No. IR4, Dec 1968, pp 381-389.

29. Szabo, B. A. and McCaig, I. W., "A Mathematical Model for Transient Free Surface Flow in Nonhomogeneous or Anisotropic Porous Media," Water Resources Bulletin, Vol 4, No. 3, Sep 1968.

30. Saul'ev, V. K., "A Method of Numerical Solution for the Diffusion Equation," Dokl. Akad, Nauk SSSR(NS), 115 (1957), Rxh (1958), 6198, pp 1077-1079.

31. Larkin, B. K., "Some Stable Explicit Difference Approximations to the Diffusion Equation," Journal of Mathematical Computation, Vol 18, No. 86, Apr 1964.

32. Allada, S. R. and Quon, D., "A Stable, Explicit Numerical Solution of the Conduction Equation for Multidimensional Nonhomogeneous Media," Heat Transfer, Chemical Engineering Progress Symposium, Series 64, Vol 62, 1966.

33. Irmay, S., "On the Meaning of the Dupuit and Pavlovskii Approximations in Aquifer Flow," Water Resources Research, Vol 5, No. 2, 1967.

34. Poorooshasb, H. B. and Forati, J., "Embankment Drainage After Instantaneous Drawdown," Proceedings, 7th International Conference on Soil Mechanics and Foundation Engineering, Mexico City, Vol 2, Aug 1969, pp 349-353.

35. Abbott, M. B., "One-Dimensional Consolidation of Multi-Layered Soils," Geotechnique, Vol 10, Dec 1960, pp 151-165.

36. Desai, C. S. and Abel, J. F., Introduction to the Finite Element Method: A Numerical Method for Engineering Analysis, Von Nostrand Reinhold Co., New York, 1972.

37. Desai, C. S., "An Approximate Solution for Unconfined Seepage," Journal, Irrigation and Drainage Division, American Society of Civil Engineers, Vol 99, No. IR1, Mar 1973, pp 71-87.

38. McCorquodale, J. A., "Variational Approach to Non-Darcy Flow," Journal, Hydraulics Division, American Society of Civil Engineers, Vol 96, No. HY11, Nov 1970, pp 2265-2278.

39. France, P. W. et al., "Numerical Analysis of Free Surface Seepage Problems," Journal, Irrigation and Drainage Division, American Society of Civil Engineers, Vol 97, No. IR1, Paper 7959, Mar 1971, pp 165-179.

40. Crandall, S. H., Engineering Analysis, McGraw-Hill, New York, 1956.

41. Finlayson, B. A. and Scriven, L. E., "The Method of Weighted Residuals--A Review," Applied Mechanics Reviews, Vol 19, No. 9, Sep 1966, pp 735-748.

42. Zienkiewicz, O. C. and Parekh, C. J., "Transient Field Problems: Two-Dimensional and Three-Dimensional Analysis by Isoparametric Finite Elements," International Journal for Numerical Methods in Engineering, Vol 2, No. 1, 1970, pp 61-71.

43. Wilson, E. L. and Nickell, R. E., "Application of the Finite Element Method to Heat Conduction Analysis," Nuclear Engineering and Design, Vol 4, 1966.

44. Zienkiewicz, O. C., Meyer, P., and Cheung, Y. K., "Solution of Anisotropic Seepage by Finite Elements," Journal, Engineering Mechanics Division, American Society of Civil Engineers, Vol 92, No. EM1, Feb 1966, pp 111-120.

45. Taylor, R. L. and Brown, C. B., "Darcy Flow Solutions With a Free Surface," Journal, Hydraulics Division, American Society of Civil Engineers, Vol 93, No. HY2, Mar 1967, pp 25-33.

46. Finn, W. D. L., "Finite-Element Analysis of Seepage Through Dams," Journal, Soil Mechanics and Foundations Division, American Society of Civil Engineers, Vol 93, No. SM6, Nov 1967, pp 41-48.

47. Volker, R. E., "Nonlinear Flow in Porous Media by Finite Elements," Journal, Hydraulics Division, American Society of Civil Engineers, Vol 95, No. HY6, Nov 1969, pp 2093-2114.

48. Witherspoon, P. A., Javandel, I., and Neuman, S. P., "Use of the Finite Element Method in Solving Transient Flow Problems in Aquifer Systems," Proceedings, Tucson Conference, International Association of Scientific Hydrology, Vol 81, 1968.

49. Zienkiewicz, O. C. and Cheung, Y. K., "Finite Elements in the Solution of Field Problems," The Engineer, Vol 220, Sep 1965, pp 507-510.

50. Neumann, S. P. and Witherspoon, P. A., "Analysis of Nonsteady Flow With a Free Surface Using the Finite Element Method," Water Resources Research, Vol 7, No. 3, Jun 1971, pp 611-623.

51. Desai, C. S., "Seepage Analysis of Earth Banks Under Drawdown," Journal, Soil Mechanics and Foundations Division, American Society of Civil Engineers, Vol 98, No. SM11, Nov 1972, pp 1143-1162.

52. _____, "Finite Element Procedures for Seepage Analysis Using an Isoparametric Element," Proceedings of the Symposium, Applications of the Finite Element Method in Geotechnical Engineering, C. S. Desai, ed., U. S. Army Engineer Waterways Experiment Station, CE, Vicksburg, Miss., May 1972, pp 799-824.

53. Ergatoudis, J., Irons, B. M., and Zienkiewicz, O. C., "Curved, Isoparametric, 'Quadrilateral' Elements for Finite Element Analysis," International Journal of Solids and Structures, Vol 4, 1968, pp 31-42.

54. Farhoomand, I. and Wilson, E., "A Nonlinear Finite Element Code for Analyzing the Blast Response of Underground Structures," Contract Report N-70-1, Jan 1970, U. S. Army Engineer Waterways Experiment Station, CE, Vicksburg, Miss.; prepared by Structural Engineering Laboratory, University of California, Berkeley, Calif., under Contract No. DACA 39-67-0020.

55. Herbert, R. and Ruston, K. R., "Ground Water Flow Studies by Resistance Networks," Geotechnique, Vol 16, No. 1, Mar 1966, pp 53-75.

56. Hvorslev, M. J., "Time Lag and Soil Permeability in Ground Water Observations," Bulletin No. 36, Apr 1951, U. S. Army Engineer Waterways Experiment Station, CE, Vicksburg, Miss.

57. Clough, G. W., "Ground Water Level in Silty and Sandy Mississippi Upper Banks," Aug 1966, Mississippi River Commission, CE, Vicksburg, Miss.

58. U. S. Army Engineer Waterways Experiment Station, CE, "Investigation of Underseepage and Its Control, Lower Mississippi River Levees," Technical Memorandum No. 3-424, Vols 1 and 2, Oct 1956, Vicksburg, Miss.

59. Krinitzsky, E. L. and Wire, J. C., "Groundwater in Alluvium of the Lower Mississippi Valley (Upper and Central Areas)," Technical Report No. 3-658, Vol 1, Sep 1964, U. S. Army Engineer Waterways Experiment Station, CE, Vicksburg, Miss.

Table 1

Comparison of Measured and Computed Heads

King's Point, Δt = 0.025 Day

Time During Drawdown days	Piezometer A			Piezometer B		
	Measured ft	Computed		Measured ft	Computed	
		k = 50	k = 40		k = 50	k = 40
0	80.7	79.0	79.0	79.5	79.3	79.3
2	79.0	76.6	76.9	77.8	76.7	77.1
6	74.7	72.1	72.3	75.2	72.2	72.4
10	70.2	68.6	68.8			
14	66.9	66.0	66.1			
17	65.0	64.5	64.6			

Table 2

Comparisons Between Measured and Computed Heads

Effect of Anisotropy, Δt = 0.05 Day

Time During Drawdown days	Piezometer A				Piezometer B			
	Measured ft	$k_x = 30$ $k_y = 30$	$k_x = 30$ $k_y = 3$	$k_x = 3$ $k_y = 30$	Measured ft	$k_x = 30$ $k_y = 30$	$k_x = 30$ $k_y = 3$	$k_x = 3$ $k_y = 30$
0	80.70	79.00	79.00	79.00	79.50	79.30	79.30	79.30
2	79.00	77.52	77.86	78.21	77.80	77.46	78.04	78.16
6	74.70	73.10	74.05	75.10	75.20	73.27	74.88	75.44
10	70.20	68.95	70.42	72.11				
14	66.90	65.68	67.14	69.52				
17	65.00	63.77	64.97	67.84				

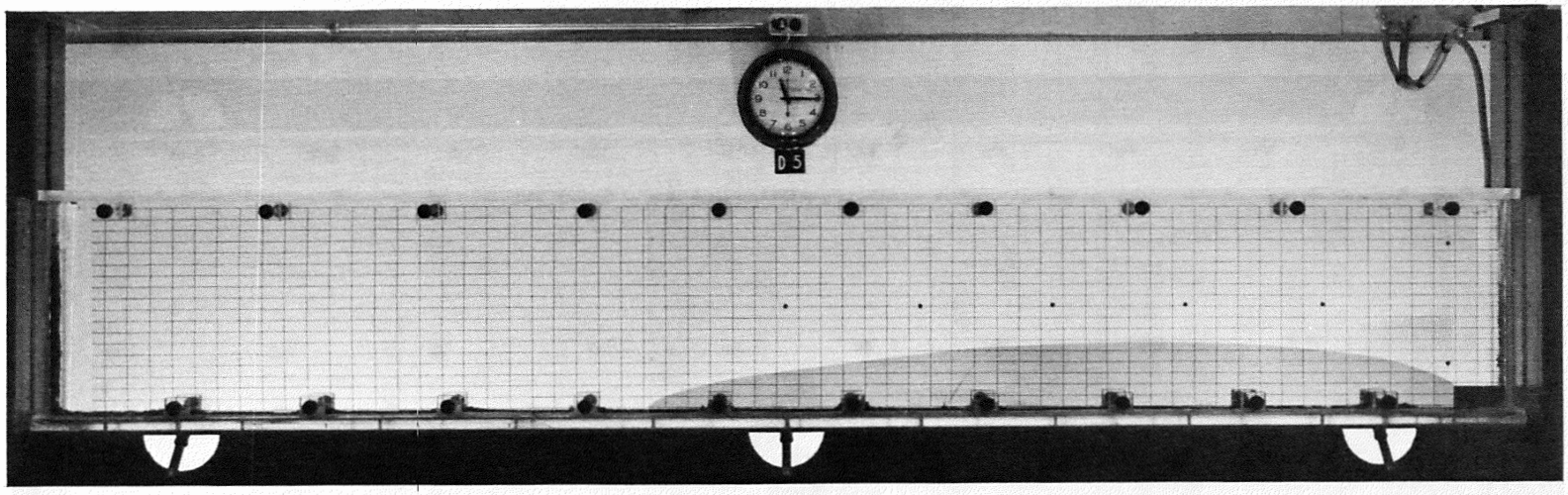

Photo 1. Typical test result: α = 90 deg

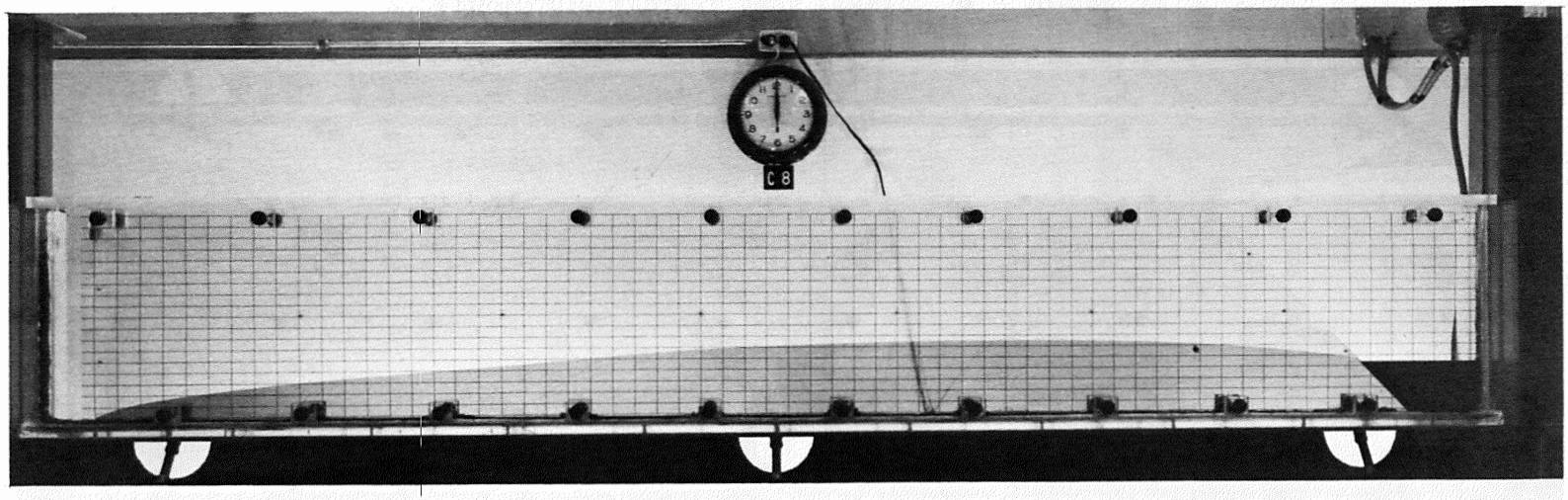

Photo 2. Typical test result: α = 45 deg

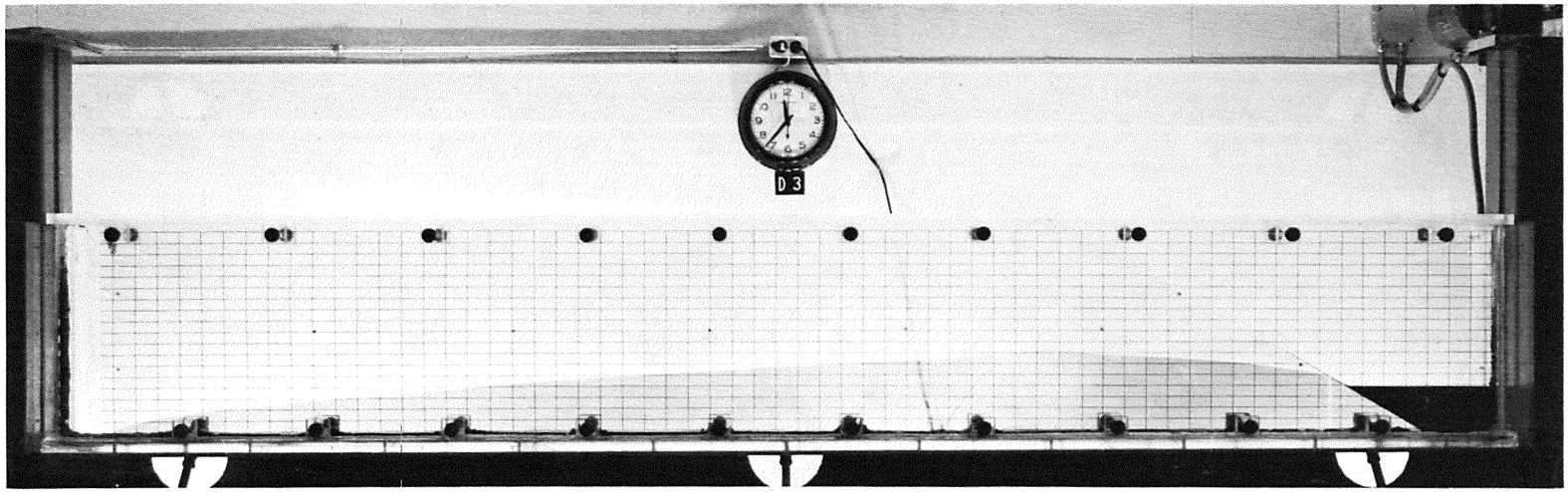

Photo 3. Typical test result: α = 30 deg

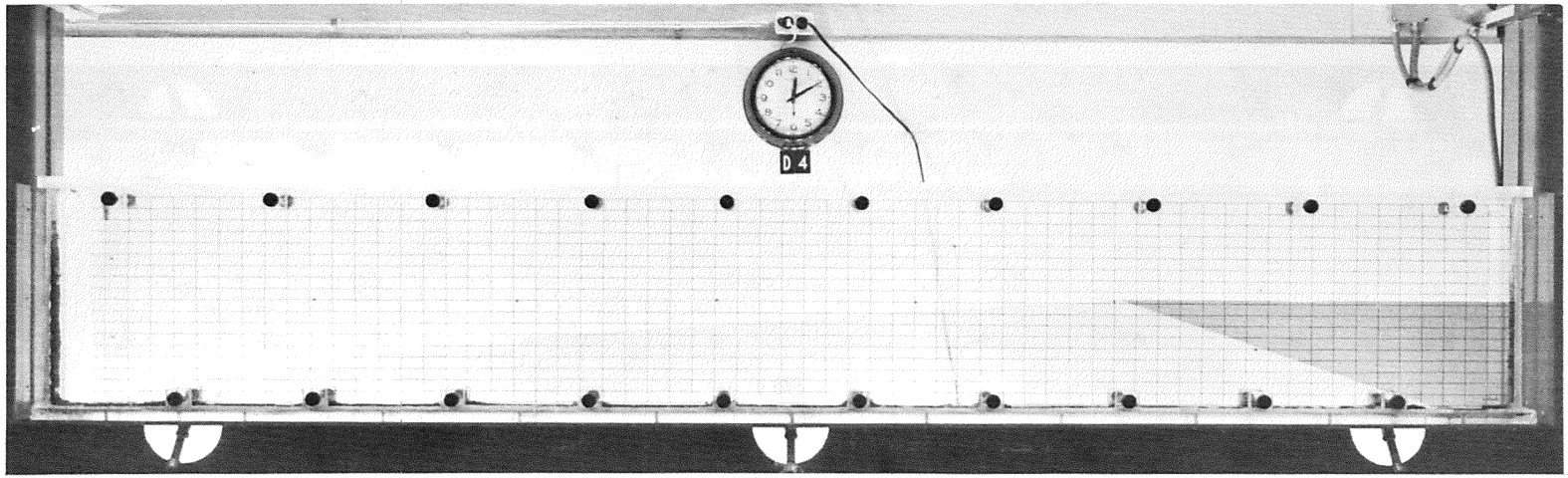

Photo 4. Typical test result: α = 18.5 deg

APPENDIX A: CLOSED-FORM SOLUTIONS

1. A closed-form mathematical solution yields an expression for the unknown sought that is valid at every point in the flow domain. In the case of a numerical procedure, the solution is obtained only at a selected number of points, nodes, or subdomains within the total flow domain. Solutions at any other points in the flow domain can usually be obtained by interpolation. Thus, subject to the basic assumptions, the closed-form solution is exact, whereas a numerical solution is an approximation. However, such physical complexities as the arbitrary shapes of a domain and arbitrary variations of material properties are very difficult to handle in a closed-form solution. For certain simple situations, closed-form solutions are possible, and some of the previously published solutions are reviewed herein.

One-Dimensional Flow

Derivation of governing equation

2. The differential equation governing unconfined flow in one direction can be derived by using equation 9a,

$$\bar{u} = -\frac{b^2 \rho g}{3\mu} \frac{\partial h}{\partial x} \qquad \text{(9a bis)}$$

The following continuity equations can be derived by considering the flow through the faces of a small element, as in fig. A1:

a. The flow through the face 1-1 is given as

$$q_{n1} = 2bhu \qquad \text{(A1a)}$$

b. The flow through the face 2-2 is given by

$$q_{n2} = 2b \left(h + \frac{\partial h}{\partial x} dx\right) \left(u + \frac{\partial u}{\partial x} dx\right) \qquad \text{(A1b)}$$

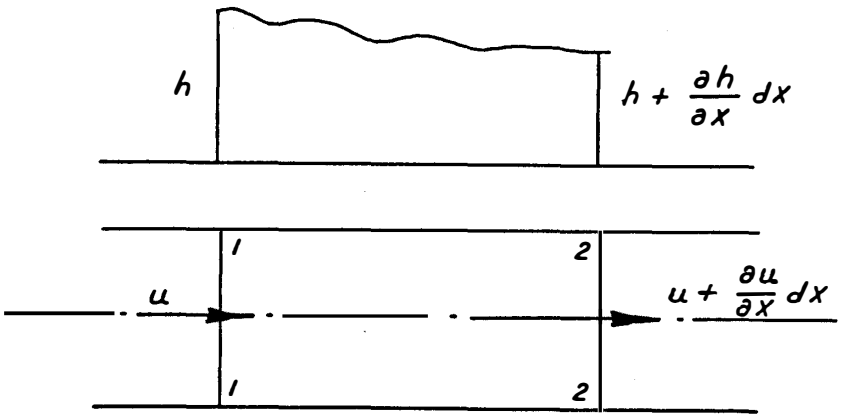

Fig. A1. Flow in an element of fluid

c. The change in flow between the faces 1-1 and 2-2 is given by

$$q_{n1} - q_{n2} = 2bhu - \left(2bhu + 2bh \frac{\partial u}{\partial x} dx + 2bu \frac{\partial h}{\partial x} dx\right) + 2b \frac{\partial h}{\partial x} \frac{\partial u}{\partial x} (dx)^2 \qquad \text{(A1c)}$$

d. The last term, being of higher order, is neglected; thus,

$$q_{n1} - q_{n2} = -2bh \frac{\partial u}{\partial x} dx - 2bu \frac{\partial h}{\partial x} dx \qquad \text{(A1d)}$$

e. Assuming the fluid to be incompressible, the change in the flow must also be equal to $2b \times dx \times n \times \frac{\partial h}{\partial t}$, where n is the effective porosity and is equal to 1 for the slit in the model. Then the complete flow equation becomes

$$-2bh \frac{\partial u}{\partial x} dx - 2bu \frac{\partial h}{\partial x} dx = 2b\, dx\, n \frac{\partial h}{\partial t} \qquad \text{(A2)}$$

Substituting the value of $\frac{\partial u}{\partial x}$ from equation 9,

$$-2bh\left(-\frac{b^2}{3} \frac{\rho g}{\mu} \frac{\partial^2 h}{\partial x^2}\right) dx - 2b \left(-\frac{b^2 \rho g}{3\mu} \frac{\partial h}{\partial x}\right) \frac{\partial h}{\partial x} dx = n \times 2b \times dx \frac{\partial h}{\partial t} \qquad \text{(A3)}$$

Simplifying equation A3 yields

$$\frac{b^2\rho g}{3\mu n}\left[h\,\frac{\partial^2 h}{\partial x^2}+\left(\frac{\partial h}{\partial x}\right)^2\right]=\frac{\partial h}{\partial t} \tag{A4}$$

3. Equation A4 is the governing differential equation for unconfined flow through the Hele-Shaw model. This equation also represents flow through porous media when the term $b^2\rho g/3\mu n$ is replaced by $k_o\rho g/\mu n$, where k_o is the permeability of soil. Furthermore, equation A4 is a nonlinear, partial differential equation. If the change in head h is small compared to the height of the aquifer, the term $(\partial h/\partial x)^2$ can be neglected and $h\,\partial^2 h/\partial x^2$ can be replaced by $\bar{h}\,\partial^2 h/\partial x^2$, where $\bar{h}$ is either the original depth of water in the aquifer or the mean height in the case of a rise of flood level.

4. Thus, the nonlinear equation is reduced to a linear partial differential equation,

$$\frac{b^2\rho g}{3\mu n}\,\bar{h}\,\frac{\partial^2 h}{\partial x^2}=\frac{\partial h}{\partial t} \tag{A5}$$

or

$$\frac{\partial h}{\partial t}=\alpha\,\frac{\partial^2 h}{\partial x^2} \tag{A6}$$

where $\alpha=\dfrac{b^2\rho g}{3\mu n}\,\bar{h}$.

Closed-form solutions

5. Linearized equation. Several closed-form solutions are available for the governing differential equation A4 with simple boundary conditions.

6. Rise of flood at constant rate. Carslow and Jaeger[1*] and Hantush[4] have derived the solution of equation A4 for the following simple boundary conditions and a bank with vertical upstream face, if the boundary conditions are

---

* Reference numbers refer to items in "Literature Cited" following the main text.

$$h(x,o) = 0$$
$$h(\infty,t) = 0$$
$$h(o,t) = ct$$

where

$h(x,t)$ = head at distance x occurring at time t

x = distance from upstream face

t = time

c = rate of rise of head at upstream face

Then the solution to equation A4 with the above boundary conditions is given as

$$h(x,t) = ct\left[(1 + 2U^2)\ \text{erfc}\ (U) - \frac{2}{\sqrt{\pi}} U \exp\ (-U^2)\right] \qquad (A7)$$

where $U = \dfrac{x}{\sqrt{4\alpha t}}$.

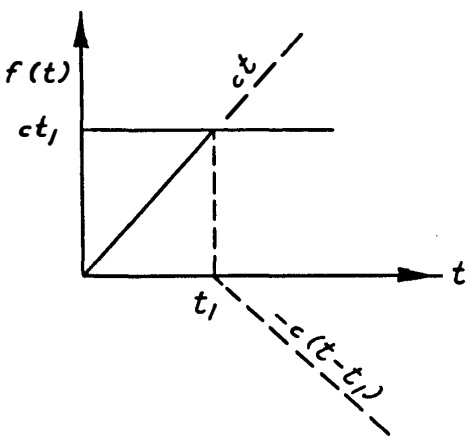

Fig. A2. Superposition of two linear functions

7. The solution for the case when the flood rises at a constant rate to a certain head and remains steady is also obtained by superposition of two linear functions, as shown in fig. A2.[7]

8. Sinusoidal rise of flood. Cooper and Rorabaugh[3] obtained the solution to equation A4 with a sinusoidal rise of flood and the boundary conditions

$$h(x,o) = 0 \qquad x \geq 0$$
$$h(\infty,t) = 0 \qquad t \geq 0$$
$$h(o,t) = \begin{cases} \dfrac{h_o}{2}(1 - \cos \omega t) & t \leq T \\ 0 & t \geq T \end{cases}$$

where

ω = frequency of flood

T = period of flood

9. The solution for the case of a rise and fall of flood level (fig. A3) up to time T and then steady conditions

$$h(x,t) = \frac{h_o}{2}\left[\operatorname{erfc}\frac{x}{2\sqrt{\alpha t}} - \operatorname{erfc}\left(\frac{x}{2\sqrt{\alpha(t-T)}}\right)\right]$$

$$+ \frac{1}{\pi}\int_0^\infty \left[e^{-Ut} - e^{-U(t-T)}\right] \sin\left(x\sqrt{\frac{U}{\alpha}}\right)\frac{U}{U^2+\omega^2}\,dU \qquad \text{(A8)}$$

is obtained by superposition of sinusoidal waves.[3]

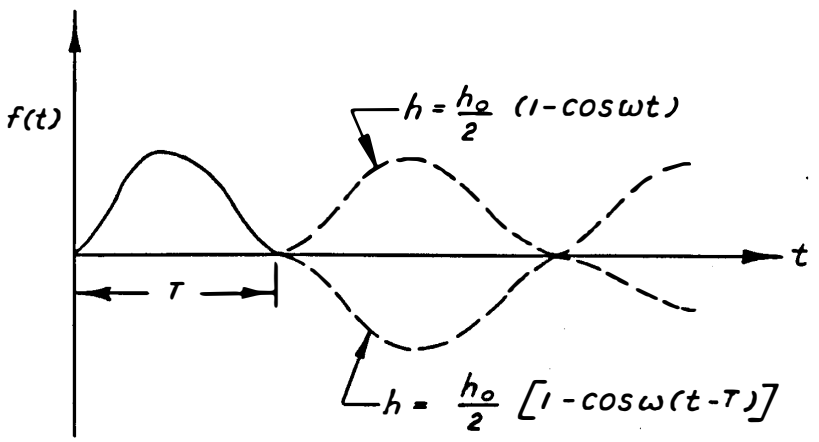

Fig. A3. Superposition of waves

10. Nonlinear equation. The results of the linearized equation are applicable only to those cases where the height of flood is small when compared to the original aquifer depth. In cases where the height of flood is not small compared to the depth of aquifer, the above results are not applicable, and the nonlinear differential equation should be considered.

11. Exponential rate of flood rise. Polubarinova-Kochina[5] has obtained a solution to the nonlinear equation A4

$$\frac{\partial h}{\partial t} = \alpha_1\left[\left(\frac{\partial h}{\partial x}\right)^2 + h\,\frac{\partial^2 h}{\partial x^2}\right] \tag{A4}$$

where $\alpha_1 = \dfrac{b^2 \rho_m g}{3\mu_m n}$, or

$$\frac{\partial h}{\partial t} = \lambda^2\,\frac{\partial^2 (h^2)}{\partial x^2} \tag{A9}$$

where $\lambda^2 = \dfrac{\alpha_1}{2}$ and the boundary conditions are

$$h(x,o) = 0$$

$$h(o,t) = ct^p \qquad p > 0$$

12. The equation is solved by assuming the solution in the form of

$$h(x,t) = ct^p\, f(\psi) \tag{A10}$$

where $\psi = x \Big/ \left\{\lambda\sqrt{c^{k-1}\, t^{\left[1+p(k-1)\right]}}\right\}$. For the special case of $p = 1$, giving a linear rate of flood rise, the solution[5] is presented as

$$h = ct - x\sqrt{\frac{c}{2\lambda^2}} \qquad \text{for} \quad 0 \le x \le \sqrt{2\lambda^2 c}\; t$$

and

$$h = 0 \qquad \text{for} \quad x > \sqrt{2\lambda^2 c}\; t \tag{A11}$$

Equation A11 shows that $\dfrac{dx}{dt} = \sqrt{2\lambda^2 c}$ and indicates that the water front travels with a constant velocity equal to $\sqrt{2\lambda^2 c}$.

Two-Dimensional Flow

Governing equation

13. The governing differential equation for two-dimensional flow can be obtained by using a procedure similar to that described in paragraph 1.[14] The equation may be expressed as

$$\frac{\partial h}{\partial t} = \frac{k_x}{n} \frac{\partial}{\partial x}\left(h \frac{\partial h}{\partial x}\right) + \frac{k_y}{n} h \frac{\partial^2 h}{\partial y^2} \qquad \text{(A12)}$$

where

k_x and k_y = permeabilities in x and y directions, respectively

n = porosity

Solution by linearization

14. It is difficult to obtain a closed-form solution to equation A12 in the nonlinear form. Brahma and Harr[2] modified equation A12 to the linearized form

$$\frac{\partial h}{\partial t} = \frac{k\bar{h}}{n}\left(\frac{\partial^2 h}{\partial x^2} + \frac{\partial^2 h}{\partial y^2}\right) \qquad \text{(A13)}$$

where

$\bar{h}$ = mean height of reservoir

k = uniform permeability

and obtained solutions by expressing equation A13 in polar coordinates r,θ (fig. A4) as

$$\frac{\partial h}{\partial t} = \frac{k\bar{h}}{n}\left(\frac{\partial^2 h}{\partial r^2} + \frac{1}{r}\frac{\partial h}{\partial r} + \frac{1}{r^2}\frac{\partial^2 h}{\partial \theta^2}\right) \qquad \text{(A14)}$$

with boundary conditions of

i. $h(r,\theta,0) = 0$ for $r > 0$, $0 < \theta < 2\alpha$

ii. $h(r,0,t) = h(r,2\alpha,t) = H$ or $= f(t)$

iii. $h(r,\theta,t) = r \sin(\alpha - \theta)$ on free surface

where

H = instantaneous head

f(t) = function giving variation of flood

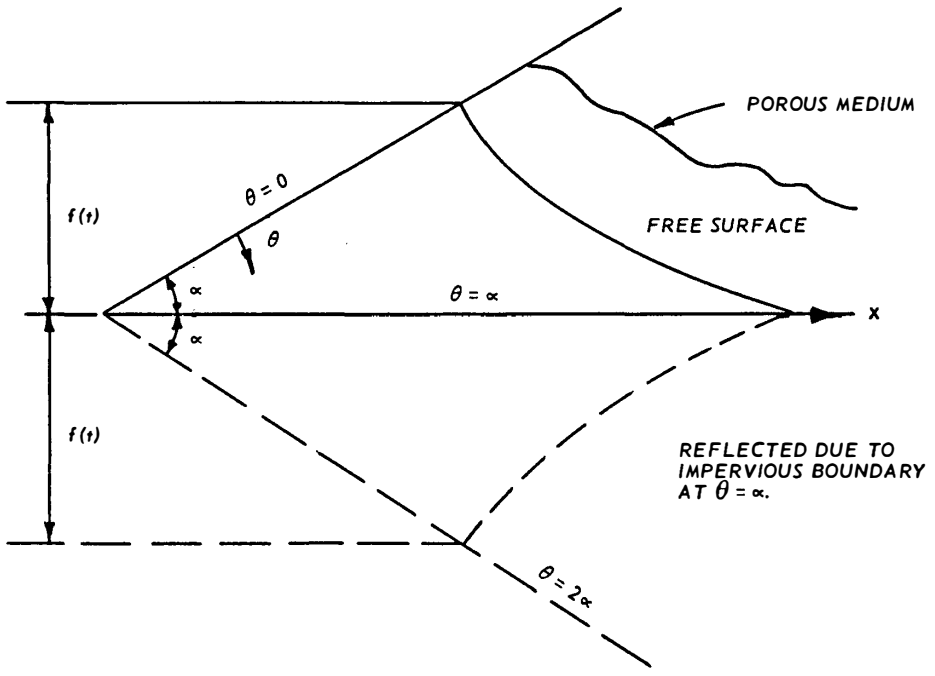

Fig. A4. Section of porous boundary to account for impervious boundary[2]

15. The solution for the case of instantaneous rise of head H is

$$\frac{h(r,\theta,t)}{H} = 1 - \frac{2}{\alpha}\sum_{n=0}^{\infty} \sin s\theta \left\{\frac{\sqrt{\pi}}{4s\sqrt{\tau}}\left[\frac{I_{s-1}}{2}\left(\frac{1}{8\tau}\right) + \frac{I_{s+1}}{2}\left(\frac{1}{8\tau}\right)\right]\exp\left(-\frac{1}{8\tau}\right)\right\} \qquad \text{(A15)}$$

where

$$s = \left(\frac{2n+1}{2}\right)\frac{\pi}{\alpha}$$

$$\tau = \frac{kt}{r^2}$$

$$k = \frac{k\bar{h}}{n}$$

I = modified Bessel function

The solution for linear rise of flood is

$$\frac{h(r,\theta,t)}{ct} = 1 - \frac{2}{c\tau} \sum_{n=o}^{\infty} \sin s\theta \int_{0}^{\infty} \left(1 - e^{-\tau u^2}\right) \frac{\tau_s(u)}{u^3} du \qquad (A16)$$

For further details on the derivation of equations A15 and A16, see reference 2. The free surface is determined from the solutions of equations A15 and A16, such that the boundary condition iii is satisfied.

Unclassified

Security Classification

DOCUMENT CONTROL DATA - R & D

(Security classification of title, body of abstract and indexing annotation must be entered when the overall report is classified)

1. ORIGINATING ACTIVITY *(Corporate author)* U. S. Army Engineer Waterways Experiment Station Vicksburg, Miss.	2a. REPORT SECURITY CLASSIFICATION Unclassified 2b. GROUP

3. REPORT TITLE

SEEPAGE IN MISSISSIPPI RIVER BANKS; Report 1, ANALYSIS OF TRANSIENT SEEPAGE USING A VISCOUS-FLOW MODEL AND THE FINITE DIFFERENCE AND FINITE ELEMENT METHODS

4. DESCRIPTIVE NOTES *(Type of report and inclusive dates)*

Report 1 of a series

5. AUTHOR(S) *(First name, middle initial, last name)*

Chandrakant S. Desai

6. REPORT DATE	7a. TOTAL NO. OF PAGES	7b. NO. OF REFS
May 1973	105	59

8a. CONTRACT OR GRANT NO.	9a. ORIGINATOR'S REPORT NUMBER(S) Technical Report S-73-5
b. PROJECT NO.	
c.	9b. OTHER REPORT NO(S) *(Any other numbers that may be assigned this report)*
d.	

10. DISTRIBUTION STATEMENT

Approved for public release; distribution unlimited.

11. SUPPLEMENTARY NOTES	12. SPONSORING MILITARY ACTIVITY
	U. S. Army Engineer Division, Lower Mississippi Valley

13. ABSTRACT

The stability of the banks of the Mississippi River is dependent in part upon seepage conditions induced by variations in the river level. Specifically, the drawdown conditions become significant for the design of stable riverbank slopes and protective structures. Conventionally, the slopes are designed on the basis of sudden drawdown conditions, which have often been found to be conservative. For realistic design analysis, it is necessary to evolve methods that permit computations of the timewise fluctuations of the phreatic surface as a consequence of the variations in the river level. Closed-form solutions for the transient, unconfined seepage posed by the foregoing situation are suitable only for simplified geometries and physical conditions. Such numerical techniques as the finite difference and finite element methods can provide general solutions for complex geometries and material properties. These methods were employed in this research. A parallel-plate, viscous-flow model was designed and constructed at the WES for the purpose of conducting tests that simulate seepage conditions and variations of external water levels in the field. This report presents a description of the viscous-flow model and the theory governing fluid flow through the model. Various experiments were performed using the model, and a special finite difference scheme was developed for solving approximate equations governing one- and two-dimensional fluid flow. Comparisons were made between the numerical and experimental solutions. A study was performed to examine the numerical characteristics of the finite difference solution scheme. The finite element method for analysis of one- and two-dimensional fluid flow situations was developed. The one-dimensional flow situation was based on an approximate equation, and the two-dimensional situation was based on the division of the transient problem into a number of steady-state problems governed by the Laplace equation. The numerical solutions were compared with typical experimental results and with field observations along typical sections of the Mississippi River. Analyses were also performed to arrive at the conclusions regarding discretization of infinite soil media as occurring in riverbanks. Applications of the proposed techniques for obtaining head distribution and flow nets in the domain of fluid seepage are presented in the report. Work to be performed and to be included in the final report (Report 2) is briefly described.

DD FORM 1 NOV 65 1473 REPLACES DD FORM 1473, 1 JAN 64, WHICH IS OBSOLETE FOR ARMY USE.

Unclassified

Security Classification

14. KEY WORDS	LINK A		LINK B		LINK C	
	ROLE	WT	ROLE	WT	ROLE	WT
Finite difference method						
Finite element method						
Mississippi River						
Parallel plate model						
Riverbanks and earth dams						
Transient unconfined seepage						